

NASA TECHNICAL NOTE



NASA TN D-5766

2.1

NASA TN D-5766



LOAN COPY: RETURN TO
AFWL (WLOL)
KIRTLAND AFB, N MEX

AN EXPERIMENTAL INVESTIGATION
OF BOUNDARY-LAYER TRANSITION
ON A 10° HALF-ANGLE CONE
AT MACH 6.9

by Michael C. Fischer

Langley Research Center

Langley Station, Hampton, Va.



0132444

1. Report No. NASA TN D-5766	2. Government Accession No.	3. Recipient's Catalog No.	
4. Title and Subtitle AN EXPERIMENTAL INVESTIGATION OF BOUNDARY-LAYER TRANSITION ON A 10° HALF-ANGLE CONE AT MACH 6.9		5. Report Date April 1970	6. Performing Organization Code
		8. Performing Organization Report No. L-6940	10. Work Unit No. 126-13-10-17-23
7. Author(s) Michael C. Fischer		11. Contract or Grant No.	
9. Performing Organization Name and Address NASA Langley Research Center Hampton, Va. 23365		13. Type of Report and Period Covered Technical Note	
		14. Sponsoring Agency Code	
12. Sponsoring Agency Name and Address National Aeronautics and Space Administration Washington, D.C. 20546		15. Supplementary Notes The information presented herein was a part of a thesis entitled "An Experimental Investigation on Unit Reynolds Number and Bluntness Effects on Boundary-Layer Transition for a 10° Half-Angle Cone at $M_\infty = 7$ " submitted in partial fulfillment of the requirements for the degree of Master of Science in Mechanical Engineering, Virginia Polytechnic Institute, Blacksburg, Virginia, June 1969.	
16. Abstract An experimental investigation was made of the effect of mass addition, local unit Reynolds number, nose bluntness, and angle of attack on the transition Reynolds number for a 10° half-angle cone with a ratio of wall to total temperature of about one-half. The tests were conducted at a Mach number of 6.9 and a free-stream unit Reynolds number range of 1.68×10^6 to 6.26×10^6 per foot (5.51×10^6 to 20.53×10^6 per meter). The results showed a significant reduction in transition Reynolds number owing to mass addition by using a low-temperature ablator. There was a significant influence of local unit Reynolds number on transition. The present data did not agree with a correlation which attempts to predict the Reynolds number for the end of transition. Correlations of transition Reynolds number with hypersonic Mach number were shown to be highly dependent on tunnel size (noise level). Transition moved forward on the leeward side of the sharp cone at angle of attack and rearward on the windward side. Transition occurred only on the leeward side of the blunted-cone configurations at angle of attack and was displaced rearward of the equivalent sharp-cone transition location. At large angle of attack there was a diminishing effect of bluntness on displacing transition rearward. Longitudinal grooves observed on the surface of the ablated models were believed to be formed by an array of streamwise Görtler-type vortices.			
17. Key Words (Suggested by Author(s)) Mass addition Unit Reynolds number Bluntness Angle of attack Boundary-layer transition Cones		18. Distribution Statement Unclassified - Unlimited	
19. Security Classif. (of this report) Unclassified	20. Security Classif. (of this page) Unclassified	21. No. of Pages 63	22. Price* \$3.00

AN EXPERIMENTAL INVESTIGATION OF BOUNDARY-LAYER
TRANSITION ON A 10° HALF-ANGLE CONE AT MACH 6.9*

By Michael C. Fischer
Langley Research Center

SUMMARY

An experimental investigation was made of the effect of mass addition, local unit Reynolds number, nose bluntness, and angle of attack on the transition Reynolds number for a 10° half-angle cone at a Mach number of 6.9. The tests were conducted over a free-stream unit Reynolds number range of 1.68×10^6 to 6.26×10^6 per foot (5.51×10^6 to 20.53×10^6 per meter). Stagnation temperature varied from 1020° R to 1280° R (567° K to 711° K), and the ratio of wall to total temperature varied from 0.45 to 0.53.

Transition Reynolds numbers for the low-temperature ablating cones were 28 to 35 percent lower than those for the sharp metal cone. There was a strong effect of local unit Reynolds number on the metal-cone transition data for the start and end of transition.

By comparing slender sharp-cone transition data from various facilities the unit Reynolds number effect was shown to be a common parameter in most wind tunnels. The present results indicated poor agreement when compared with a correlation which attempts to predict the Reynolds number for the end of transition based on parameters upon which tunnel noise was assumed to have a functional dependence. Correlations of transition Reynolds number with local hypersonic Mach number were shown to be limited in their meaning if no consideration was given to tunnel size and thus, presumably, noise level. The location of transition moved forward on the leeward side at angle of attack and rearward on the windward side for the sharp-tipped cone. For the blunt-tipped-cone configurations transition occurred only on the leeward side at angle of attack and was displaced rearward of the equivalent sharp-cone locations. At large angle of attack there was a diminishing effect of bluntness on displacing transition rearward of the equivalent sharp-cone location. Longitudinal grooves were observed on the surface of the ablated-cone models. These longitudinal grooves were believed to be formed by an array of stream-wise Görtler-type vortices which were attached to the rearward facing step formed at the interface of the nonablating tip and the ablation material.

*The information presented herein was a part of a thesis entitled "An Experimental Investigation on Unit Reynolds Number and Bluntness Effects on Boundary-Layer Transition for a 10° Half-Angle Cone at $M_\infty = 7$ " submitted in partial fulfillment of the requirements for the degree of Master of Science in Mechanical Engineering, Virginia Polytechnic Institute, Blacksburg, Virginia, June 1969.

INTRODUCTION

In recent years there has been considerable interest in studying transition in the hypersonic speed range encountered by reentry vehicles. (See refs. 1 to 9.) Associated with boundary-layer transition are increased surface heating associated with a turbulent boundary layer and possible effects on the aerodynamic characteristics. Ablation of the protective heat shield may alter the transition location because of effects of nose shape changes, mass addition, and surface roughness. There are limited experimental investigations dealing with the effects of mass addition on boundary-layer transition (refs. 10 to 12); however, results of these investigations are not conclusive.

The purpose of this experimental investigation was to study the effects of nose bluntness, mass addition, local unit Reynolds number, and angle of attack on boundary-layer transition for a slender cone in a hypersonic free stream. The tests were conducted with a metal 10° half-angle cone, instrumented for heat transfer, with four interchangeable nose tips, and with four cones of identical external geometry as the metal cone which were composed of paradichlorobenzene ($C_6H_4Cl_2$), a low-temperature ablator.

Free-stream unit Reynolds number varied from 1.68×10^6 to 6.26×10^6 per foot (5.51×10^6 to 20.53×10^6 per meter) for a range of tunnel stagnation pressures from 186 to 609 pounds per square inch absolute (128×10^4 to 420×10^4 newtons/meter²). The free-stream Mach number was a function of unit Reynolds number with a value between 6.82 and 6.86, with tunnel stagnation temperature of $1150^\circ R \pm 130^\circ R$ ($639^\circ K \pm 72^\circ K$). The metal cone was tested for an angle-of-attack range from 0° to 8° , while the tests with the ablating cone were conducted at an angle of attack of 0° .

SYMBOLS

A_{tr}	cross-sectional area of cone at start of transition
C	constant in power-law relation
C_F	mean turbulent skin-friction coefficient
C_f	local skin-friction coefficient
c	tunnel test-section circumference
c_1	tunnel test-section circumference used as reference in Pate and Schueler's correlation, 48 inches (122 cm)

c_p	specific heat at constant pressure
F_c	function in Spalding-Chi theory
h	height of rearward facing step
k	thermal conductivity
L	center-line distance from tunnel throat to model leading edge
M	Mach number
\dot{m}	mass ablation rate
N_{St}	Stanton number, $\frac{\dot{q}}{\rho_\infty u_\infty c_p (T_{aw} - T_w)}$
N_{Pr}	Prandtl number
n	exponent in power-law relation
p	pressure
\dot{q}	rate of heat flow per unit area
R	unit Reynolds number, $\rho u / \mu$
R_s	local Reynolds number based on surface distance from cone apex, $\rho u s / \mu$
r_n	nose radius
s	distance along cone surface from stagnation point
T	temperature
t	time
u	velocity

Δy	wall thickness
α	angle of attack
δ	boundary-layer thickness
δ^*	boundary-layer displacement thickness
η	recovery factor
θ_c	cone half-angle
λ	spacing between adjacent longitudinal vortices
μ	viscosity
ρ	density
ϕ	cone peripheral angle measured from top ray

Subscripts:

aw	adiabatic-wall conditions
l	local conditions at boundary-layer edge
lam	laminar
t	stagnation conditions
tr	transition
w	wall conditions
∞	free-stream conditions

Primes denote quantities evaluated at reference-temperature conditions.

TEST FACILITY

This experimental investigation was conducted in the Langley 11-inch hypersonic tunnel with the nominal Mach 7 two-dimensional air nozzle. The facility is capable of operating over a range of stagnation pressures from 73.5 to 610 psia (50.7×10^4 to 421×10^4 N/m²) and a range of free-stream unit Reynolds numbers of 0.8×10^6 to 6.3×10^6 per foot (2.6×10^6 to 20.7×10^6 per meter). Free-stream stagnation temperature can be varied over the range of 1000° R to 1280° R (556° K to 711° K), and free-stream Mach number varies slightly depending on unit Reynolds number. The test-section circumference is 44 inches (111.7 cm), and the nozzle length from throat to center of test section is 54 inches (137.2 cm). A schematic of the Langley 11-inch hypersonic tunnel is shown in figure 1.

DESCRIPTION OF MODELS

Nonablating Metal Model

The metal model used in this investigation was a 10° half-angle cone with four detachable nose tips as shown in figure 2. This cone had an axial length of 12 inches (30.5 cm) with the sharp tip installed and a base diameter of 4.23 inches (10.75 cm). The cone model was rolled from an 0.063-inch-thick (0.160-cm) inconel 610 sheet and spun on a lathe to the nominal wall thickness of 0.030 inch (0.0762 cm). Inconel was chosen because of the material's low thermal conductivity which reduces conduction effects and also because it has favorable machining properties.

The detachable nose tips were machined separately from an inconel shaft to obtain uniform wall thicknesses and were threaded to allow for accurate installation on the cone frustum. The nose tips were blunted in such a manner that the radius at the shoulder joining the stagnation nose region with the conical region was half the radius r_n at the stagnation point. The dimensions of each tip are as follows:

Nose tip	r_n		Length	
	in.	cm	in.	cm
A	0	0	2.25	5.72
B	.15	.38	1.75	4.45
C	.30	.76	1.25	3.18
D	.60	1.52	.60	1.52

Ablating Models

The ablating models used in this investigation were identical in external geometry to the sharp metal model and were composed of paradichlorobenzene ($C_6H_4Cl_2$). This low-temperature melting-subliming material has uniform ablation rates with time and has a molecular weight of 147. A sharp stainless steel nose tip prevented blunting and maintained sharp-cone conditions at the boundary-layer edge. In addition a phenolic nylon spacer was used to insulate the hot steel tip from the ablation material, thus preventing recession at the interface because of conduction. (See fig. 3 for a typical ablation model.)

Four ablation models were made – one for each run – because each model could be tested only once. The models were formed in a specially designed mold where they were pressed into the desired conical shape which resulted in a material density of about 167 lbm/ft^3 (2675 kg/m^3). The tunnel mounting sting was molded into the cone base during the forming process. Details of the ablation-model molding technique are presented in appendix A. The final step was to turn the models down to a true conical shape by using a lathe and then install the sharp tip. Because of the high density, the material displayed excellent machining properties and the surface finish was smooth. The lengths of each ablation cone varied from 11.25 to 12.13 inches (28.6 to 30.8 cm).

Instrumentation

The metal model was instrumented with 38 thermocouples for measuring wall temperature and determining heat-transfer rates. Table I lists the thermocouples and gives their surface locations. All thermocouples were 30-inch (0.010-inch-diameter (0.0254-cm)) chromel-alumel wires which were individually spotwelded to the inside surface of the model skin along the cone ray where $\phi = 0^\circ$. The reference temperature of each thermocouple was maintained at 77° F (298.2° K) by using a cold junction box.

The ablation models were not instrumented because of the nature of the ablation material. For these models transition was determined by surface recession measurements which gave a direct indication of the relative local heating rate.

TEST CONDITIONS AND PROCEDURE

A total of 59 runs were conducted for this investigation. The tunnel stagnation pressure varied from 186 to 609 psia (128×10^4 to $420 \times 10^4 \text{ N/m}^2$) for a range of free-stream unit Reynolds numbers of 1.68×10^6 to 6.26×10^6 per foot (5.51×10^6 to 20.53×10^6 per meter). The free-stream Mach number varied from 6.82 to 6.86 depending on unit Reynolds number, and the stagnation temperature was between 1020° R and 1280° R (567° K to 711° K). Details of the test conditions are given in table II.

The test procedure for the metal cone consisted of evacuating the test section to a vacuum of about 3 to 4 millimeters of mercury and preheating the test air with an electrical resistance heater. While the heater was being brought up to the desired temperature, the preheated air was bypassed to the atmosphere. The bypass was closed off when the selected temperature was attained. A fast-response pressure-regulating valve enabled steady-state flow conditions to be established in the test section within 2 to 4 seconds. A series of screens in the settling chamber reduced the vorticity and contamination of the air. Each test run with the metal cone was approximately 10 seconds in length. After each test run, the metal model was air cooled in preparation for the next test run. A temperature-time history of each thermocouple was recorded by using three 18-channel oscillographs. Stagnation pressure and temperature were recorded separately for each run.

The test procedure for the ablating cones was basically the same as for the metal cone. Run time for the ablating models was about 30 seconds. A recession-indicator apparatus was mounted on the ablated cone and photographs were taken to record the results. These recession measurements were made at three peripheral angles about the cone $\phi = 0^\circ, 90^\circ, \text{ and } 180^\circ$ to determine whether any unsymmetrical transition was present.

EXPERIMENTAL HEAT-TRANSFER DATA REDUCTION

The convective heat-transfer rate \dot{q}_{conv} to the metal-cone surface was calculated by using the equation

$$\dot{q}_{\text{conv}} = \rho_w c_{p,w} \Delta y \frac{dT_w}{dt}$$

The value of the wall density ρ_w was taken to be 530 lbm/ft³ (8490 kg/m³), and the specific heat varied with the wall temperature as $c_{p,w} = 0.1041 + 0.000335T_w$ Btu/^oF-lbm (436 + 1.402 T_w J/^oK-kg). The thickness of the wall at each thermocouple station was measured and varied over the range from 0.028 to 0.041 inch (0.071 to 0.104 cm). The temperature-time derivative dT_w/dt was determined by measuring the slope of each thermocouple trace at the instant constant flow conditions were established in the test section (between 2 and 4 seconds). Corrections for radiative heat transfer both from the tunnel wall to the model or from the model to the surrounding environment were insignificant because of the low temperatures encountered (maximum $T_w \approx 120^\circ \text{ F}$ (322.0^o K)). The heat-transfer measurements were made under nonisothermal wall conditions, with the model wall temperature varying a maximum of about 40^o F (277.6^o K) over the model length. Estimates of the error in the measurements owing to heat conduction \dot{q}_{cond}

along the wall were made by using the equation for one-dimensional heat conduction along a cone surface

$$\dot{q}_{\text{cond}} = k_w \Delta y \left(\frac{d^2 T_w}{ds^2} + \frac{1}{s} \frac{dT_w}{ds} \right)$$

Conduction effects were minimized by the thin skin of the model. The maximum correction due to conduction was calculated to be about 3 percent, with most of the corrections being less than 2 percent of the measured heat-transfer data. For this reason corrections due to heat-conduction effects were neglected.

The adiabatic-wall temperature was calculated from the equation

$$T_{\text{aw}} = T_t \left[\eta + \frac{T_l}{T_t} (1 - \eta) \right]$$

where η is the recovery factor and was taken as $\eta = \sqrt{N_{\text{Pr}}}$ for laminar flow and $\eta = \sqrt[3]{N_{\text{Pr}}}$ for turbulent flow. A Prandtl number of 0.72 was used for all calculations.

The convective heat transfer was converted to a Stanton number by the equation

$$N_{\text{St},\infty} = \frac{\dot{q}}{\rho_\infty u_\infty c_p (T_{\text{aw}} - T_w)}$$

where a specific heat of $c_p = 0.24 \text{ Btu/}^\circ\text{F-lbm}$ ($1004 \text{ J/}^\circ\text{K-kg}$) for air was used.

TEST RESULTS AND DISCUSSION

Transition Reynolds Number

Effect of mass addition.- Transition Reynolds numbers for the sharp-tipped metal cone at $\alpha = 0^\circ$, as determined from heat-transfer distributions, and for the ablating cones, as determined from recession measurements, are shown in figure 4 against local unit Reynolds number. For the metal cone the start of transition was taken as the location where the laminar heat-transfer data began to increase and where this increase was continued downstream. The end of transition was taken as the peak heating point. The start of transition for the ablating cones was taken as the location where surface recession began to increase from the observed laminar value. The details of the heat transfer and recession measurements are presented subsequently herein. The unshaded symbols are from the test runs conducted at the higher stagnation temperatures, thereby resulting in a ratio of wall to total temperature T_w/T_t of about 0.46. The shaded symbols (metal

cone only) represent transition data determined at a T_w/T_t of about 0.52 by decreasing the total temperature from about 1210° R (672° K) to about 1055° R (586° K).

Transition Reynolds numbers for the ablating cones were about 28 to 35 percent lower than those for the metal cone for nondimensional mass ablation rates of $\dot{m}_{lam}/\rho_\infty u_\infty A_{tr} = 0.0041$ to 0.0063. In this expression, \dot{m}_{lam} represents the amount of mass injected into the laminar boundary layer and A_{tr} is the cross-sectional area of the cone at the start of transition. As a comparison, results from Larson and Mateer (ref. 10) showed no noticeable effect of mass addition on transition for a 5° half-angle ablating camphor cone at $M_\lambda = 6.8$ with a maximum $\dot{m}_{lam}/\rho_\infty u_\infty A_{tr}$ of about 0.005. DiCristina (ref. 11) reported a 12-percent reduction in transition Reynolds number at $M_\lambda = 7.8$ for an 8° half-angle ablating paradichlorobenzene cone with a maximum $\dot{m}_{lam}/\rho_\infty u_\infty A_{tr}$ of about 0.007. A recent study by Marvin and Akin (ref. 12) for a porous 5° half-angle cone (air injection) at $M_\lambda = 6.8$ and with $\dot{m}_{lam}/\rho_\infty u_\infty A_{tr} = 0$ to 0.028 showed a 0- to 68-percent decrease in transition Reynolds number. The greater effect of mass addition on transition for the investigation of reference 12 may be due to the low molecular weight of the injected gas (air).

In the present ablation tests a rearward facing step formed at the interface of the ablation material and the nonablating tip. The maximum height of this step (at end of test run) was about 0.040 inch (0.102 cm). This step was not believed to influence transition significantly based on studies in reference 10 with oversized tips on a metal-cone model at nearly the same local Mach number as in the present experiment. For the tests of reference 10, the rearward facing step was 0.050 to 0.100 inch (0.127 to 0.254 cm) and the transition Reynolds number was reduced a maximum of 10 percent. The effect of the steps on transition is more pronounced in the lower supersonic Mach number range, as noted in reference 13.

Effect of local unit Reynolds number.- The unit Reynolds number effect on transition was significant for both the metal-cone and ablating-cone transition Reynolds numbers. From the faired lines through the data in figure 4, power-law relations of the form $R_{s,tr} = C(R_\lambda/ft)^n$ were calculated. Values of the power-law exponent for the tests in this facility were $n = 0.41$ for the ablating cones at $T_w/T_t = 0.47$ (start of transition, $T_t \approx 1280^\circ R$ (711° K)), $n = 0.57$ for the metal cone at about $T_w/T_t = 0.46$ to 0.52 (start of transition, $T_t \approx 1055^\circ R$ to 1210° R (586° K to 672° K)), and $n = 0.80$ for the metal cone at $T_w/T_t = 0.52$ (end of transition, $T_t \approx 1055^\circ R$ (586° K)).

In order to determine how the unit Reynolds number effect of this investigation compares with those from studies in other facilities, cone transition data were collected in figure 5. An attempt was made to choose only data for slender sharp cones at an angle of attack of 0° where the ratio of wall to total temperature was $T_w/T_t \approx 0.5$ (as



for the present tests). Two sets of data had significant deviations from the desired wall temperature ratio (refs. 3 and 4); however, they were used because no effect of wall temperature ratio on transition was found. The line associated with each data symbol (except that of ref. 3) indicates the average of the data for transition Reynolds number as a function of local unit Reynolds number. The data of reference 3 were obtained at one value of unit Reynolds number. Only one data symbol for each study is shown, although each line is the result of many experimental points. The numbers given for each solid line represent the local Mach number at the edge of the boundary layer for the particular investigation.

All data in figure 5 indicate a substantial effect of local unit Reynolds number on transition Reynolds number (similar slopes) except for the data of reference 10 (square symbols). For the data of reference 10 in which a weaker unit Reynolds number effect existed, this behavior was tentatively attributed to the test facility (NASA Ames 3.5-foot hypersonic wind tunnel) where cold helium gas was injected into the subsonic portion of the tunnel nozzle for the purpose of insulating the wall from the hot free-stream flow. It is known (ref. 14) that the acoustic energy radiated from a jet boundary is a function of the molecular weight of the jet. Therefore the low-molecular-weight helium-air wind-tunnel boundary layer may have influenced the transition results of reference 10.

The unit Reynolds number parameter has never really been established as the most appropriate parameter describing the behavior of transition Reynolds numbers with increasing tunnel or range pressure. In fact the investigations of Laufer would suggest that at least one of the factors would be a Reynolds number associated with tunnel size (refs. 15 and 16). Nagel (ref. 17) analyzed the unit Reynolds number effect in terms of the formation and growth of turbulent spots, wind-tunnel noise, and stability theory. He also emphasized the requirement of a characteristic Reynolds number based on tunnel size for purposes of explaining transition behavior. Reshotko (ref. 18) noted that in addition to the usual parameters affecting transition, other significant parameters are a dimensionless frequency or wavelength and an orientation factor that is representative of the initial disturbance spectrum. Reshotko accounted for the unit Reynolds number effect in terms of dimensionless frequency parameters. The investigations of Pate and Schueler (ref. 19) and Wagner and others (ref. 20) showed the dependence of transition Reynolds numbers in conventional wind tunnels on radiated pressure fluctuations from the turbulent tunnel-wall boundary layer. The level of radiated pressure fluctuations from a turbulent boundary layer (nondimensionalized by free-stream mean static pressure) decreases with increasing unit Reynolds number. From a study of previous investigations dealing with measurement of tunnel noise, Pate and Schueler found the main parameters affecting the radiated pressure field were tunnel-wall boundary-layer displacement thickness, the wall mean shear, and the tunnel test-section size. By using

these factors, Pate and Schueler developed an empirical correlation which was independent of local unit Reynolds number and Mach number. The correlation was based on transition data from flat-plate and hollow-cylinder models (extrapolated to zero-bluntness leading edge) tested in nine different wind tunnels over a free-stream Mach number range of 3 to 8 and a free-stream unit Reynolds number range from 0.60×10^6 to 13.20×10^6 per foot (1.95×10^6 to 43.30×10^6 per meter). In addition, preliminary data by Pate and Schueler, as discussed by Morkovin (ref. 21), contain a similar correlation based on 10^0 half-angle sharp cones tested in various tunnels over a similar Mach and unit Reynolds number range.

The data for the start and end of transition for the present tests are compared with Pate and Schueler's cone correlation (from ref. 21) in figure 6. In order to maintain compatibility, the displacement thickness δ^* and the turbulent mean skin-friction coefficient C_F were determined for the present study by the same method used by Pate and Schueler. The mean skin-friction coefficient was determined by Van Driest (ref. 22) by using the center-line length from the nozzle throat to the cone tip L as a characteristic dimension. To determine δ^* , a correlation method of Maxwell and Jacobs (ref. 23) presented in Pate and Schueler's paper was used. The tunnel circumference c for the present tests was 44 inches (111.7 cm), and the reference circumference used in the correlation c_1 was 48 inches (122 cm).

The transition data used by Pate and Schueler were based on the Reynolds number for the end of transition. Therefore the ticked circular symbols in figure 4 of this investigation (end of transition) should be used for comparison purposes. The data representing the end of transition for the present investigation lie above the cone correlation while the data for the start of transition lie below the cone correlation. The disagreement of the end-of-transition data for the present study with the correlation in figure 6 does not verify or disprove the effect of tunnel aerodynamic noise on the transition results.

The correlations of Pate and Schueler are limited to wind tunnels having turbulent wall boundary layers. In addition, as pointed out by Pate and Schueler, the correlations cannot be applied to free-flight results because of the restrictions imposed by C_F and δ^* and also because the correlations are based on finite-sized wind tunnels. The recent study by Potter (ref. 24) showed a definite unit Reynolds number effect in ballistic-range tests and tends to cast doubt on the correlations of Pate and Schueler. In Potter's tests, noise measurements verified that the noise levels in the free stream normally generated by turbulent tunnel-wall boundary layers were practically nonexistent.

Potter's range test results are presented in figure 7 and are compared with the transition data of the present study and that of reference 2. The significant result is that the unit Reynolds number effect is nearly the same for the three cases ($n \approx 0.6$).

Also note that the levels of transition Reynolds numbers are quite similar (if Potter's data were extrapolated to lower R_L/ft), a result which is somewhat unexpected for three reasons. First, with the almost complete absence of radiated free-stream pressure disturbances, Potter's transition Reynolds numbers should have been larger in magnitude (if noise radiated from the nozzle walls is of major importance). Second, the nose radius of 0.005 inch (0.0127 cm) for Potter's cones would also produce a higher level of transition Reynolds numbers as compared with a sharp tip. Third, the wall temperature ratio of Potter's tests ($T_w/T_t \approx 0.16$) places the results in a region where the boundary layer may be expected to have greater stability so that a beneficial effect on transition (higher $R_{S,tr}$) prevailed. The low level of Potter's transition results was discussed by Morkovin (ref. 21) where he postulated that perhaps the combined effects of surface roughness at the low wall temperature ratio and the high local unit Reynolds number were responsible. The surface roughness was measured by Potter and reported as 10 microinches ($0.25 \mu m$) root mean square.

Clearly the situation suggests that more investigations must be conducted to determine and define the most appropriate parameters to explain what has been designated the unit Reynolds number effect, which by nature, is surely a combination of many inter-related and perhaps still unidentified parameters.

Effect of total temperature.- In the present investigation, the total temperature was varied from about $1055^\circ R$ ($586^\circ K$) to $1210^\circ R$ ($672^\circ K$) to assess the effect of a slight change in total-temperature level on transition (sharp metal cone only). From figure 4, the data obtained at $T_t \approx 1210^\circ R$ ($672^\circ K$) agree with those obtained at $T_t \approx 1055^\circ R$ ($586^\circ K$) and thereby indicate that there was no measurable effect of a change in total temperature on transition. However a change in total-temperature level can affect the transition Reynolds number. Mack's theoretical analysis (ref. 25) shows that a significant increase in total temperature will make the velocity profile less stable (through the temperature effect on Sutherland's viscosity). Stetson and Rushton (ref. 1) and Sheetz (ref. 26) showed experimentally that transition Reynolds numbers were lowest for the runs conducted at the highest stagnation temperature. Also temperature spottiness in the free stream may increase with increasing total temperature and thus affect transition. Recent results by Maddalon (ref. 27) at $M_\infty \approx 20$ in helium indicate however that sound (rather than temperature spottiness) is the dominant disturbance mode in moderately heated hypersonic tunnels.

Effect of local Mach number.- In figure 5, there seems to exist a general relation between transition Reynolds number and local Mach number; that is, as the local Mach number increases, in general, so does the Reynolds number for transition.

In figure 8(a) the transition data for the present tests are compared with data from the investigations of figure 5 to indicate the effect of local Mach number on the start of

transition. The vertical line at all but one of the data points with a bar at the top and bottom represents the range of transition Reynolds numbers with unit Reynolds numbers for the particular investigation. The solid-line curve is the relation suggested by Lees and Reshotko (ref. 28). The general trend of this curve in the higher Mach number region ($M_2 > 9$) agrees with correlations of other investigators. For this particular curve, transition Reynolds number is related to local Mach number as $R_{s, tr} \propto M_2^4$. In contrast, a correlation suggested by Larson and Mateer (ref. 10) uses the highest transition Reynolds numbers measured when comparing data from various facilities at similar test conditions so as to assess the effects of various flow variables on transition. In figure 8(a) the correlation of reference 10 considers only the highest or the upper bound of the data presented, as represented by the dashed-line curve. This dependence of transition Reynolds number on local Mach number was constructed, by definition, from data at high local unit Reynolds number; this accounts for the deviation from the suggested relation of Lees and Reshotko.

In an attempt to provide further insight into the local Mach number effect on the start of transition, the correlation of Softley and others (ref. 4) for a local unit Reynolds number of 2.00×10^6 per foot (6.56×10^6 per meter) is shown as the solid-line curve in figure 8(b). The shape of the correlation of reference 4 is based mainly on the data points obtained by Stetson and Rushton (ref. 1) and Larson and Mateer (ref. 10) for $M_2 < 8$. (See fig. 8(b).) The fact that the facilities used in references 1 and 10 are large, with circumferences of 94.2 inches (239.3 cm) and 131.8 inches (334.8 cm), respectively, explains the higher transition Reynolds numbers measured there. Characteristic Reynolds numbers based on the local unit Reynolds number of 2.00×10^6 per foot (6.56×10^6 per meter) and the corresponding tunnel circumference are shown in figure 8(b) for the data of references 1 and 10.

A data point representing the present study, with a tunnel circumference of 44 inches (111.7 cm), is shown in figure 8(b) for the Reynolds number based on tunnel circumference. Also shown are transition data from Stainback (ref. 2) for the Reynolds number based on a tunnel circumference of 56.5 inches (143.5 cm). Another correlation could therefore be made based on transition data obtained in facilities with smaller diameter test sections, as represented by the dashed-line curve in figure 8(b). Based on the results of Pate and Schueler (ref. 19) and Wagner and others (ref. 20), correlations of the type shown in figure 8(b) are vague in nature and show only gross effects since the contributions of free-stream disturbances (radiated noise and temperature spottiness) and total temperature level to the individual transition results are unknown.

Effect of angle of attack and nose bluntness.- Transition data for the sharp-tipped cone and for the blunt-tipped configurations (noses B and D) tested at angle of attack are

presented in figure 9 as a function of the surface distance to transition s_{tr} nondimensionalized by the surface distance to transition for a sharp cone at $\alpha = 0^\circ$ (s_{tr})_{sharp, $\alpha=0^\circ$} . Also shown for comparison purposes are the data of Stetson and Rushton (ref. 1) for an 8° half-angle cone at $M_7 = 4.8$.

For the sharp-tipped-cone configuration (circular symbols) of this investigation, small values of angle of attack resulted in a significant shift of transition rearward on the windward ray or forward on the leeward ray. Transition moved off the windward ray of the sharp-cone model for $\alpha > 2^\circ$, but remained at essentially the same location on the leeward side as the angle of attack was increased from $\alpha = 2^\circ$ to 8° . This sharp-tip transition behavior is similar to that observed by Stetson and Rushton and could be due to cross flow or secondary flow instabilities. An inflection point occurs in the cross-flow velocity profile which promotes boundary-layer instability on the leeward side.

For the blunt-cone configurations, transition occurred only for angles of attack of $\alpha = 2^\circ$ to 8° on the leeward ray. There was no transition noted at an angle of attack of 0° with the blunt tips because of the reduction in local unit Reynolds number as a result of the high entropy, low local Mach number flow which had passed through the curved part of the bow shock. The conditions at the boundary-layer edge will become essentially sharp-cone conditions when this entropy layer is swallowed by the boundary layer. For the present blunt-cone tests, sharp-cone conditions were not attained anywhere on the cone surface at $\alpha = 0^\circ$.

The transition locations on the leeward ray for the blunt-cone configurations were approaching those on the sharp-tip cone at high angles of attack. (See fig. 9.) Stetson and Rushton noted that on the windward side at high angles of attack there was no effect of bluntness on the transition location, and that this condition was approached on the leeward side also. Stetson and Rushton's data indicate that transition moves forward on both the leeward and windward rays of the blunt-cone configurations at angle of attack.

Surface features on ablated models.- An interesting surface feature was noted on the ablated models after a test run. Examination of the models revealed the presence of streamwise longitudinal grooves extending the entire length of the model. These grooves were believed to be formed by an array of vortices which formed behind the rearward facing step. Görtler (ref. 29) studied these counterrotating streamwise vortices in his analysis of boundary-layer instability over concave walls. In order for Görtler vortices to form, a concavity in the surface must be present, but this could be in the form of random surface irregularities or forward and rearward facing steps (present case), all of which produce concave curvature of the streamlines.

The surface features observed during the present tests are shown in figure 10(a). For the two lowest unit Reynolds numbers at which the ablating models were tested, the

grooves were difficult to detect and virtually impossible to record on film. However for the two highest unit Reynolds numbers ($R_L = 4.87 \times 10^6$ and 6.14×10^6 per foot (15.97×10^6 and 20.14×10^6 per meter)), the grooves were a more dominant feature. Oblique lighting was used to give the photographs in figure 10(a). Presented in figure 10(b) is a figure from a paper by Ginoux (ref. 30) which illustrates the behavior of Görtler-type vortex spacing as a function of boundary-layer thickness and step height. Ginoux constructed the shaded region by using his data and those of others at low supersonic speeds. The circular symbols represent the data measured for the present investigation which do not agree with the trend suggested by Ginoux. The disagreement may be due to the large Mach number difference and to the fact that the present tests were conducted with an axisymmetric model (cone) compared with a flat plate for the studies of Ginoux.

Considerable interest was generated recently by the discovery of cross-hatch surface patterns on recovered reentry bodies. These patterns exist only in turbulent-flow regions and were noted in ballistic-range tests with plastic cone models (see ref. 31) and also in wind-tunnel tests with camphor cone models. (See refs. 10 and 32.) These cross-hatch patterns are believed to be formed from a breakdown of the longitudinal vortices which are present. Larson and Mateer (refs. 10 and 32) noted that for the cross hatching to occur, the boundary layer had to be not only turbulent but also supersonic and relatively thin (high surface pressure). For the present investigation with a maximum surface pressure of 0.556 psia (0.384×10^4 N/m²), no cross-hatch surface patterns were observed.

Heat-Transfer Distribution

Metal cone, sharp tip ($\alpha = 0^\circ$).- Experimental Stanton number distributions for the sharp-tipped metal cone at $\alpha = 0^\circ$ are compared with laminar and turbulent theory (presented in appendix B) in figure 11. For the turbulent theory the flow was assumed turbulent from the sharp tip when the transition data were not fully turbulent. When fully turbulent flow was attained on the cone, a correction to the turbulent theory was made by assuming a virtual origin at the peak heating point (ref. 33). However for fully turbulent flow both theories are shown (virtual origin at sharp tip and at peak heating point).

The beginning of transition for the metal cone in this investigation was taken to be the location where the laminar heat-transfer data began to increase and where this increase was continued downstream. The end of transition was taken as the highest Stanton number. Arrows designate the start and end of transition. In this paper Stanton numbers are referenced to free-stream conditions so that direct comparisons can be made to show the effect of (1) angle of attack on sharp-cone heating levels, (2) angle of attack on blunt-cone heating levels, and (3) bluntness on cone-surface heating levels.

The factor for converting the sharp-cone free-stream Stanton numbers to local Stanton numbers is $N_{St,l} = N_{St,\infty}/2.2$.

The first 12 test runs presented in figure 11 were made at a ratio of wall to total temperature of $T_w/T_t = 0.51$ to 0.53 ($T_t \approx 1055^\circ \text{ R}$ (586° K)). The last five test runs presented were conducted at $T_w/T_t = 0.45$ to 0.47 ($T_t \approx 1210^\circ \text{ R}$ (672° K)) to determine whether there was any effect of a slight increase in total-temperature level on the transition location.

For the two lowest local unit Reynolds numbers (fig. 11(a)) the flow over the cone remained laminar. However at a local unit Reynolds number of $R_l = 3.46 \times 10^6$ per foot (11.35×10^6 per meter) the flow over the rearward part of the cone became transitional, as indicated by the arrow in figure 11(b).

As the local unit Reynolds number was increased further, the start of transition generally moved forward (figs. 11(c) and 11(d)), and finally, at $R_l = 7.01 \times 10^6$ per foot (22.99×10^6 per meter), fully turbulent flow was established on the rear of the cone (fig. 11(e)).

For the remaining three test runs at $T_w/T_t \approx 0.52$, the location of the start of transition again generally moved forward with increasing local unit Reynolds number, while the location of the end of transition remained stationary except for the last test run (see fig. 11(f)) where the end of transition moved forward.

The first of the five test runs with $T_w/T_t \approx 0.46$ was made at $R_l = 3.77 \times 10^6$ per foot (12.36×10^6 per meter) (fig. 11(g)). For this local unit Reynolds number, the start of transition occurred near the base of the cone. As the local unit Reynolds number was increased, the start of transition generally moved forward and fully developed turbulent flow was established at the highest local unit Reynolds number $R_l = 6.88 \times 10^6$ per foot (22.57×10^6 per meter) (fig. 11(i)).

Metal cone, sharp tip (angle of attack).- The experimentally measured Stanton number distributions for the sharp-tipped metal cone tests conducted at $\alpha = 0^\circ$ to 8° are shown in figure 12. The heating distribution for $\alpha = 0^\circ$ is shown in each part of figure 12 for comparison. In figure 12(a) the results for the leeward ray are presented. The location of the start and end of transition moved forward rather abruptly for $\alpha = 2^\circ$. For $\alpha = 4^\circ$, 6° , and 8° , the start of transition moved forward of the first heat-transfer measuring station. Estimates were made of the location of the start of transition for these three cases ($\alpha = 4^\circ$, 6° , and 8°) by assuming that the ratios of $(R_{s,tr})_{end}/(R_{s,tr})_{start}$ for these cases were the same as for $\alpha = 2^\circ$.

Figure 12(b) shows the results obtained for the windward ray. The start of transition was shifted backwards on the model at $\alpha = 2^\circ$, and moved completely off the cone

for $\alpha = 4^\circ$, 6° , and 8° . Note the increase in the level of laminar heating with increasing angle of attack on the windward ray.

Metal cone, blunt tips ($\alpha = 0^\circ$).- The experimentally measured heat transfer to the blunt-tip configurations for $\alpha = 0^\circ$ are presented in figure 13 as a function of surface distance nondimensionalized by nose radius s/r_n . For comparison purposes, the corresponding sharp-cone Stanton number distributions (from fig. 11) are also shown. The wall temperature ratio for the blunt-cone tests varied over the range of $T_w/T_t = 0.52$ to 0.53.

The heat-transfer results for nose B ($r_n = 0.15$ inch (0.381 cm)) are presented in figures 13(a) and 13(b). As shown in the figures, the boundary layer remained laminar and the heating distribution was slightly below that of an equivalent sharp cone for a range of free-stream unit Reynolds numbers of 2.01×10^6 to 6.10×10^6 per foot (6.59×10^6 to 20.01×10^6 per meter).

The results for nose C ($r_n = 0.30$ inch (0.762 cm)) are presented in figures 13(c) and 13(d) and indicate that the flow over the cone remained laminar for a range of free-stream unit Reynolds numbers of 2.13×10^6 to 6.08×10^6 per foot (6.99×10^6 to 19.94×10^6 per meter). In figures 13(e) and 13(f) the results for nose D ($r_n = 0.60$ inch (1.52 cm)) are presented for a range of free-stream unit Reynolds numbers of 2.10×10^6 to 6.21×10^6 per foot (6.89×10^6 to 20.37×10^6 per meter). For nose D as with the other two tips, the flow over the cone remained laminar and the level of heating was slightly below that of an equivalent sharp cone.

Metal cone, blunt tips (angle of attack).- The heating-rate distributions for the blunt-tipped configurations (noses B and D) tested at $\alpha = 0^\circ$ to 8° , are shown in figure 14. Again the heating-rate distribution for $\alpha = 0^\circ$, where purely laminar flow existed, is shown as a comparison. On the leeward ray (fig. 14(a)), for the nose tip with $r_n = 0.15$ inch (0.38 cm), the start of transition occurred slightly more than halfway back on the model at $\alpha = 2^\circ$. As the angle of attack was increased further, transition moved forward on the model and, at $\alpha = 8^\circ$, transition moved just forward of the first measuring station. For $\alpha = 8^\circ$, the transition location was estimated at the location shown by the arrow. On the windward ray ($\alpha = 4^\circ$ and 8°) the heating distribution was above the level for $\alpha = 0^\circ$ and remained laminar.

In figure 14(b) the heating distributions for nose D with $r_n = 0.60$ inch (1.52 cm) are shown. For $\alpha = 2^\circ$, the flow remained laminar over the leeward ray of the model. Transition first occurred near the rear of the cone for $\alpha = 4^\circ$ and moved forward as the angle of attack was increased up to 8° . Note that the transitional heating for these tests up to $\alpha = 8^\circ$ never exceeded the laminar heating rate for $\alpha = 0^\circ$. On the windward side, at $\alpha = 4^\circ$ and 8° , the flow remained laminar and the heating distribution was above the level measured at $\alpha = 0^\circ$.

Ablating cones.- Photographs of each of the four ablated models with the recession indicator attached are presented in figure 15 for local unit Reynolds numbers of 2.47×10^6 to 6.14×10^6 per foot (8.10×10^6 to 20.14×10^6 per meter). Also shown for each model are enlargements of the recessed area made by using a cylindrical lens which magnified the vertical axis by a factor of 3. These enlargements enabled an accurate location of the start of transition to be chosen, defined as the location where recession began to increase from the observed laminar value. Recession measurements of this type were made at three peripheral locations about each model, $\phi = 0^\circ$, 90° , and 180° , to detect any unsymmetrical transition. Because there was little if any unsymmetrical transition observed, only the photographs for $\phi = 0^\circ$ are shown. However the average of the three readings was taken as the transition location. From the cylindrical-lens enlargements, the amount of mass loss into the laminar boundary layer was calculated. This mass loss was divided by the length of the run to determine a laminar mass ablation rate $\dot{m}_{1\text{lam}}$.

For the lowest local unit Reynolds number (fig. 15(a)), the local heating rate was low so that little surface recession occurred. As the unit Reynolds number was increased, the local heating rate increased also and a measurable amount of recession was observed. (See fig. 15.) The ablating cones were tested at the highest stagnation temperatures (about 1280° R (711° K)) to obtain the maximum mass ablation rates.

Schlieren photographs were taken of the ablating models to aid in defining the general flow-field characteristics. Typical schlieren photographs are shown in figure 16 at test times of 3 and 30 seconds. The photograph at $t = 30$ seconds shows that a recompression shock from the rearward facing step formed at the interface of the non-ablating tip and the ablation material. More emphasis was given to the recession measurements for defining transition, and the schlieren photographs were used mainly to define the general flow-field characteristics.

CONCLUSIONS

From this experimental investigation of laminar, transitional, and turbulent flow over a sharp and blunt-tipped metal 10° half-angle cone and over sharp ablating 10° half-angle cones the following conclusions were made:

1. Transition Reynolds numbers for the low-temperature ablating cones were 28 to 35 percent lower than those for the metal, nonablating sharp cone, thereby indicating a significant influence of mass addition on transition.

2. Transition Reynolds numbers for the start and end of transition for the sharp metal cone at a ratio of wall to total temperature of about 0.46 to 0.52 displayed a significant effect of local unit Reynolds number.

3. A comparison of transition data on slender sharp cones from various facilities indicated an influence of local unit Reynolds number. The present data did not agree with Pate and Schueler's correlation which attempts to predict the Reynolds number for the end of transition based on parameters upon which tunnel noise was assumed to have a functional dependence.

4. Correlations of transition Reynolds number with local hypersonic Mach number are limited in their meaning if no considerations are given to tunnel size and thus, presumably, noise level.

5. For the sharp metal cone at angle of attack, transition moved forward on the leeward side and rearward on the windward side. Transition occurred only on the leeward ray of the blunted-cone configurations at angle of attack and was displaced rearward of the equivalent sharp-cone transition location. At large angle of attack there was a diminishing effect of bluntness on displacing transition rearward of the equivalent sharp-cone location.

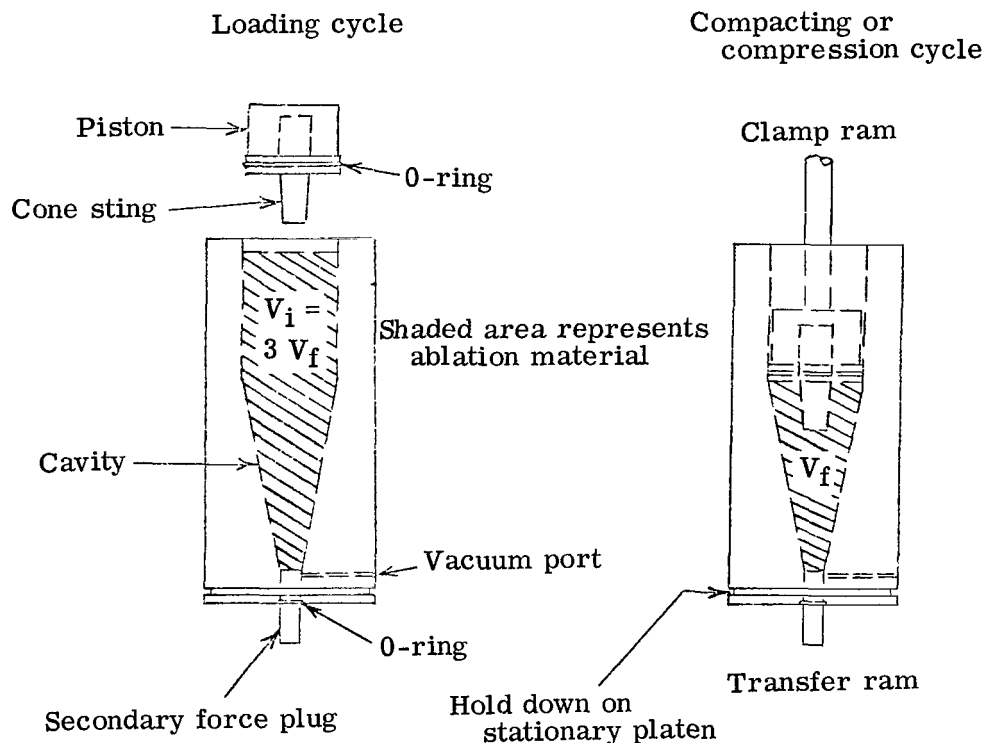
6. Longitudinal grooves observed on the surface of the ablated models were believed to be formed by an array of streamwise Görtler-type vortices which were attached to the rearward facing step formed at the interface of the nonablating tip and the ablation material.

Langley Research Center,
National Aeronautics and Space Administration,
Langley Station, Hampton, Va., February 11, 1970.

APPENDIX A

ABLATION-MODEL MOLDING TECHNIQUE

In reference 10, where low-temperature subliming ablation models (camphor) were formed by casting, severe surface cracks and distortions occurred on the models during a test. The structural integrity of low-temperature ablation models formed by ordinary casting methods is poor, and therefore an alternate technique was developed. For the present investigation a mold was designed so that the models could be pressed into the desired shape as shown in the following sketch:



The mold consists of a cavity, a primary force plug (piston), and a secondary force plug. Initial volume of the ablation material V_i should be about three times the final desired cone volume V_f (three-to-one bulk factor). A cone support sting is fitted into the piston (slip fit) and subsequently molded into the base of the cone. Both force plugs have O-rings to make a hermetical seal. A vacuum is applied prior to the compression cycle to remove all trapped air in the mold. A hydraulic press is used to ram the piston into the mold with a suitable pressure. To ensure an equal distribution of pressure throughout the

APPENDIX A - Concluded

mold, sufficient force is applied to the secondary force plug to just overcome the original force on the piston. When the piston is observed to begin slight movement out of the mold, the force on the secondary force plug is adjusted to balance the force on the piston, thus restricting any further movement. The positions of the primary and secondary force plugs are then adjusted to ensure that the final molded configuration has the correct shape. The material is now in a viscous hydrostatic state and is allowed to solidify under this pressure for a period of about 2 hours to attain maximum structural integrity. Then the pressure is reduced slowly and the cone frustum is removed from the mold. The concept involved in this compacting process is that a material will enter a fluid state under a sufficiently high pressure. This pressure varies with different materials. For the present material, paradichlorobenzene ($C_6H_4Cl_2$), a pressure of about 7100 psi ($4894 \times 10^4 \text{ N/m}^2$) based on piston area was used, but this pressure may be greater than that actually required to produce a viscous hydrostatic state. A sharp steel tip is installed to prevent excess nose blunting during a test. The surface finish can be as smooth as desired simply by obtaining a smooth finish on the inside wall of the mold. If it is desired to machine the cone on a lathe, the machining characteristics are excellent. Numerous wind-tunnel tests with these models indicate a significant improvement in structural integrity over the methods previously used. No surface cracks or distortions occurred during these tests. Maintenance of a smooth, undistorted surface is important in eliminating undesirable surface roughness effects on the results. Another problem associated with models made from low-temperature ablation materials is sublimation at room temperature prior to testing since immediate testing of the models is often not possible. The models are therefore refrigerated after they are fabricated to inhibit the sublimation process. Owing to the high density of the models made by the present technique, there is a significant reduction in deformation because of sublimation between the casting and testing period.

APPENDIX B

THEORETICAL HEAT TRANSFER

Laminar Theory

The local heating rate on a flat plate can be expressed in terms of a Stanton number and reference-temperature conditions by using the modified Reynolds analogy

$$N'_{St} = \frac{C'_f}{2(N'_{Pr})^{2/3}}$$

An expression developed by Blasius (ref. 34) for the local skin friction on a flat plate in terms of the local Reynolds number can be expressed for compressible flow as

$$C'_f = \frac{0.664}{\sqrt{R'_s}}$$

and when combined with the Reynolds analogy gives

$$N'_{St} = \frac{0.332}{(N'_{Pr})^{2/3} \sqrt{R'_s}}$$

From Pai (ref. 35) the Mangler transformation for the local Stanton number for axially symmetric laminar flow over a sharp cone is $\sqrt{3}$ times that for a flat plate at the same local Reynolds number, Mach number, total temperature, and wall temperature ratio.

Rewriting the flat-plate laminar heat-transfer expression to that for a cone and converting to free-stream conditions with $N_{Pr} = 0.72$ gives

$$N_{St,\infty} = 4.317 \frac{T_l^{1/4}}{p_\infty M_\infty} \sqrt{\frac{p_l M_l \mu' T_\infty}{T'_s}}$$

where a reference temperature defined by Monaghan (ref. 36)

$$\frac{T'_s}{T_l} = 0.575 \frac{T_w}{T_l} + 0.425 + 0.0328 M_l^2$$

was used.

APPENDIX B - Concluded

Turbulent Theory

The modified turbulent theory of Spalding and Chi was used, as given by the charts of Neal and Bertram (ref. 37). This theory is based on the Karman form of the Reynolds analogy factor

$$\frac{2N_{St}}{C_f} = \left[1 + 5\sqrt{\frac{F_c C_f}{2}} \left(N_{Pr} - 1 + \log_e \frac{5N_{Pr} + 1}{6} \right) \right]^{-1}$$

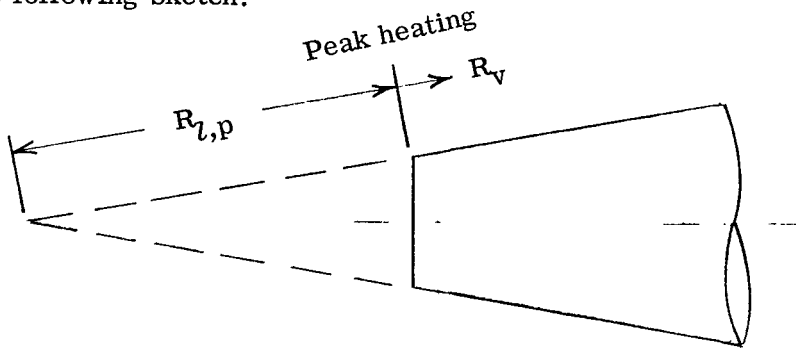
where

$$F_c = \left(\frac{T_{aw}}{T_l} - 1 \right) \left\{ \sin^{-1} \frac{2\sqrt{\frac{T_{aw}}{T_l} - 1} \left[\frac{T_{aw}}{T_l} - \frac{T_w}{T_l} - \sqrt{\frac{T_w}{T_l}} \left(2 - \frac{T_{aw}}{T_l} - \frac{T_w}{T_l} \right) \right]}{\left(\frac{T_{aw}}{T_l} + \frac{T_w}{T_l} \right)^2 - 4 \frac{T_w}{T_l}} \right\}^{-2}$$

The results from the charts of reference 37 were for a flat plate but were directly applied to a cone with a correction for the virtual origin by the transformation in appendix B of reference 33. This transformation gives the ratio of the local skin friction on a truncated cone t_c to that on a flat plate f_p as

$$\frac{(C_f R_v^{1/n})_{t_c}}{(C_f R_v^{1/n})_{f_p}} = \left(\frac{2n - 1}{n - 1} \right)^{1/n} \left[\left(1 + \frac{R_{l,p}}{R_v} \right) - \frac{R_{l,p}}{R_v} \left(\frac{R_{l,p}}{R_v} \right)^{n/n-1} \right]^{-1/n}$$

For this equation n was taken as 4 and the values of the Reynolds numbers used are defined in the following sketch:



When the flow over the cone was laminar or transitional, the theoretical prediction for turbulent flow was calculated by assuming the virtual origin to be at the sharp tip.

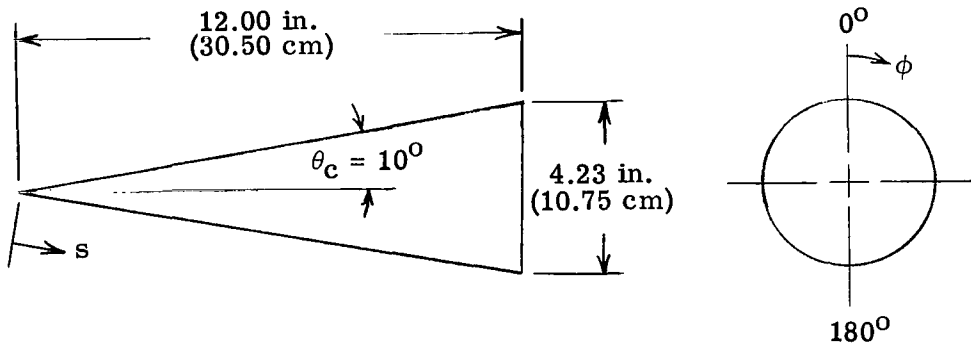
REFERENCES

1. Stetson, Kenneth F.; and Rushton, George H.: A Shock Tunnel Investigation of the Effects of Nose Bluntness, Angle of Attack and Boundary Layer Cooling on Boundary Layer Transition at a Mach Number of 5.5. AIAA Pap. No. 66-495, June 1966.
2. Stainback, P. Calvin (With appendix by P. Calvin Stainback and Kathleen C. Wicker): Effect of Unit Reynolds Number, Nose Bluntness, Angle of Attack, and Roughness on Transition on a 5° Half-Angle Cone at Mach 8. NASA TN D-4961, 1969.
3. Sanator, R. J.; DeCarlo, J. P.; and Torrillo, D. T.: Hypersonic Boundary-Layer Transition Data for a Cold-Wall Slender Cone. AIAA J. (Tech. Notes), vol. 3, no. 4, Apr. 1965, pp. 758-760.
4. Softley, E. J.; Graber, B. C.; and Zempel, R. E.: Experimental Observation of Transition of the Hypersonic Boundary Layer. AIAA J., vol. 7, no. 2, Feb. 1969, pp. 257-263.
5. Maddalon, Dal V.; and Henderson, Arthur, Jr.: Boundary-Layer Transition on Sharp Cones at Hypersonic Mach Numbers. AIAA J., vol. 6, no. 3, Mar. 1968, pp. 424-431.
6. Everhart, Philip E.; and Hamilton, H. Harris: Experimental Investigation of Boundary-Layer Transition on a Cooled 7.5° Total-Angle Cone at Mach 10. NASA TN D-4188, 1967.
7. Nagamatsu, H. T.; Sheer, R. E., Jr.; and Graber, B. C.: Hypersonic Laminar Boundary-Layer Transition on 8-Foot-Long, 10° Cone, $M_1 = 9.1-16$. AIAA J., vol. 5, no. 7, July 1967, pp. 1245-1252.
8. Nagamatsu, H. T.; and Sheer, R. E., Jr.: Boundary-Layer Transition on a Highly Cooled 10° Cone in Hypersonic Flows. Rep. No. 64-RL-(3622 C), Gen. Elec. Res. Lab., Mar. 1964.
9. Potter, J. Leith; and Whitfield, Jack D.: Boundary-Layer Transition Under Hypersonic Conditions. AEDC-TR-65-99, U.S. Air Force, May 1965.
10. Larson, Howard K.; and Mateer, George G.: Transition Measurements on Cones in Hypersonic Flow and Preliminary Observations of Surface Ablation Grooves. NASA paper presented at Boundary Layer Transition Specialists Study Group Meeting (San Bernardino, Calif.), July 1967.
11. DiCristina, V.: Three-Dimensional Laminar Boundary Layer Transition on a Sharp 8° Cone at Mach No. 10. AIAA Pap. No. 69-12, Jan. 1969.

12. Marvin, Joseph G.; and Akin, Clifford M.: Combined Effects of Mass Addition and Nose Bluntness on Boundary-Layer Transition. AIAA Pap. No. 69-706, June 1969.
13. Chapman, Dean R.; Kuehn, Donald M.; and Larson, Howard K.: Investigation of Separated Flows in Supersonic and Subsonic Streams With Emphasis on the Effect of Transition. NACA Rep. 1356, 1958.
14. Lighthill, M. J.: Jet Noise. AIAA J., vol. 1, no. 7, July 1963, pp. 1507-1517.
15. Laufer, John: Sound Radiation From a Turbulent Boundary Layer. Tech. Rep. No. 32-119 (Contract No. NASw-6), Jet Propulsion Lab., California Inst. Technol., Nov. 1, 1961.
16. Laufer, John: Some Statistical Properties of the Pressure Field Radiated by a Turbulent Boundary Layer. Phys. Fluids, vol. 7, no. 8, Aug. 1964.
17. Nagel, A. L.: Analysis of the Unit Reynolds Number Effect in Hypersonic Flat Plate Boundary Layer Transition. Proceedings of the 1968 Heat Transfer and Fluid Mechanics Institute, Ashley F. Emery and Creighton A. Depew, eds., Stanford Univ. Press, c.1968, pp. 51-64.
18. Reshotko, Eli: Stability Theory as a Guide to the Evaluation of Transition Data. AIAA Pap. No. 68-669, June 1968.
19. Pate, S. R.; and Schueler, C. J.: An Investigation of Radiated Aerodynamic Noise Effects on Boundary-Layer Transition in Supersonic and Hypersonic Wind Tunnels. AIAA Pap. No. 68-375, Apr. 1968.
20. Wagner, R. D., Jr.; Maddalon, D. V.; Weinstein, L. M.; and Henderson, A., Jr.: Influence of Measured Free-Stream Disturbances on Hypersonic Boundary-Layer Transition. AIAA Pap. No. 69-704, June 1969.
21. Morkovin, Mark V.: Critical Evaluation of Transition From Laminar to Turbulent Shear Layers With Emphasis on Hypersonically Traveling Bodies. AFFDL-TR-68-149, U.S. Air Force, Mar. 1969. (Available from DDC as AD 686 178.)
22. Van Driest, E. R.: Turbulent Boundary Layer in Compressible Fluids. J. Aeronaut. Sci., vol. 18, no. 3, Mar. 1951, pp. 145-160, 216.
23. Maxwell, H.; and Jacobs, J. L.: Nondimensional Calculation of Turbulent Boundary-Layer Development in Two-Dimensional Nozzles of Supersonic Wind Tunnels. AEDC-TN-61-153, U.S. Air Force, Jan. 1962.
24. Potter, J. Leith: Observations on the Influence of Ambient Pressure on Boundary-Layer Transition. AEDC-TR-68-36, U.S. Air Force, Mar. 1968.

25. Mack, L. M.: Effect of Free-Stream Temperature on the Inviscid Stability of the Compressible Laminar Boundary Layer. Supporting Research and Advanced Development, Space Programs Sum. No. 37-39, Vol. IV (Contract No. NAS 7-100), Jet Propulsion Lab., California Inst. Technol., June 30, 1966, pp. 145-146.
26. Sheetz, Norman W., Jr.: Free-Flight Boundary Layer Transition Investigations at Hypersonic Speeds. AIAA Pap. No. 65-127, Amer. Inst. Aeronaut. Astronaut., Jan. 1965.
27. Maddalon, Dal V.: Effect of Varying Wall Temperature and Total Temperature on Transition Reynolds Number at Mach 6.8. AIAA J. (Tech. Notes), vol. 7, no. 12, Dec. 1969, pp. 2355-2357.
28. Lees, Lester; and Reshotko, Eli: Stability of the Compressible Laminar Boundary Layer. J. Fluid Mech., vol. 12, pt. 4, 1962, pp. 555-590.
29. Görtler, H.: On the Three-Dimensional Instability of Laminar Boundary Layers on Concave Walls. NACA TM 1375, 1954.
30. Ginoux, Jean J.: Streamwise Vortices in Laminar Flow. Recent Developments in Boundary Layer Research, Pt. I, AGARDograph 97, May 1965, pp. 395-422.
31. Canning, Thomas N.; Wilkins, Max E.; and Tauber, Michael E.: Boundary-Layer Phenomena Observed on the Ablative Surfaces of Cones Recovered After Flights at Speeds up to 7 km/sec. Fluid Physics of Hypersonic Wakes, Vol. 2, AGARD CP No. 19, May 1967.
32. Larson, H. K.; and Mateer, G. G.: Cross-Hatching - A Coupling of Gas Dynamics With the Ablation Process. AIAA Pap. No. 68-670, June 1968.
33. Bertram, Mitchel H.; and Neal, Luther, Jr.: Recent Experiments in Hypersonic Turbulent Boundary Layers. Presented at the AGARD Specialists' Meeting on Recent Developments in Boundary-Layer Research (Naples, Italy), May 10-14, 1965.
34. Blasius, H.: The Boundary Layers in Fluids With Little Friction. NACA TM 1256, 1950.
35. Pai, Shih-I: Viscous Flow Theory. I - Laminar Flow. D. Van Nostrand Co., Inc., c.1956.
36. Monaghan, R. J.: An Approximate Solution of the Compressible Laminar Boundary Layer on a Flat Plate. R. & M. No. 2760, Brit. A.R.C., 1953.
37. Neal, Luther, Jr.; and Bertram, Mitchel H.: Turbulent-Skin-Friction and Heat-Transfer Charts Adapted From the Spalding and Chi Method. NASA TN D-3969, 1967.

TABLE I.- THERMOCOUPLE LOCATIONS ON INSTRUMENTED CONE MODEL



Thermocouple	s		ϕ , deg	Thermocouple	s		ϕ , deg
	in.	cm			in.	cm	
1	2.48	6.30	↓	20	7.13	18.11	↓
2	2.68	6.81		21	7.38	18.75	
3	2.88	7.32		22	7.63	19.38	
4	3.13	7.95		23	7.88	20.02	
5	3.38	8.59		24	8.18	20.78	
6	3.63	9.22		25	8.38	21.29	
7	3.88	9.86		26	8.63	21.92	
8	4.13	10.49		27	8.88	22.56	
9	4.38	11.13		28	9.13	23.19	
10	4.63	11.76		29	9.38	23.83	
11	4.88	12.40		30	9.63	24.46	
12	5.13	13.03		31	9.88	25.10	
13	5.38	13.67		32	10.13	25.73	
14	5.63	14.30		33	10.38	26.37	
15	5.88	14.94		34	10.63	27.00	
16	6.13	15.57		35	10.88	27.64	
17	6.38	16.21		36	11.13	28.27	
18	6.63	16.84		37	11.38	28.91	
19	6.88	17.48		38	11.63	29.54	

TABLE II.- TEST CONDITIONS OF EXPERIMENTAL INVESTIGATION

α , deg	p_t		T_t		T_w/T_t	M_∞	M_L	R_∞		R_L		s_{tr}				$R_{s,tr}$	
	psia	N/m ²	°R	°K				Per foot	Per meter	Per foot	Per meter	Start		End		Start	End
												ft	m	ft	m		
Nose A (sharp tip)																	
0	186	128×10^4	1055	586	0.52	6.82	5.52	1.88×10^6	6.17×10^6	2.78×10^6	9.12×10^6	---	---	---	---	-----	-----
0	201	139	1060	589	.52	6.82	5.52	2.02	6.63	3.00	9.84	---	---	---	---	-----	-----
0	226	156	1040	578	.53	6.82	5.52	2.34	7.68	3.46	11.35	0.780	0.238	---	---	2.70×10^6	-----
0	256	177	1035	575	.53	6.83	5.52	2.66	8.72	3.94	12.92	.780	.238	---	---	3.07	-----
0	288	199	1050	583	.52	6.84	5.53	2.91	9.54	4.33	14.20	.780	.238	---	---	3.38	-----
0	360	248	1060	589	.52	6.85	5.54	3.58	11.74	5.30	17.39	.634	.193	---	---	3.36	-----
0	404	279	1055	586	.52	6.86	5.54	4.02	13.19	6.00	19.68	.612	.187	---	---	3.67	-----
0	439	303	1040	578	.53	6.86	5.54	4.52	14.83	6.69	21.94	.591	.180	---	---	3.95	-----
0	482	332	1070	594	.52	6.86	5.54	4.70	15.42	7.01	23.00	.591	.180	0.884	0.269	4.15	6.20×10^6
0	519	358	1075	597	.51	6.86	5.54	5.01	16.43	7.48	24.53	.591	.180	.884	.269	4.42	6.61
0	547	377	1070	594	.52	6.86	5.54	5.33	17.48	7.95	26.08	.550	.168	.884	.269	4.37	7.02
0	609	420	1043	579	.53	6.86	5.54	6.21	20.37	9.18	30.11	.529	.161	.821	.250	4.86	7.54
0	301	208	1180	656	.47	6.84	5.53	2.53	8.30	3.77	12.37	.780	.238	---	---	2.94	-----
0	368	254	1194	663	.47	6.85	5.54	3.03	9.94	4.50	14.76	.780	.238	---	---	3.51	-----
0	437	301	1200	667	.46	6.86	5.54	3.56	11.68	5.29	17.35	.675	.206	---	---	3.57	-----
0	516	356	1225	681	.46	6.86	5.54	4.07	13.35	6.05	19.84	.612	.187	---	---	3.70	-----
0	604	416	1250	694	.45	6.86	5.54	4.61	15.12	6.88	22.57	.529	.161	.905	.276	3.64	6.22
a ₂	454	313	1020	567	---	6.86	---	4.61	15.12	-----	-----	.275	.084	.575	.175	-----	-----
a ₄	454	313	1025	569	---	6.86	---	4.54	14.89	-----	-----	.183	.056	.384	.117	-----	-----
a ₆	458	316	1025	569	---	6.86	---	4.56	14.96	-----	-----	.183	.056	.384	.117	-----	-----
a ₈	458	316	1035	575	---	6.86	---	4.49	14.73	-----	-----	.210	.064	.445	.136	-----	-----
b ₂	452	312	1020	567	---	6.86	---	4.61	15.12	-----	-----	.800	.244	---	---	-----	-----
b ₄	475	328	1050	583	---	6.86	---	4.46	14.63	-----	-----	---	---	---	---	-----	-----
b ₆	475	328	1030	572	---	6.86	---	4.61	15.12	-----	-----	---	---	---	---	-----	-----
b ₈	452	312	1020	567	---	6.86	---	4.61	15.12	-----	-----	---	---	---	---	-----	-----
Nose B, $r_n = 0.15$ in. (0.38 cm)																	
0	197	136×10^4	1050	583	0.52	6.82	---	2.01×10^6	6.59×10^6	-----	-----	---	---	---	---	-----	-----
0	294	203	1050	583	.52	6.84	---	2.99	9.81	-----	-----	---	---	---	---	-----	-----
0	369	254	1035	575	.53	6.85	---	3.80	12.46	-----	-----	---	---	---	---	-----	-----
0	424	292	1025	569	.53	6.86	---	4.43	14.53	-----	-----	---	---	---	---	-----	-----
0	516	356	1068	593	.52	6.86	---	5.06	16.60	-----	-----	---	---	---	---	-----	-----
0	608	419	1050	583	.52	6.86	---	6.10	20.01	-----	-----	---	---	---	---	-----	-----
a ₂	614	423	1050	583	---	6.86	---	6.12	20.07	-----	-----	0.600	0.183	---	---	-----	-----
a ₄	608	419	1050	583	---	6.86	---	6.11	20.04	-----	-----	.432	.132	---	---	-----	-----
a ₆	610	421	1050	583	---	6.86	---	6.13	20.11	-----	-----	.244	.074	---	---	-----	-----
a ₈	601	414	1045	581	---	6.86	---	6.08	19.94	-----	-----	.150	.046	---	---	-----	-----
b ₄	606	418	1053	585	---	6.86	---	6.06	19.88	-----	-----	---	---	---	---	-----	-----
b ₈	612	422	1048	582	---	6.86	---	6.17	20.24	-----	-----	---	---	---	---	-----	-----

aLeeward.

bWindward.

TABLE II.- TEST CONDITIONS OF EXPERIMENTAL INVESTIGATION -- Concluded

α , deg	P_t		T_t		T_w/T_t	M_∞	M_L	R_∞		R_L		s_{tr}				$R_{s,tr}$	
	psia	N/m ²	°R	°K				Start		End		ft	m	ft	m	Start	End
								Per foot	Per meter	Per foot	Per meter						
Nose C, $r_n = 0.30$ in. (0.76 cm)																	
0	200	138×10^4	1020	567	0.53	6.82	---	2.13×10^6	6.99×10^6	-----	-----	---	---	---	---	-----	---
0	288	199	1060	589	.52	6.84	---	2.88	9.45	-----	-----	---	---	---	---	-----	---
0	363	250	1050	583	.52	6.85	---	3.67	12.04	-----	-----	---	---	---	---	-----	---
0	435	300	1055	586	.52	6.86	---	4.36	14.30	-----	-----	---	---	---	---	-----	---
0	520	359	1080	600	.52	6.86	---	4.98	16.33	-----	-----	---	---	---	---	-----	---
0	606	418	1050	583	.52	6.86	---	6.08	19.94	-----	-----	---	---	---	---	-----	---
Nose D, $r_n = 0.60$ in. (1.52 cm)																	
0	197	136×10^4	1020	567	0.53	6.82	---	2.10×10^6	6.89×10^6	-----	-----	---	---	---	---	-----	---
0	280	193	1055	586	.52	6.84	---	2.81	9.22	-----	-----	---	---	---	---	-----	---
0	365	252	1035	575	.53	6.85	---	3.77	12.37	-----	-----	---	---	---	---	-----	---
0	436	301	1045	581	.53	6.86	---	4.44	14.56	-----	-----	---	---	---	---	-----	---
0	508	350	1040	578	.53	6.86	---	5.18	16.99	-----	-----	---	---	---	---	-----	---
0	604	416	1035	575	.53	6.86	---	6.21	20.37	-----	-----	---	---	---	---	-----	---
a ₂	616	425	1060	589	---	6.86	---	6.09	19.98	-----	-----	---	---	---	---	-----	---
a ₄	604	416	1050	583	---	6.86	---	6.07	19.91	-----	-----	0.700	0.213	---	---	-----	---
a ₆	603	416	1050	583	---	6.86	---	6.06	19.88	-----	-----	.553	.169	---	---	-----	---
a ₈	602	415	1050	583	---	6.86	---	6.06	19.88	-----	-----	.430	.131	---	---	-----	---
b ₄	608	419	1053	585	---	6.86	---	6.08	19.94	-----	-----	---	---	---	---	-----	---
b ₈	604	416	1032	573	---	6.86	---	6.26	20.53	-----	-----	---	---	---	---	-----	---
Ablation model (sharp tip)																	
0	222	153×10^4	1263	702	0.46	6.82	5.52	1.68×10^6	5.51×10^6	2.47×10^6	8.10×10^6	0.689	0.210	---	---	1.70×10^6	---
0	337	233	1280	711	.47	6.85	5.54	2.42	7.94	3.56	11.67	.576	.176	---	---	2.05	---
0	446	308	1265	703	.46	6.86	5.54	3.28	10.76	4.87	15.97	.482	.147	---	---	2.35	---
0	580	400	1280	711	.46	6.86	5.54	4.16	13.64	6.14	20.14	.417	.127	---	---	2.56	---

^aLeeward.

^bWindward.

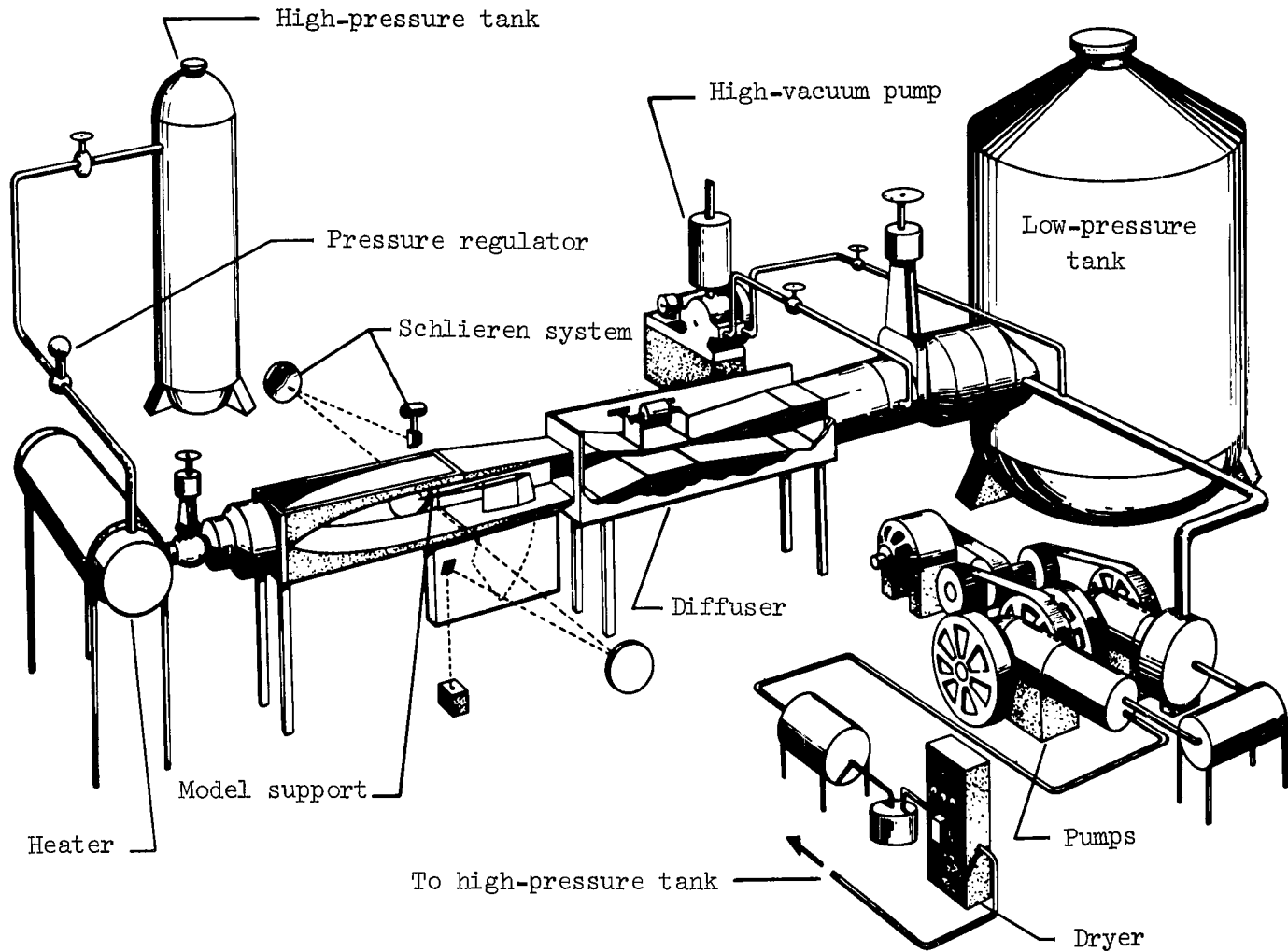


Figure 1.- Schematic of Langley 11-inch hypersonic tunnel.

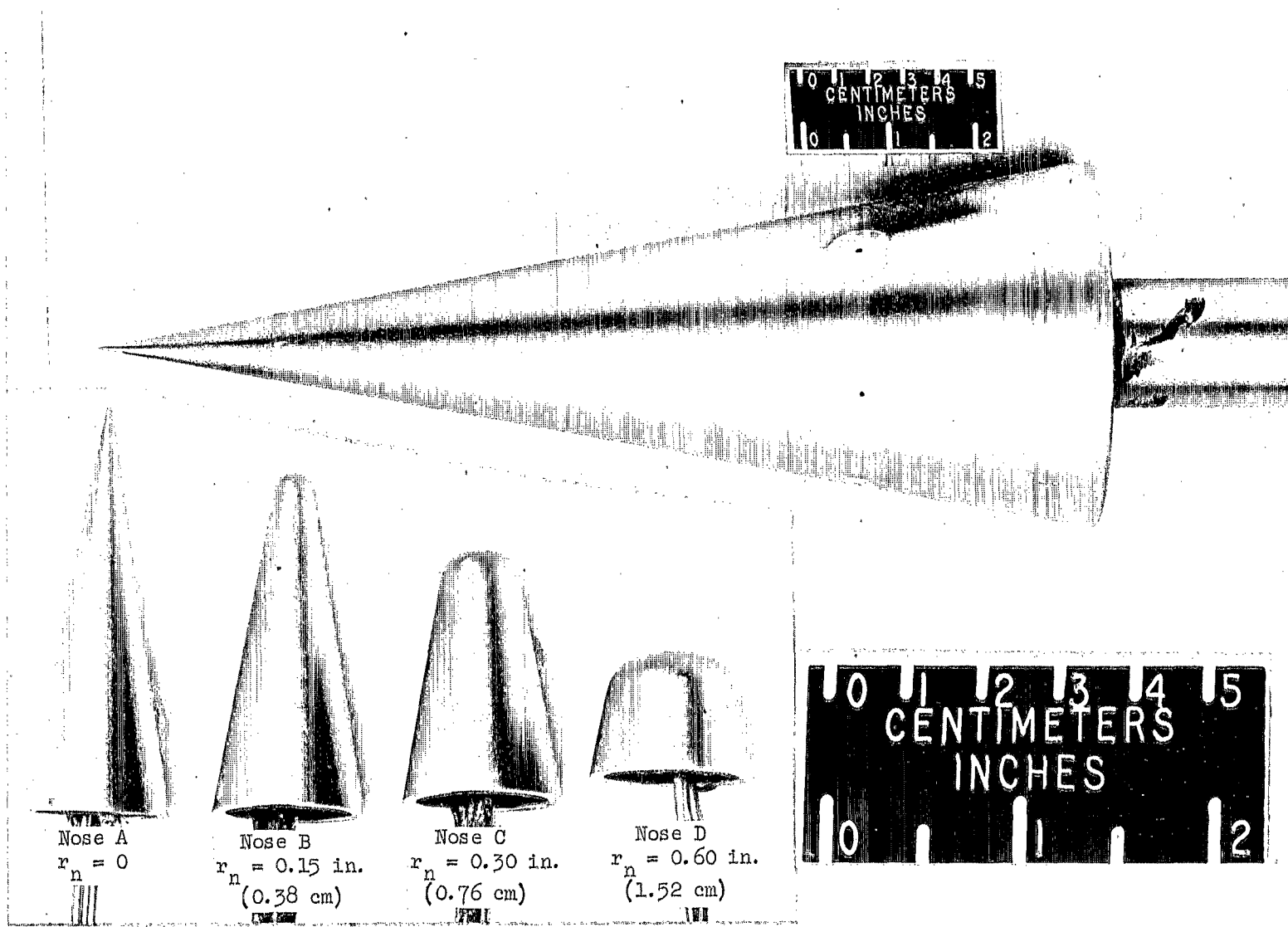
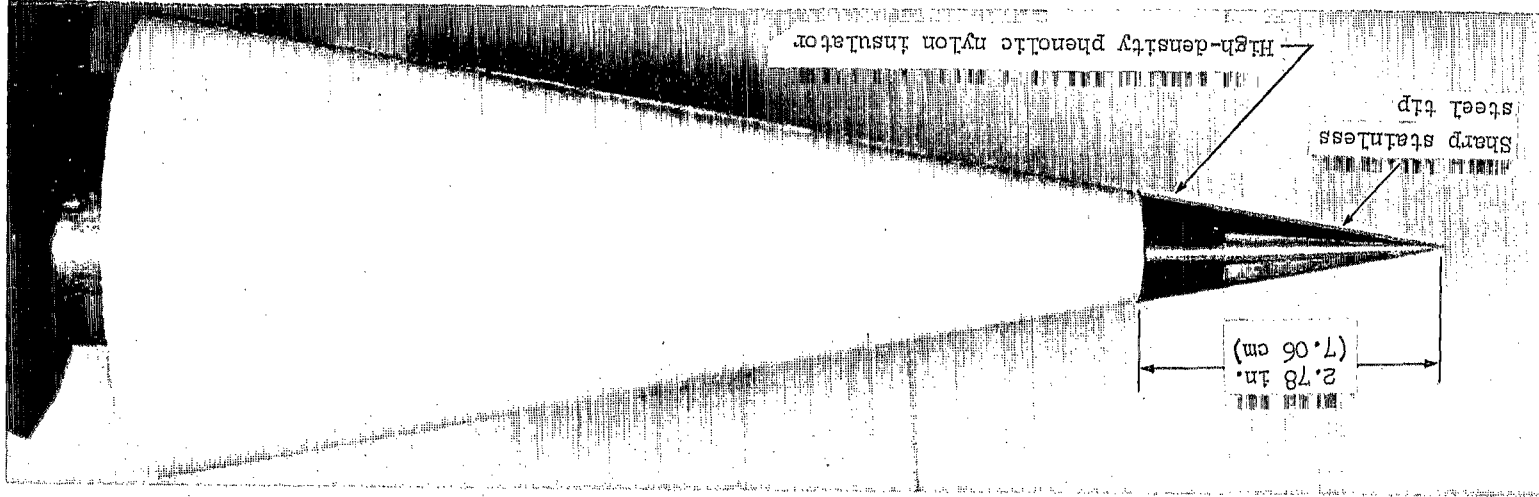


Figure 2.- Photograph of model and nose tips.

L-70-1540



Weight \approx 5.0 lbm (2.3 kg)

Base diameter \approx 4.2 in. (10.8 cm)

Half angle = 10°

Length \approx 12.0 in. (30.5 cm)

L-70-1541

Figure 3.- Typical ablation model.

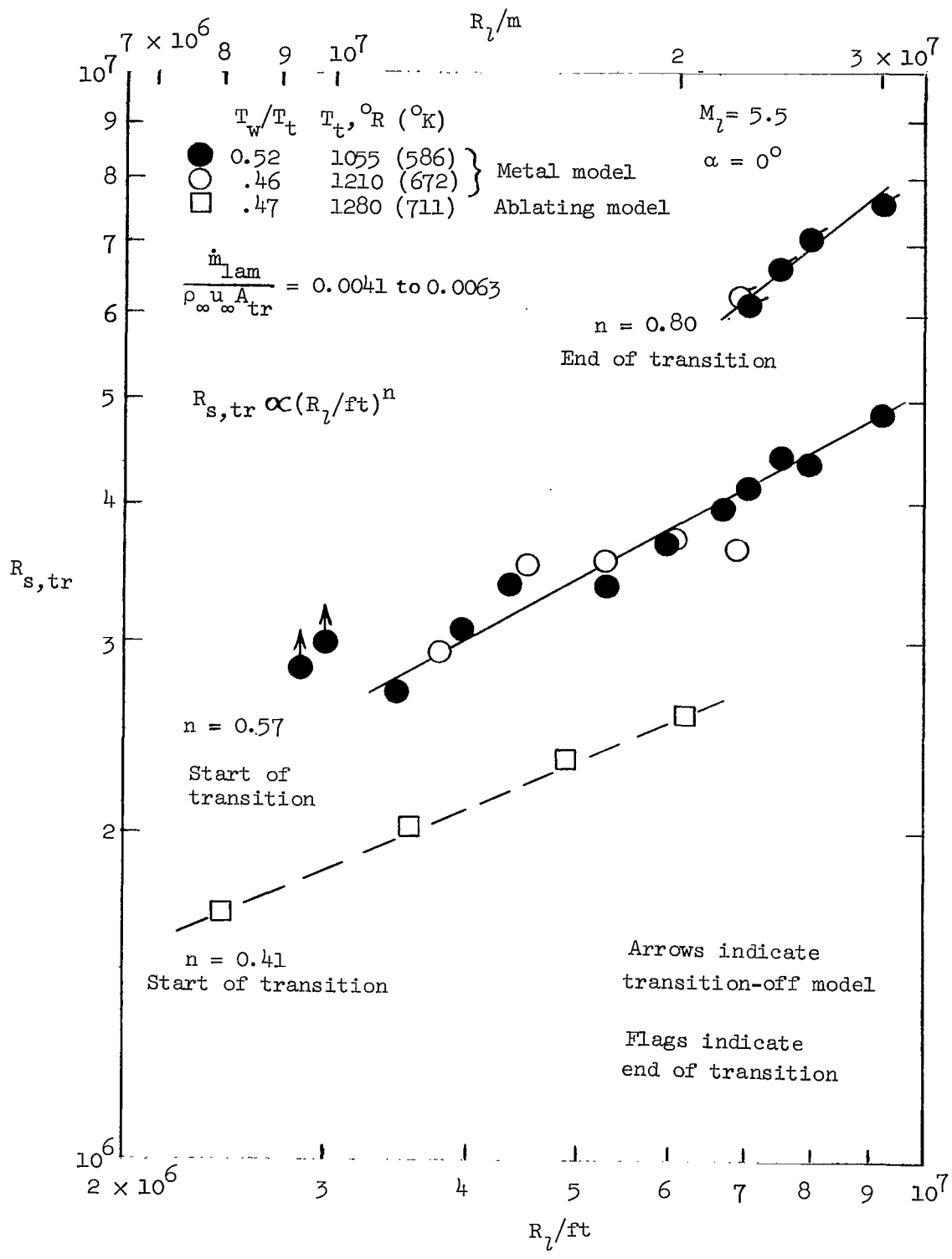


Figure 4.- Effect of mass addition and local unit Reynolds number on transition Reynolds number. $\alpha = 0^\circ$.

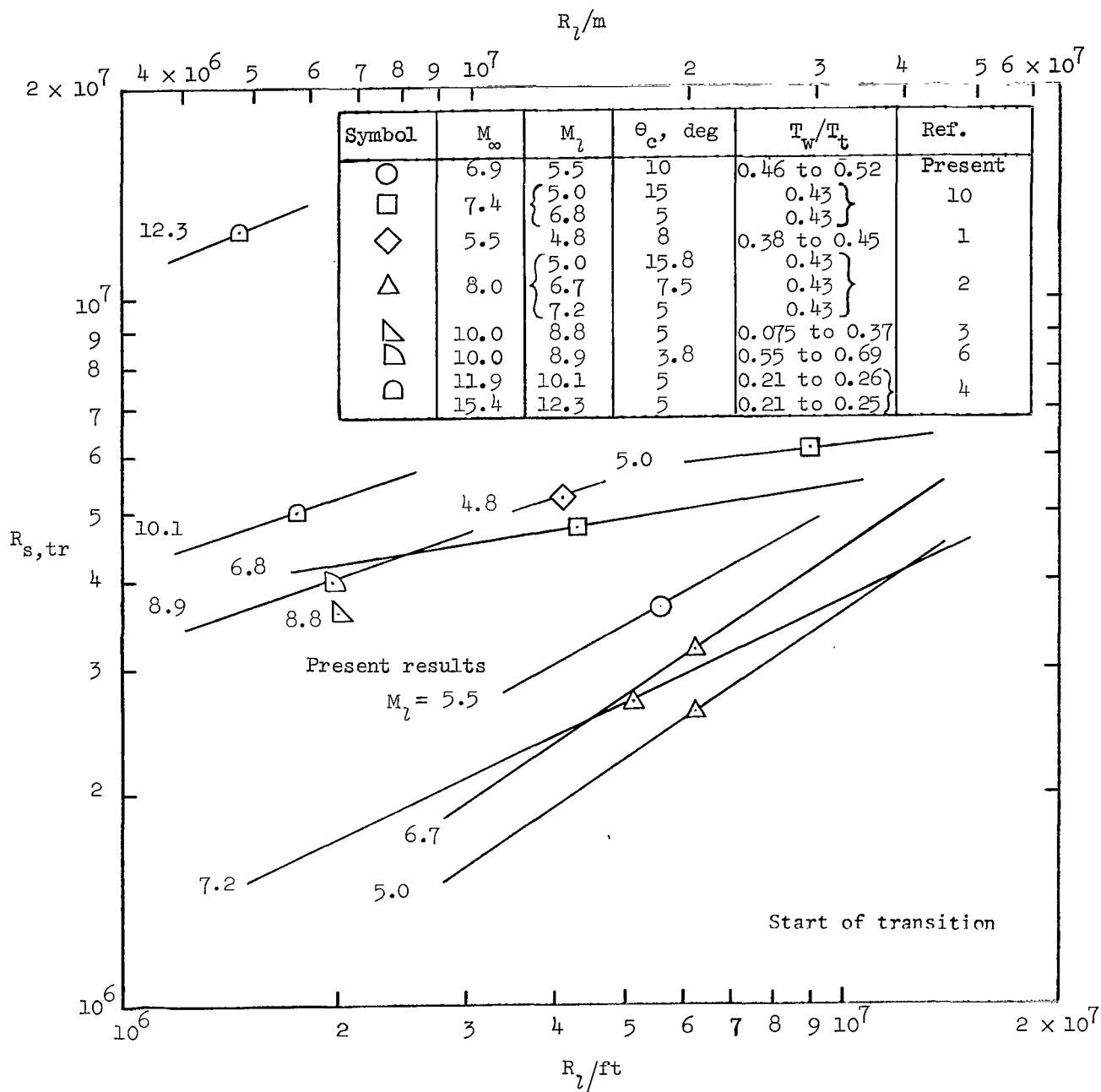


Figure 5.- Effect of local unit Reynolds number on transition Reynolds number for slender sharp cones from various facilities.

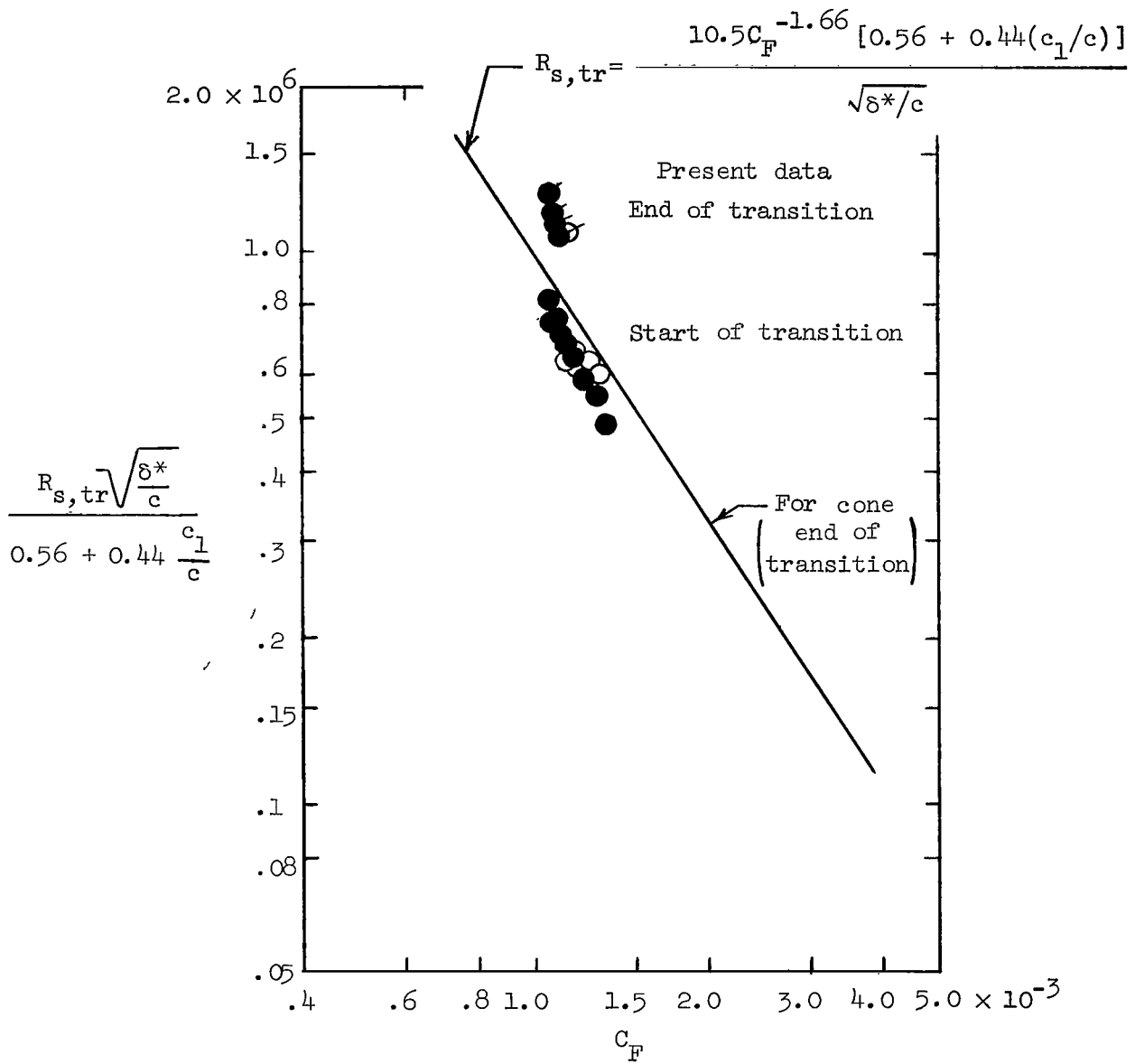


Figure 6.- Comparison of present results with Pate and Schueler's correlation.

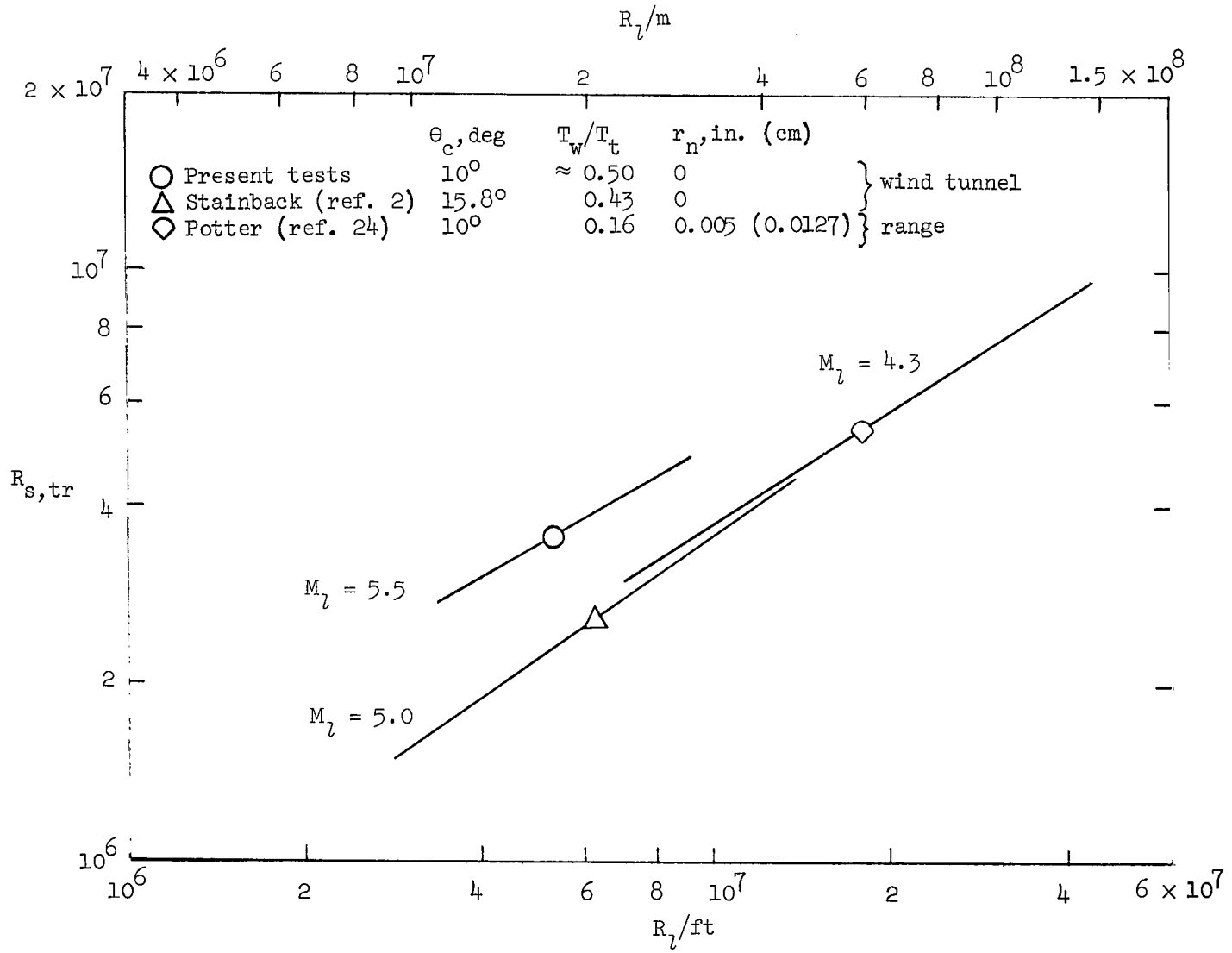
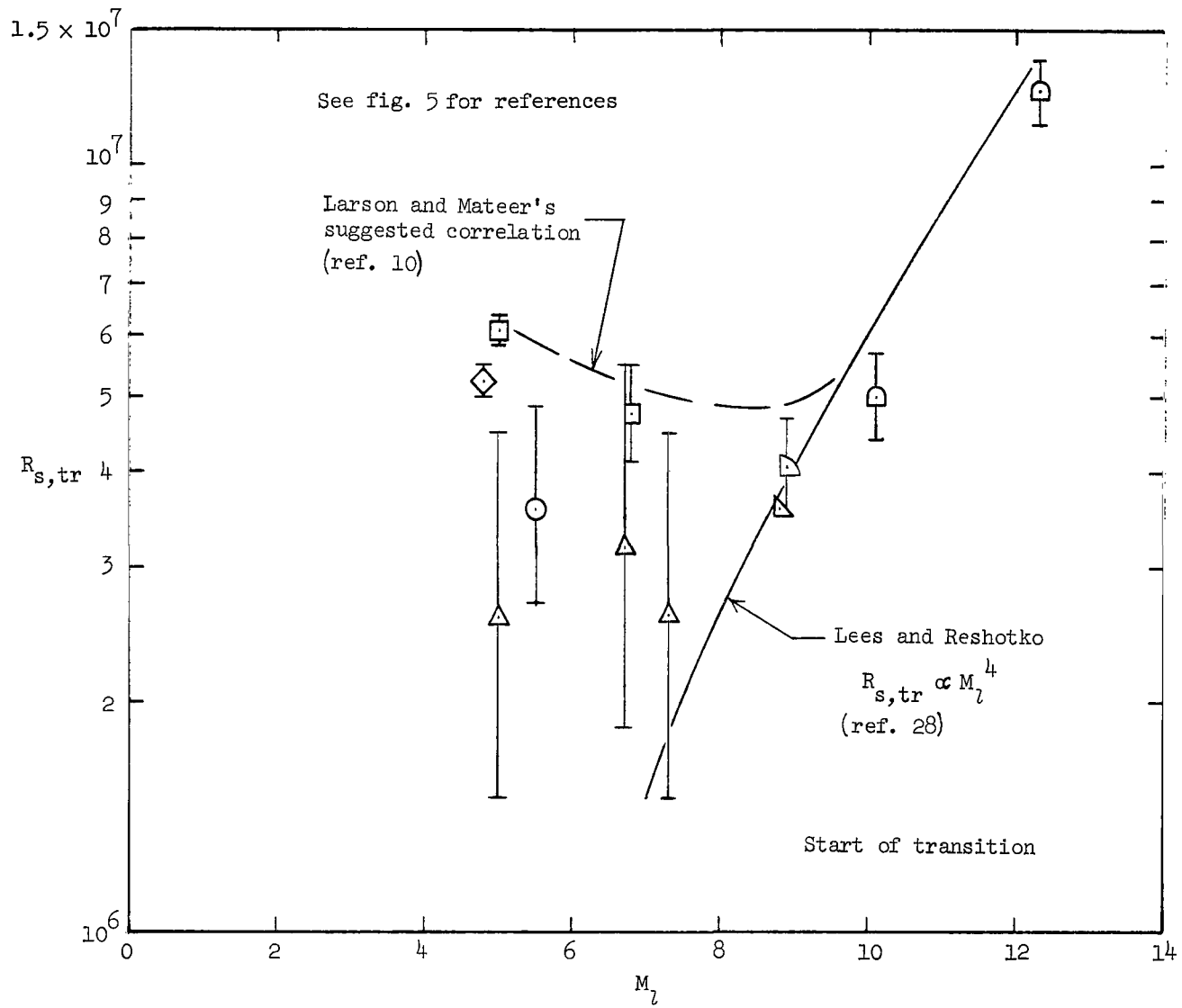
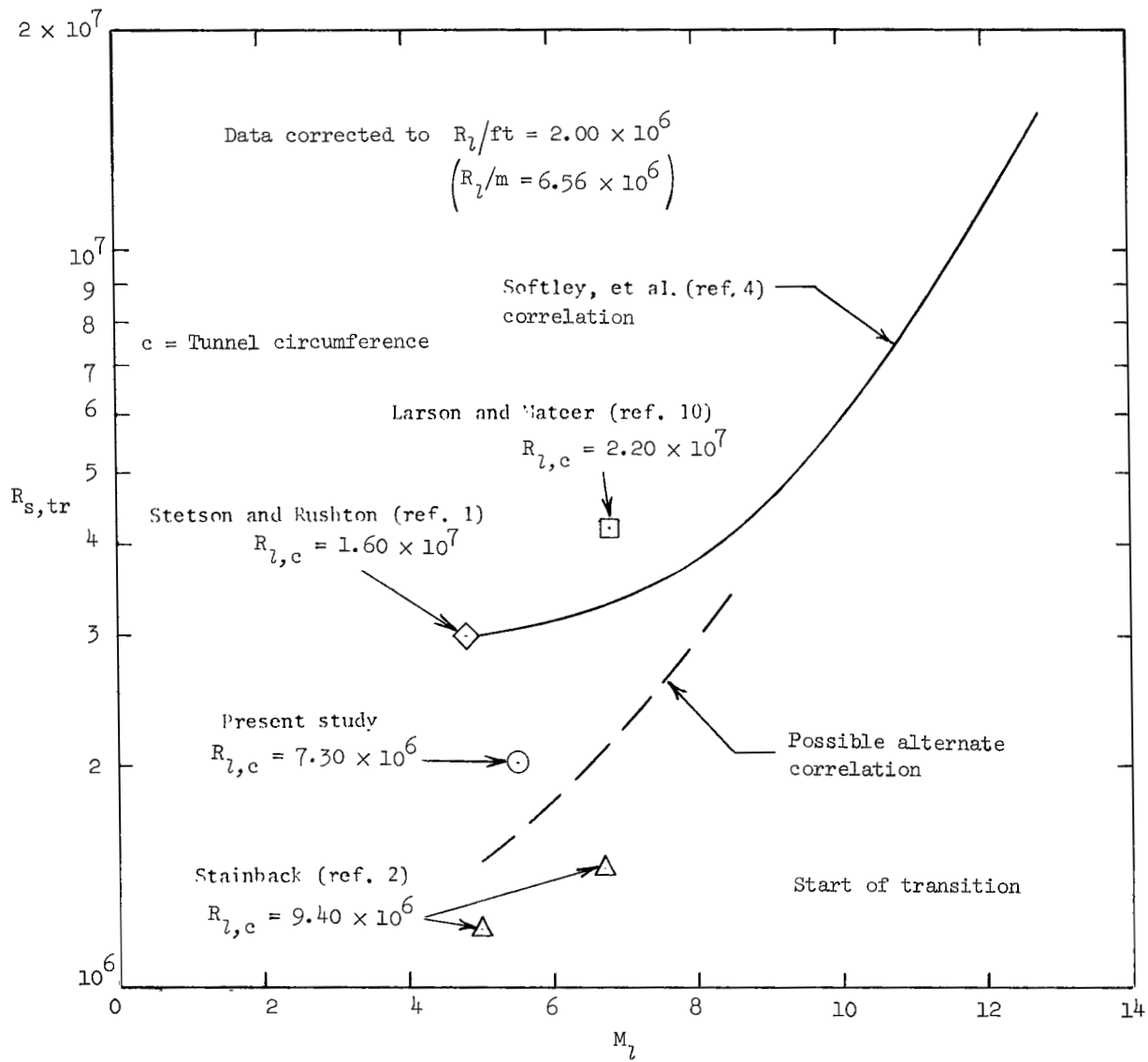


Figure 7.- Comparison of tunnel and ballistic-range transition data.



(a) Variable local unit Reynolds number.

Figure 8.- Effect of local Mach number on transition Reynolds number for slender sharp cones from various facilities.



(b) $R_L/ft = 2.00 \times 10^6$ ($R_L/m = 6.56 \times 10^6$).

Figure 8.- Concluded.

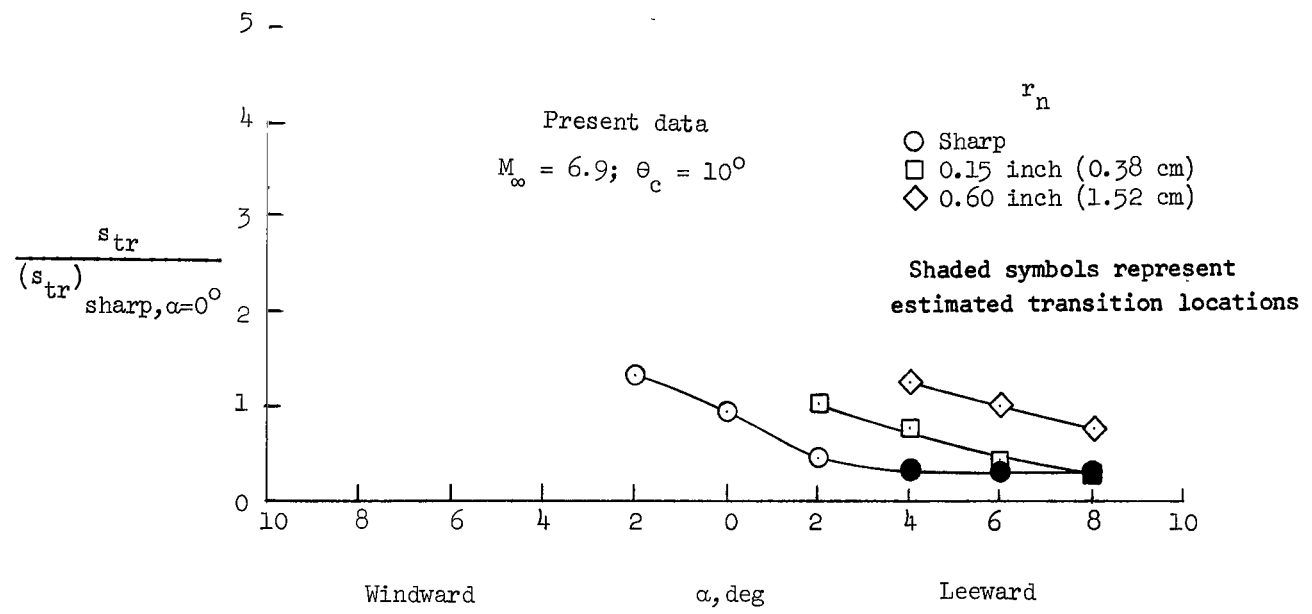
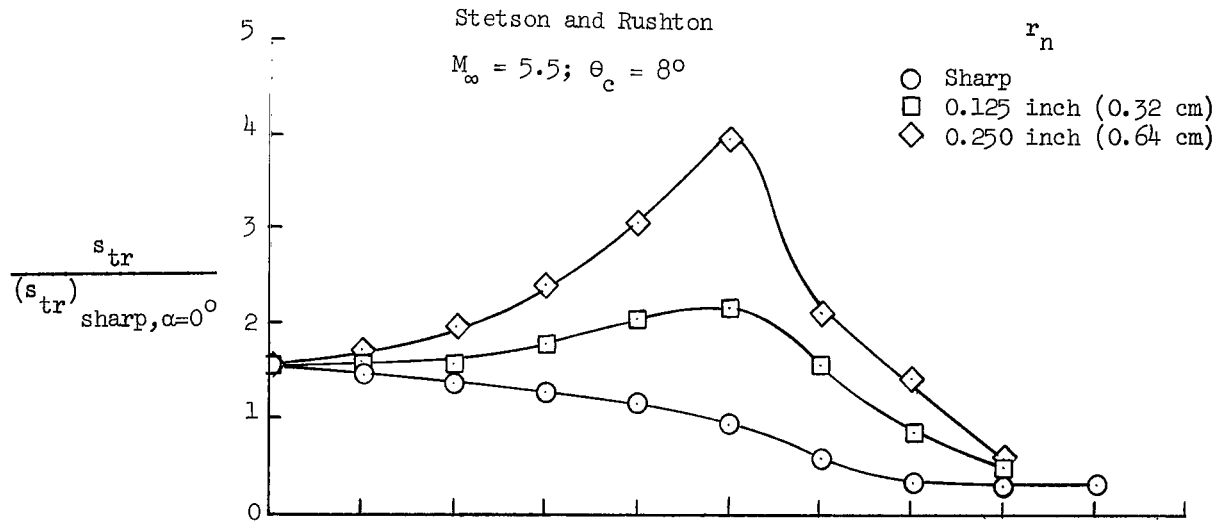
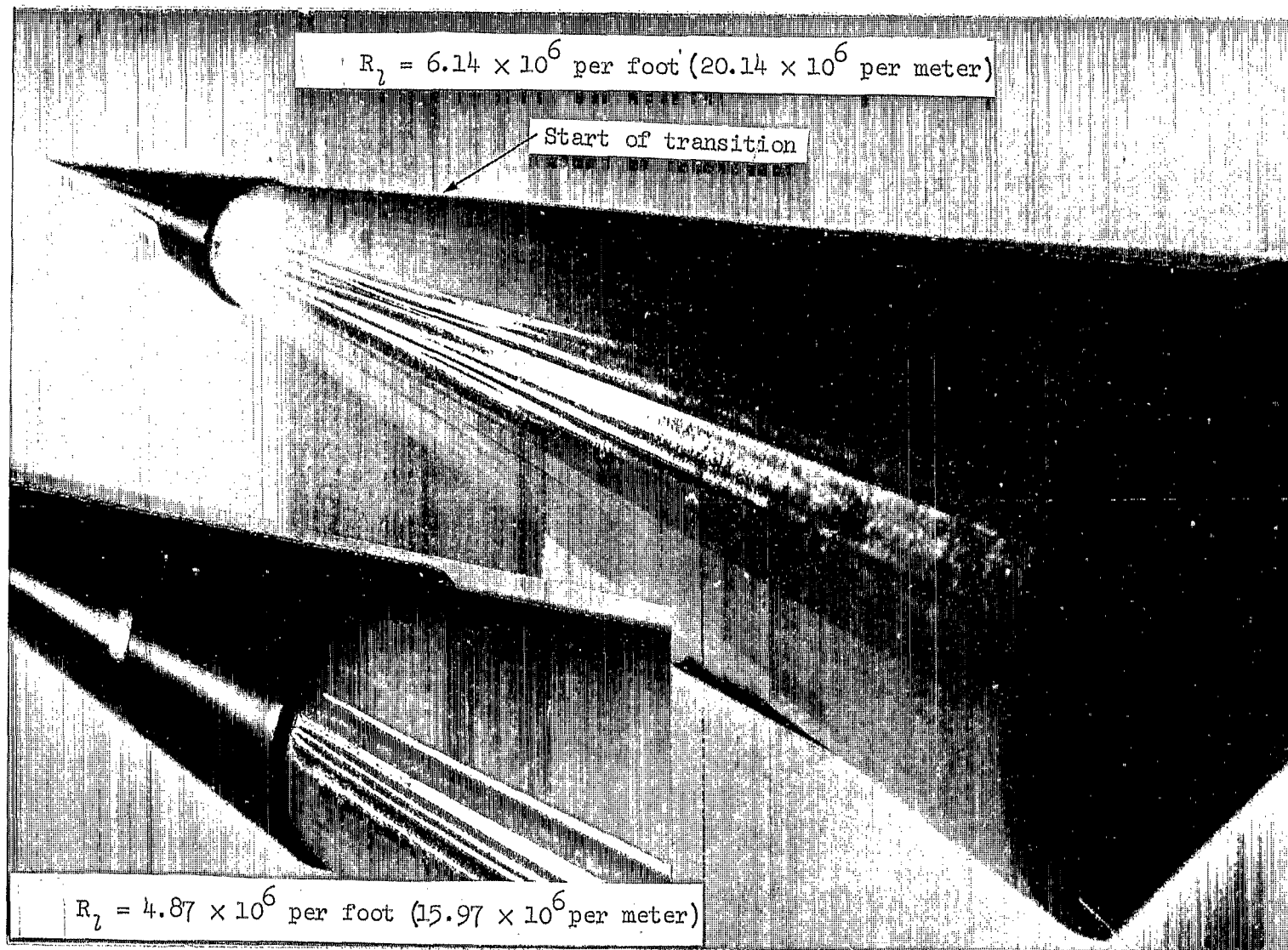


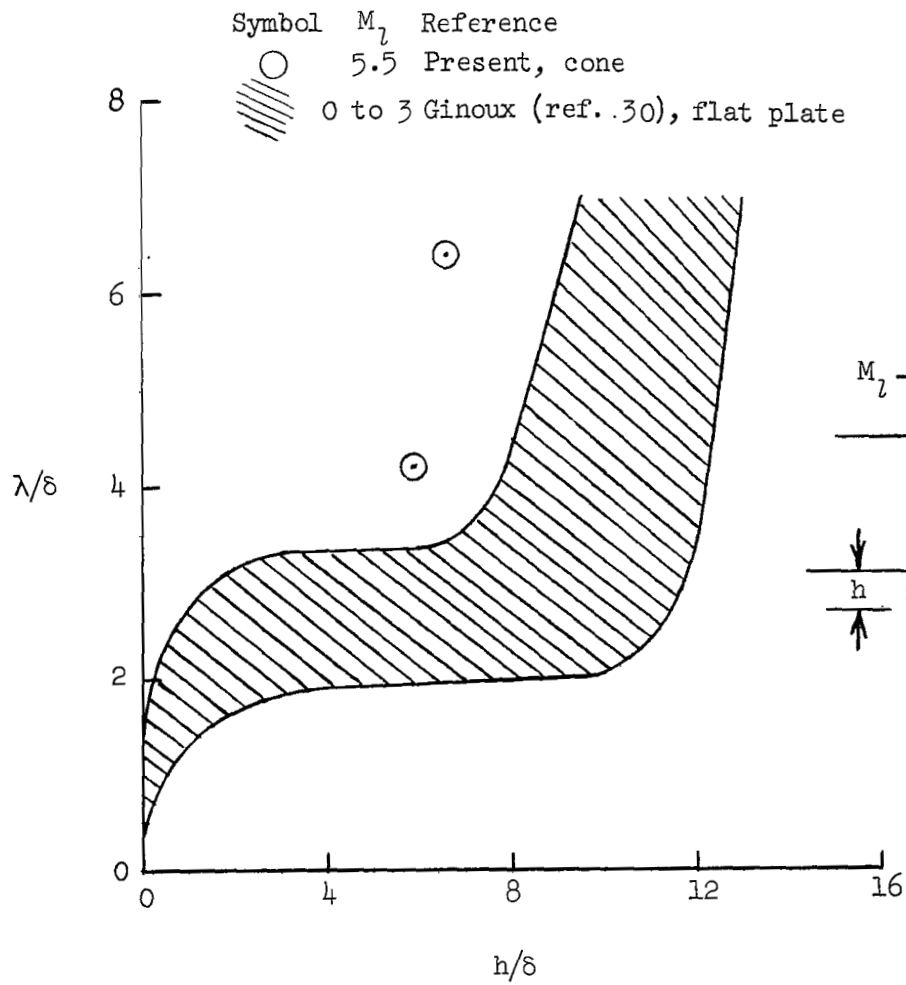
Figure 9.- Boundary-layer transition on sharp and blunt cones at angle of attack.



(a) Grooves observed on ablated models.

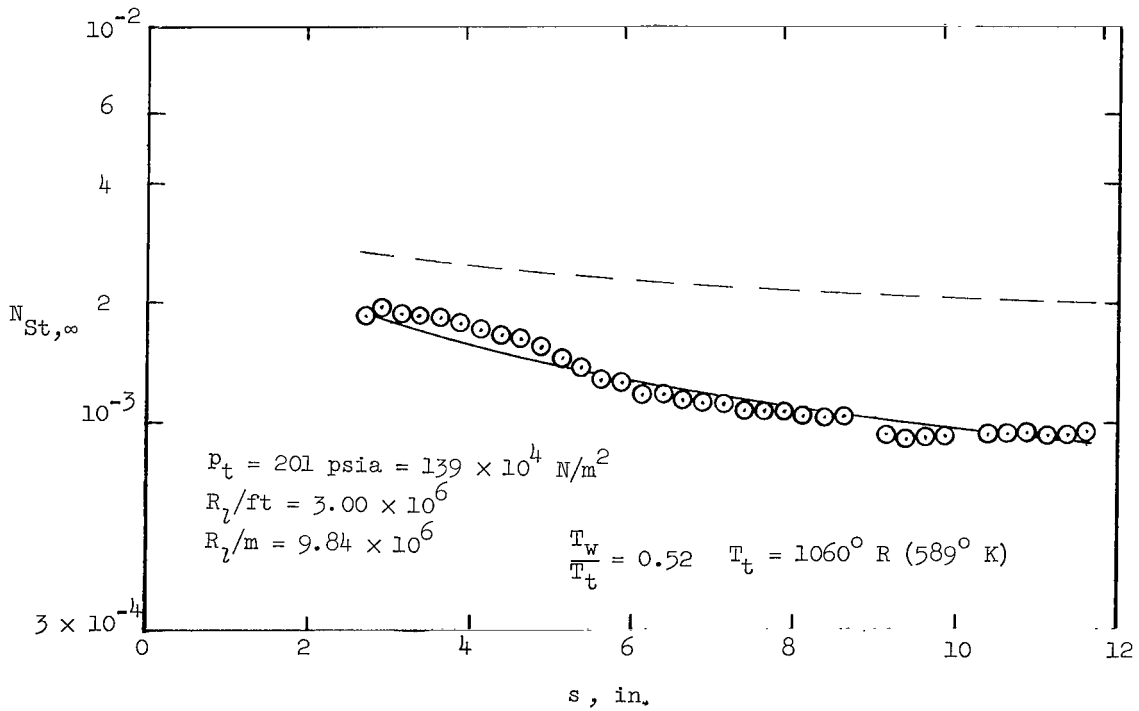
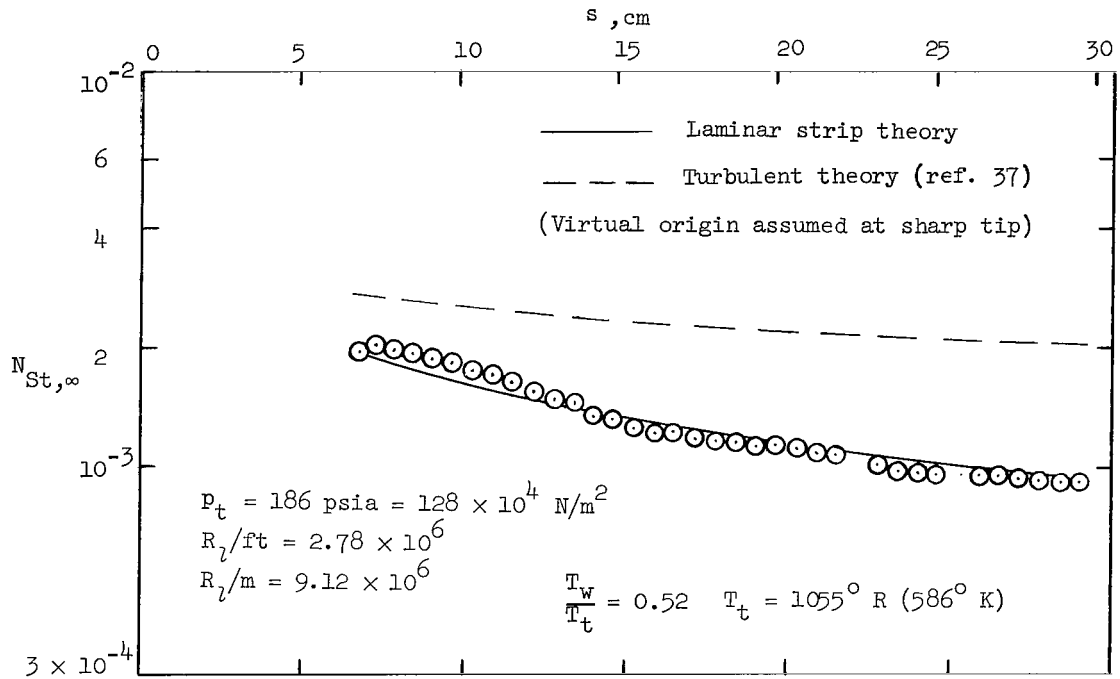
Figure 10.- Longitudinal grooves formed by vortices.

L-70-1542



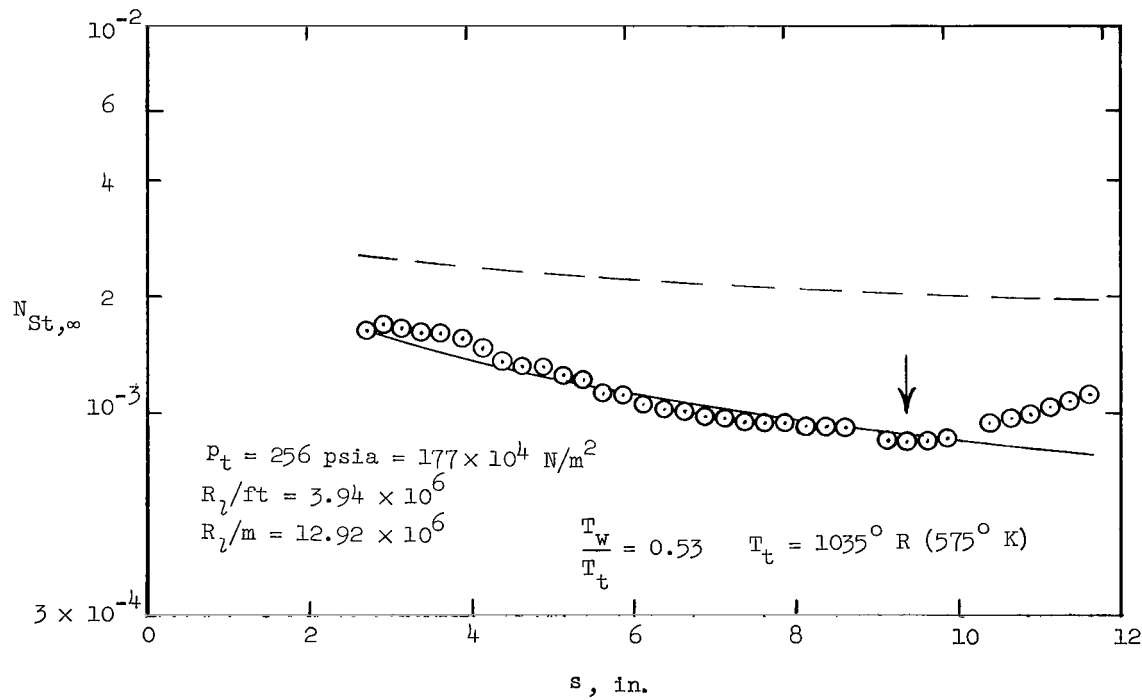
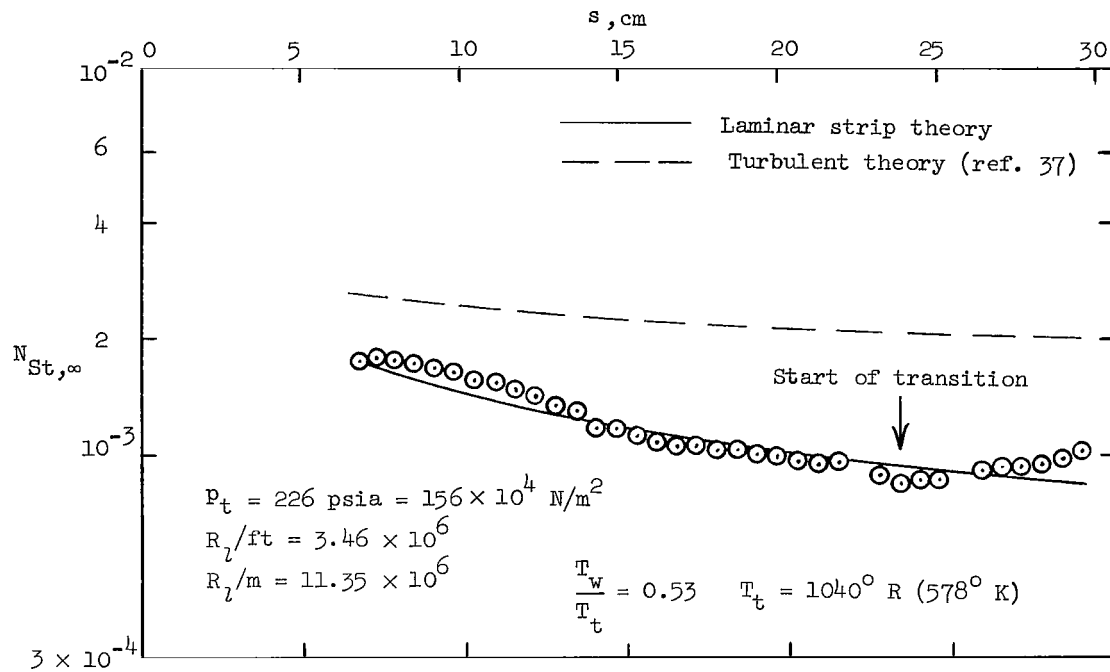
(b) Spacing of adjacent vortices.

Figure 10.- Concluded.



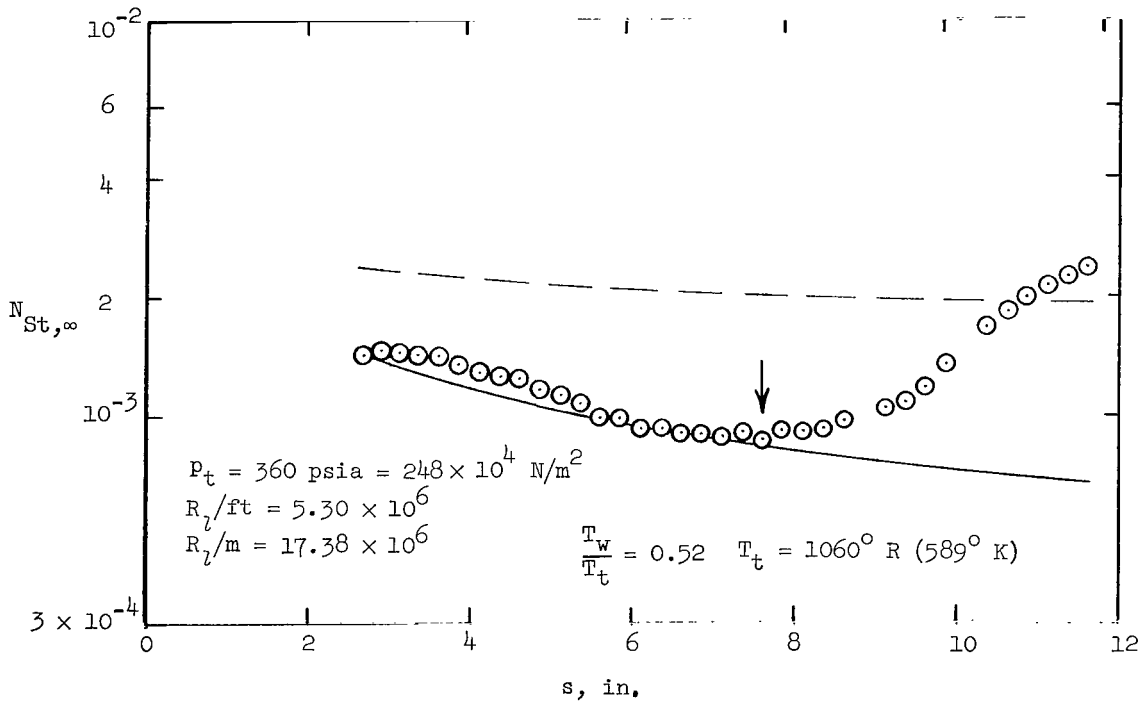
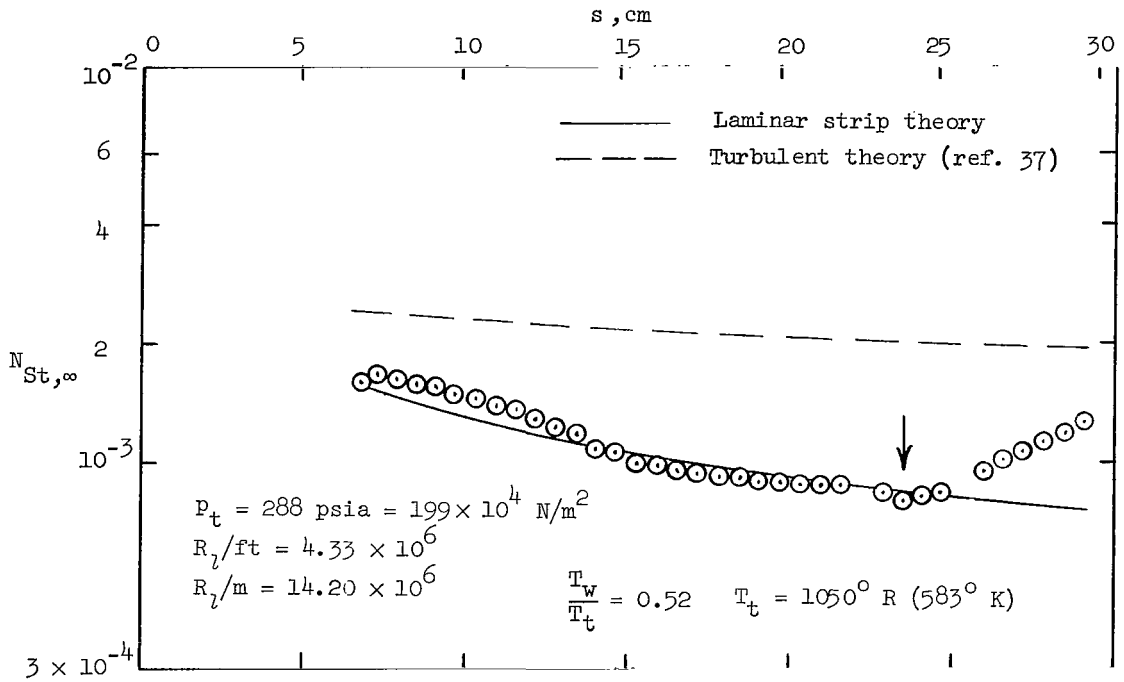
(a) $R_l/ft = 2.78 \times 10^6$ to 3.00×10^6 ($R_l/m = 9.12 \times 10^6$ to 9.84×10^6).

Figure 11.- Stanton number distributions for sharp-tipped metal cone. $\alpha = 0^\circ$.



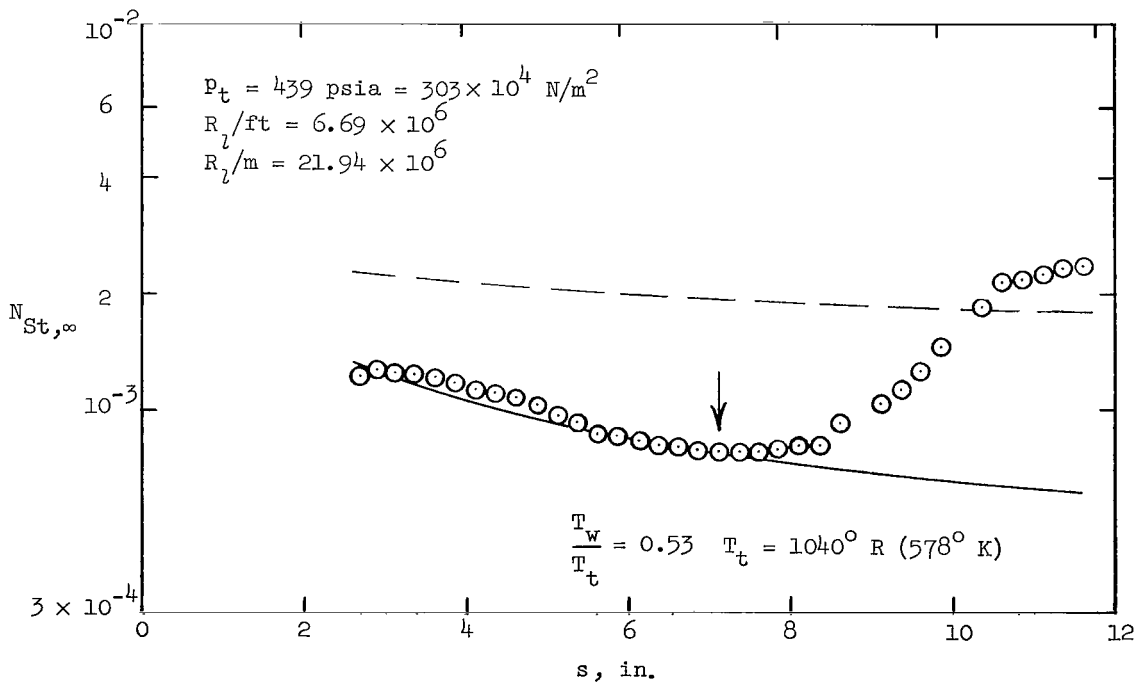
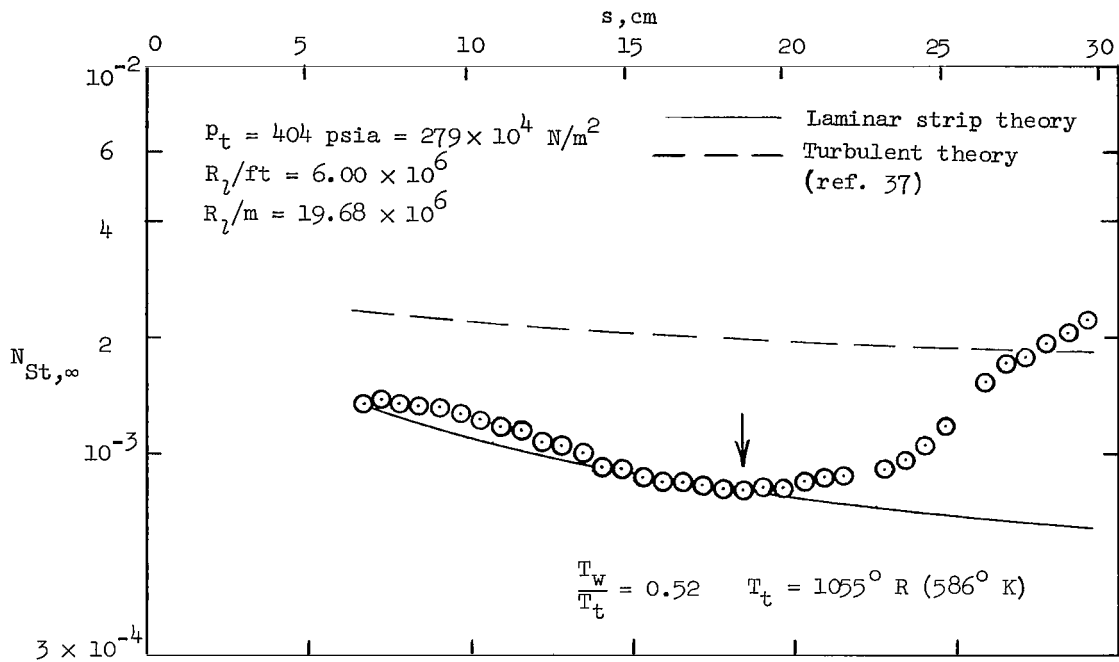
(b) $R_l/\text{ft} = 3.46 \times 10^6$ to 3.94×10^6 ($R_l/\text{m} = 11.35 \times 10^6$ to 12.92×10^6).

Figure 11.- Continued.



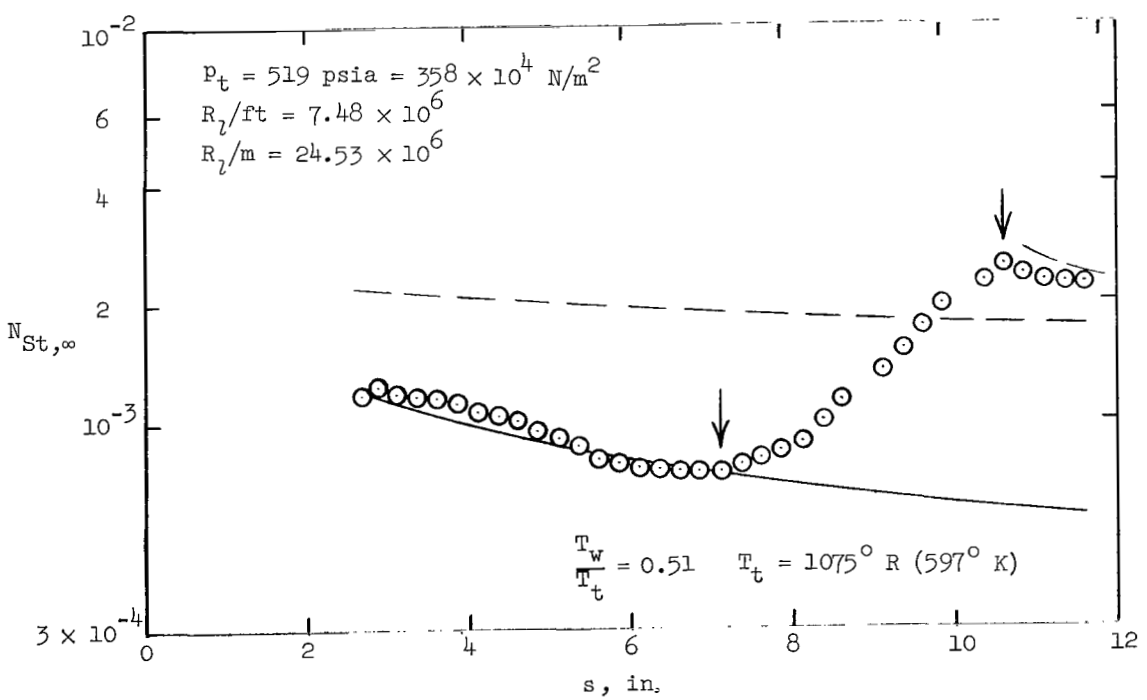
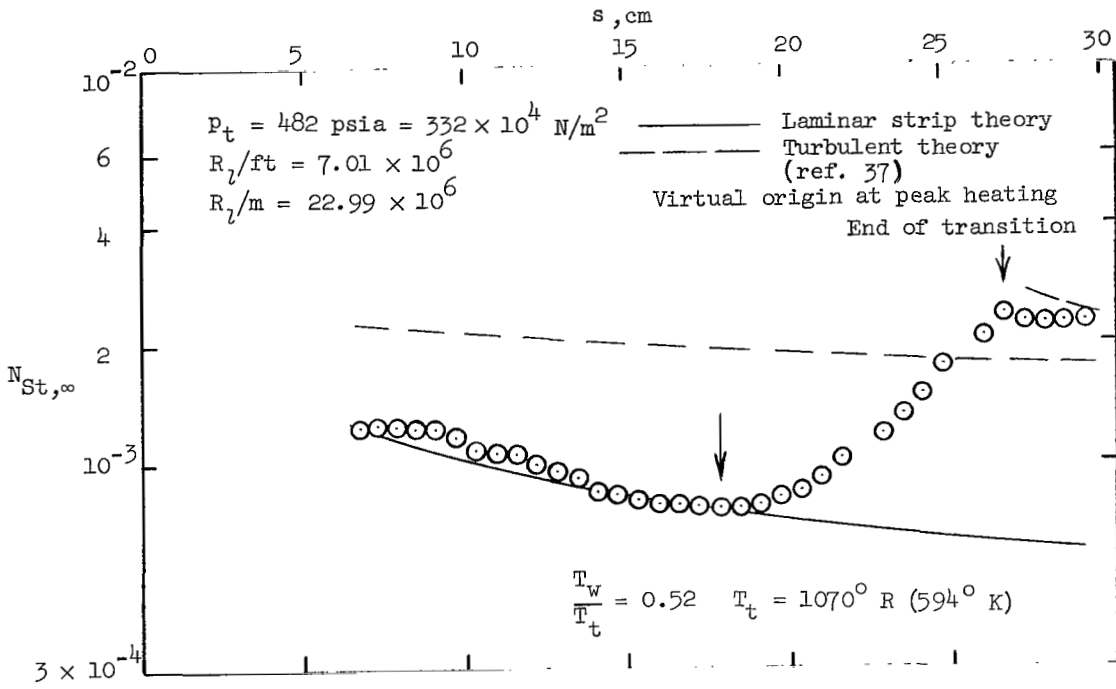
(c) $R_\gamma/\text{ft} = 4.33 \times 10^6$ to 5.30×10^6 ($R_\gamma/\text{m} = 14.20 \times 10^6$ to 17.38×10^6).

Figure 11.- Continued.



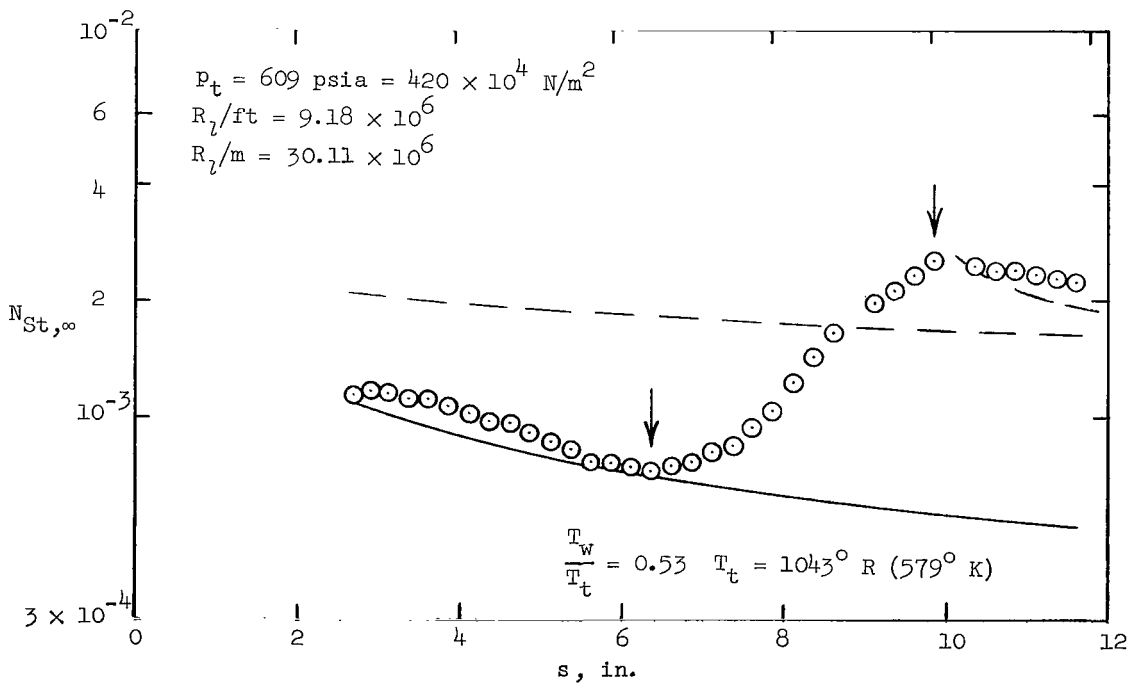
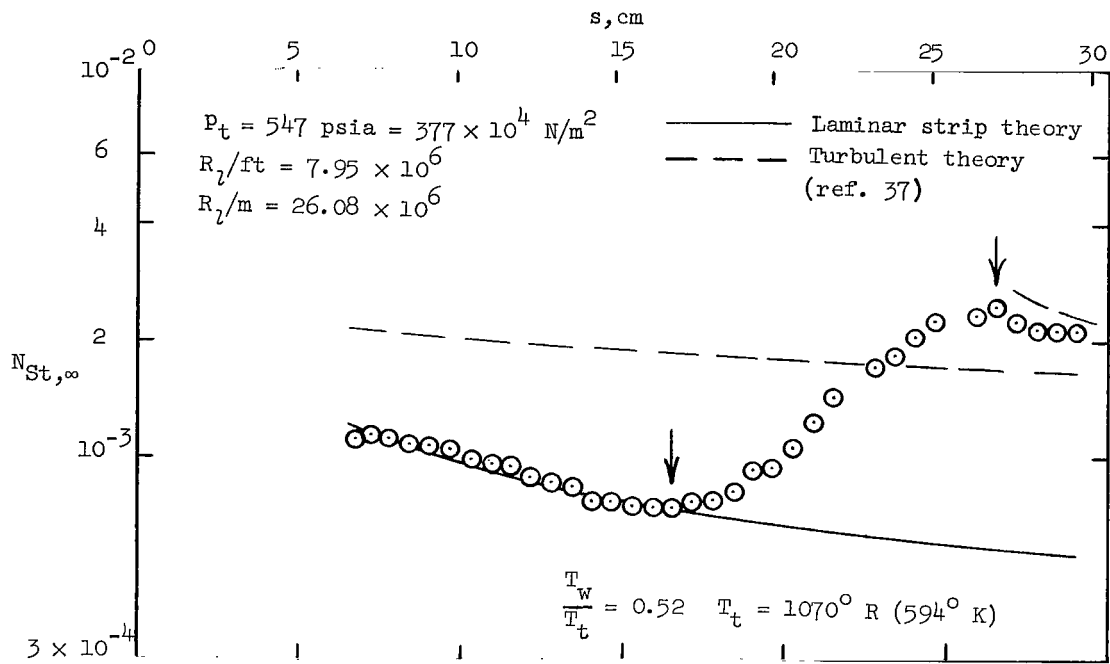
(d) $R_L/ft = 6.00 \times 10^6$ to 6.69×10^6 ($R_L/m = 19.68 \times 10^6$ to 21.94×10^6).

Figure 11.- Continued.



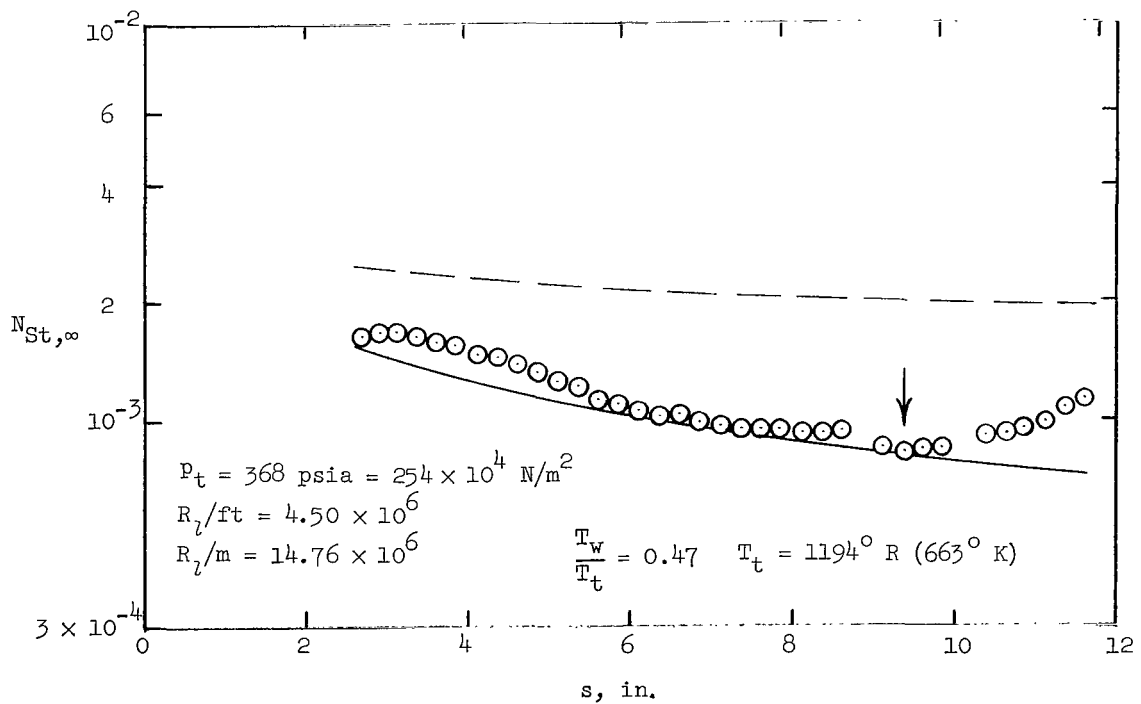
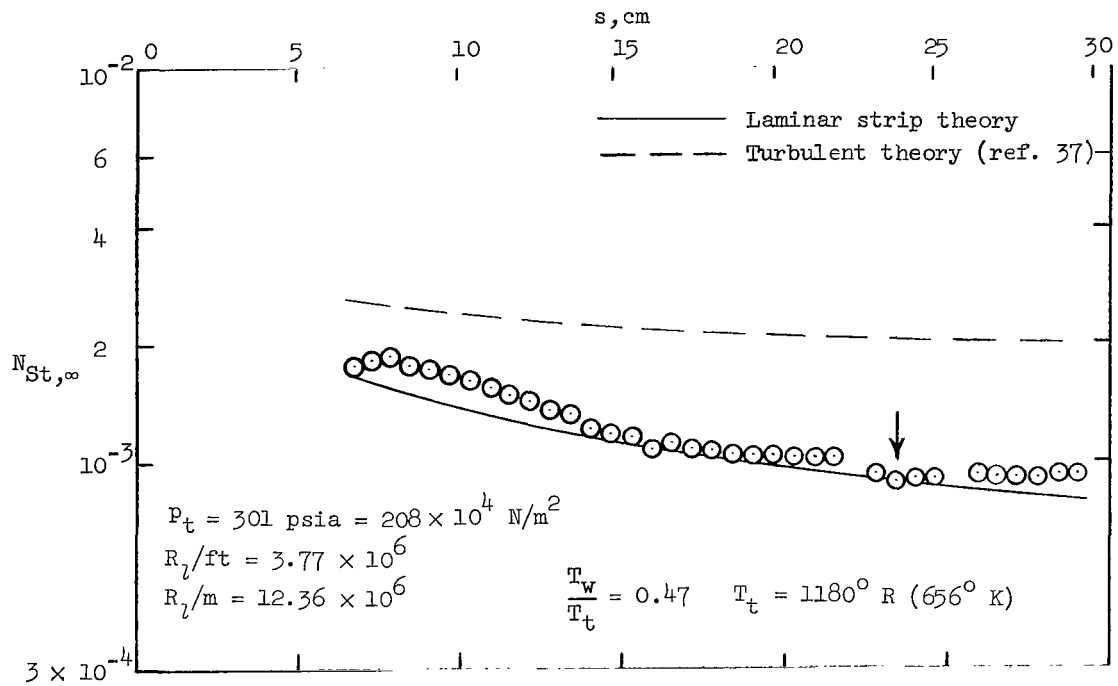
(e) $R_l/ft = 7.01 \times 10^6$ to 7.48×10^6 ($R_l/m = 22.99 \times 10^6$ to 24.53×10^6).

Figure 11.- Continued.



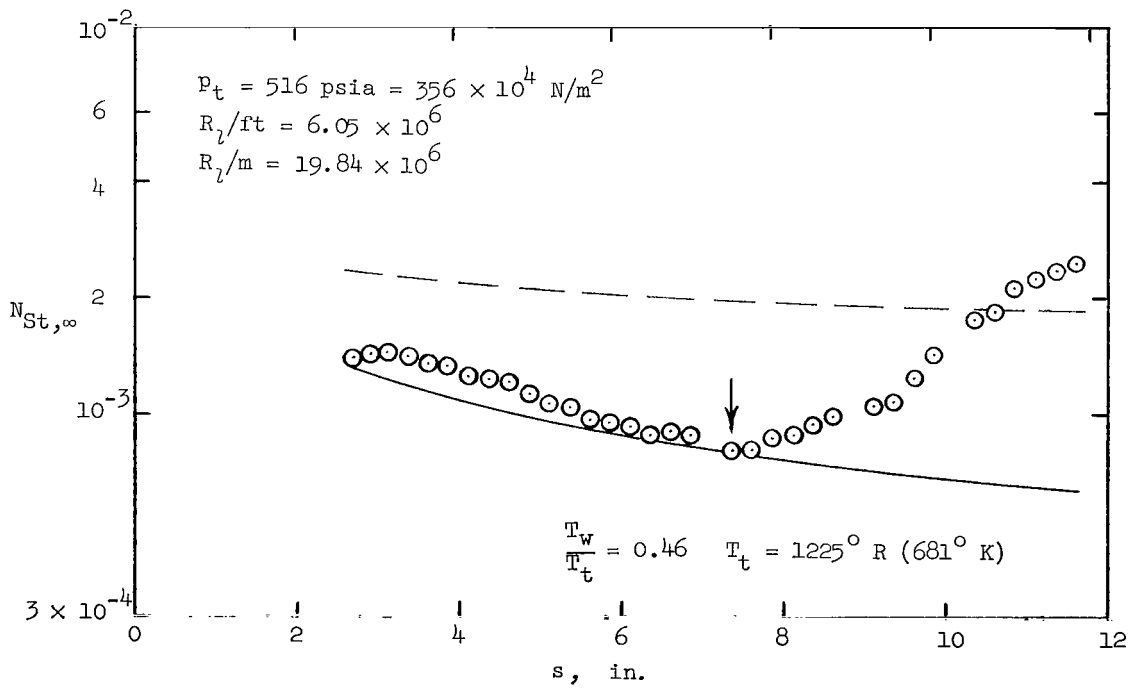
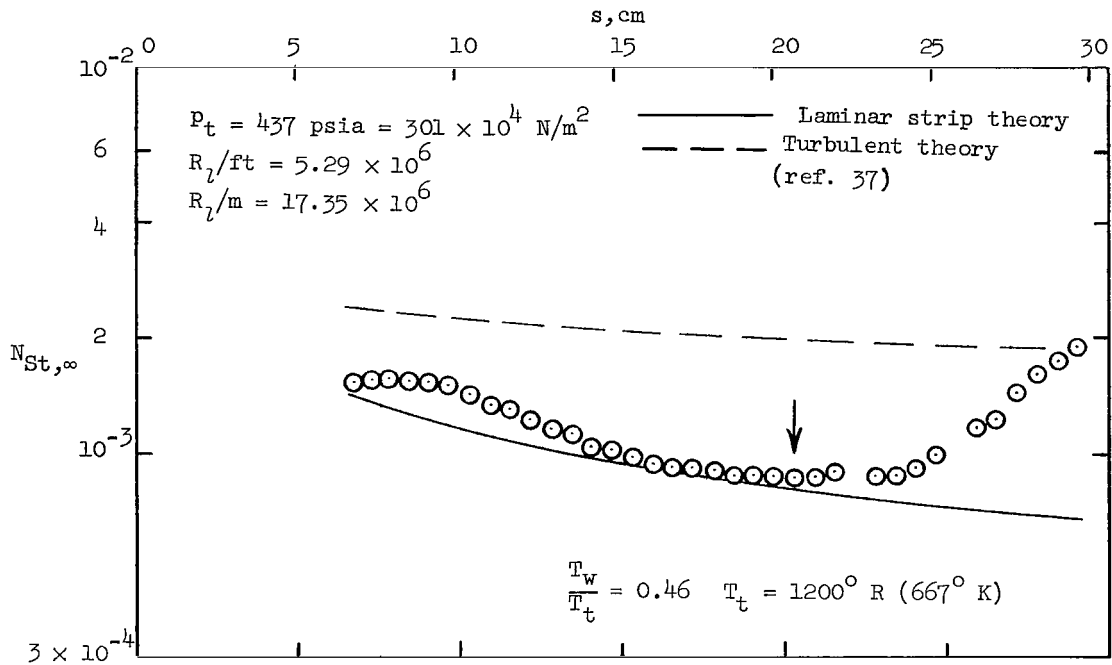
(f) $R_L/ft = 7.95 \times 10^6$ to 9.18×10^6 ($R_L/m = 26.08 \times 10^6$ to 30.11×10^6).

Figure 11.- Continued.



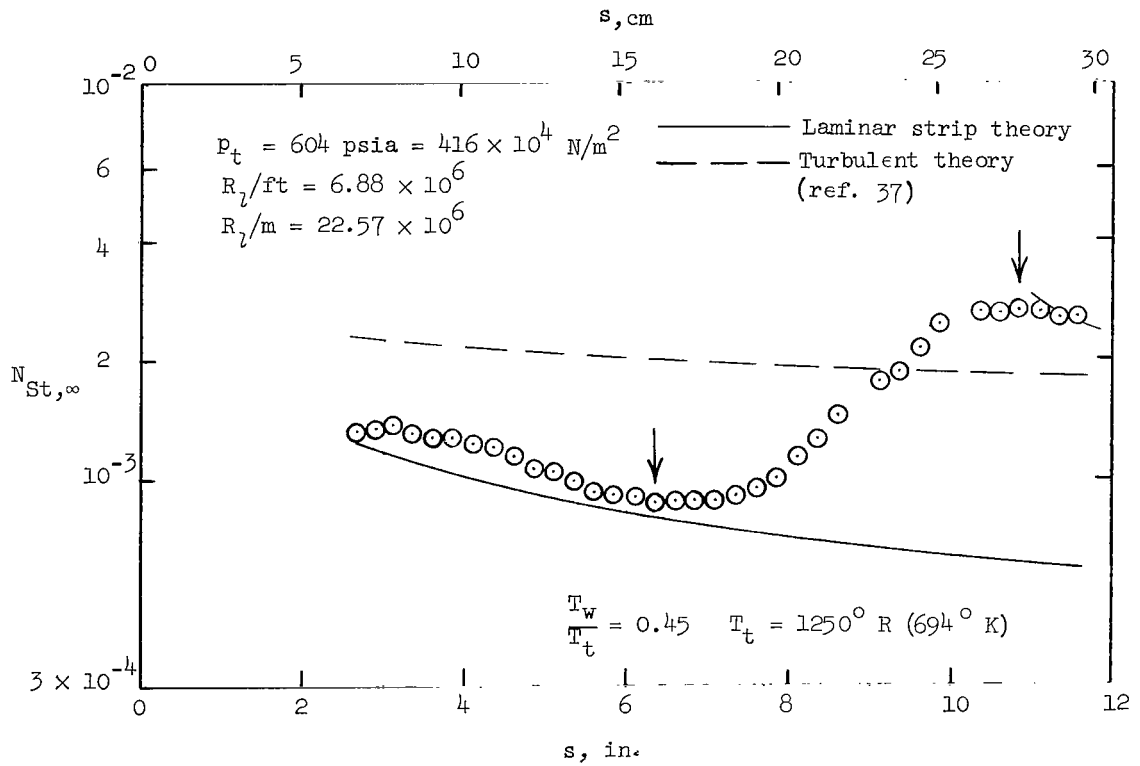
(g) $R_t/\text{ft} = 3.77 \times 10^6$ to 4.50×10^6 ($R_t/\text{m} = 12.36 \times 10^6$ to 14.76×10^6).

Figure 11.- Continued.



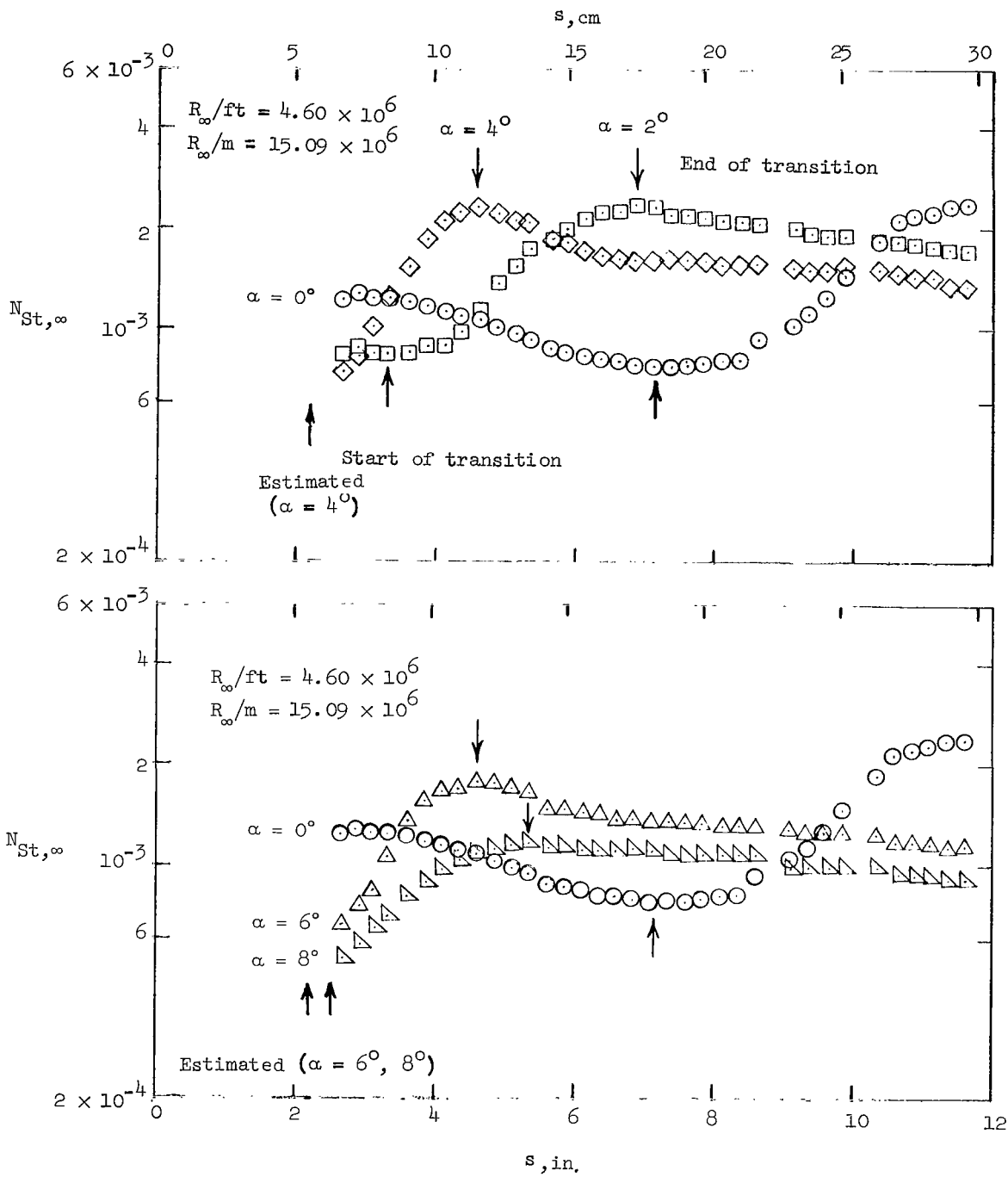
(h) $R_L/ft = 5.29 \times 10^6$ to 6.05×10^6 ($R_L/m = 17.35 \times 10^6$ to 19.84×10^6).

Figure 11.- Continued.



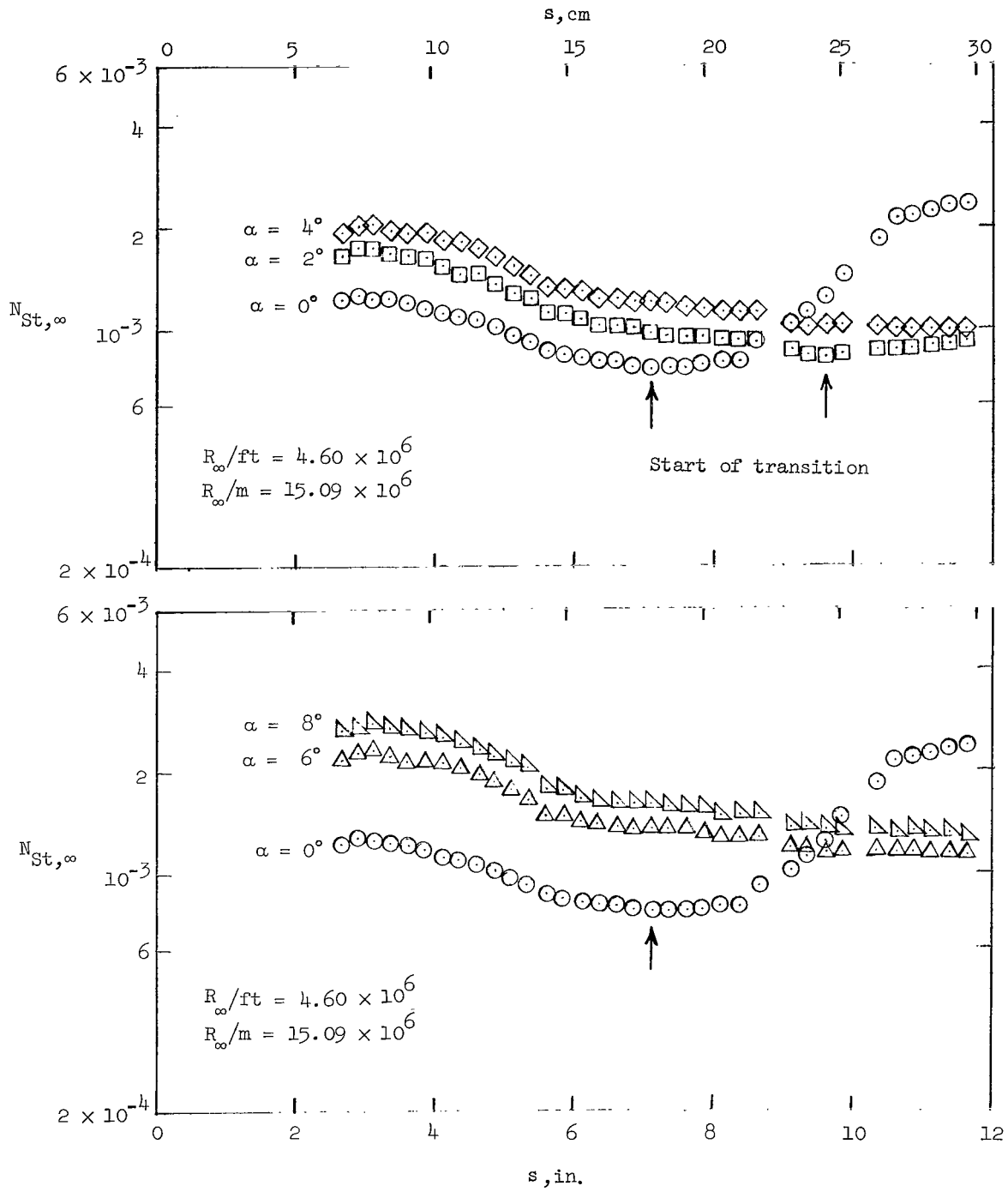
(i) $R_t/ft = 6.88 \times 10^6$ ($R_t/m = 22.57 \times 10^6$).

Figure 11.- Concluded.



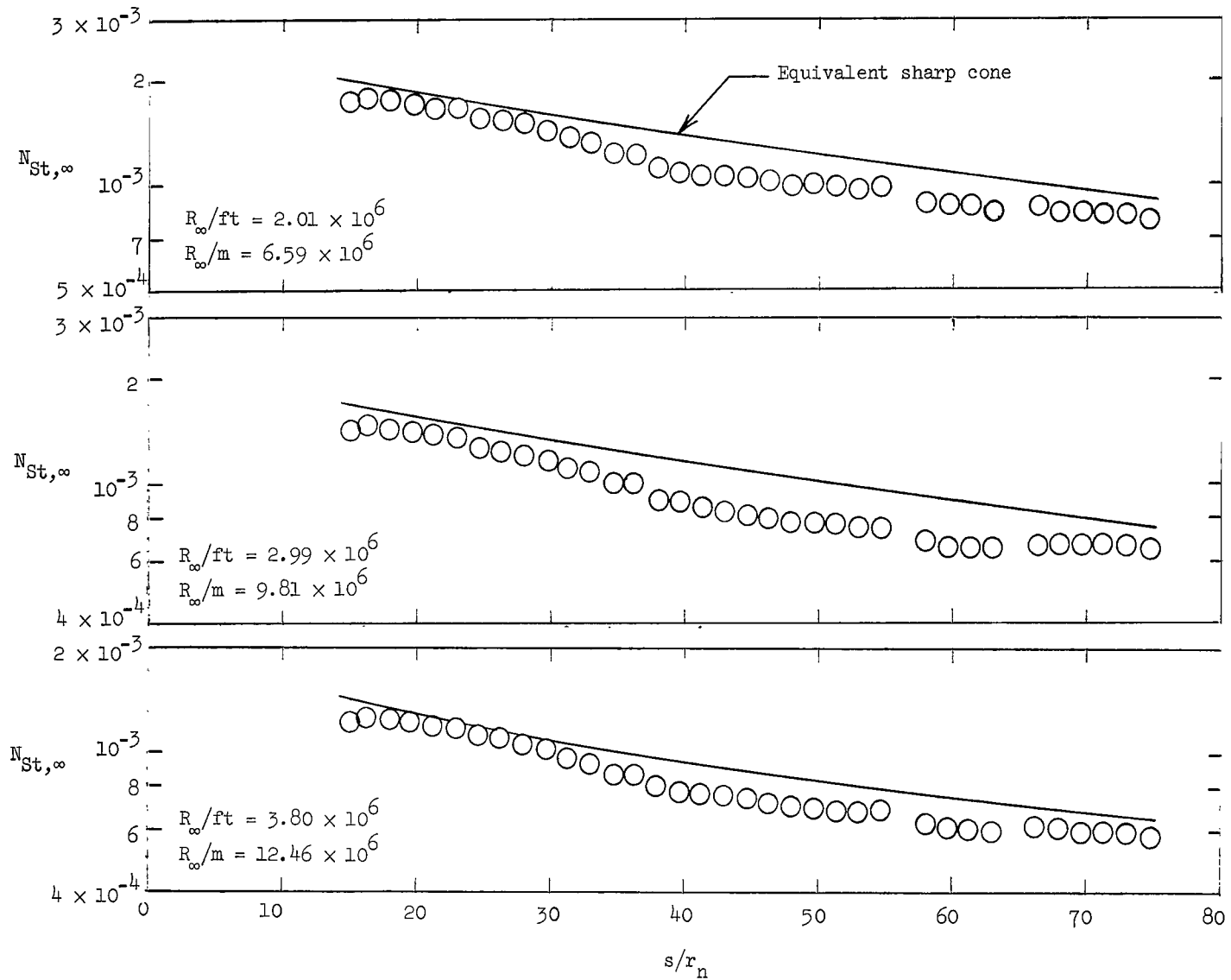
(a) $\alpha = 2^\circ$ to 8° (leeward ray).

Figure 12.- Stanton number distributions for sharp-tipped metal cone at angle of attack.



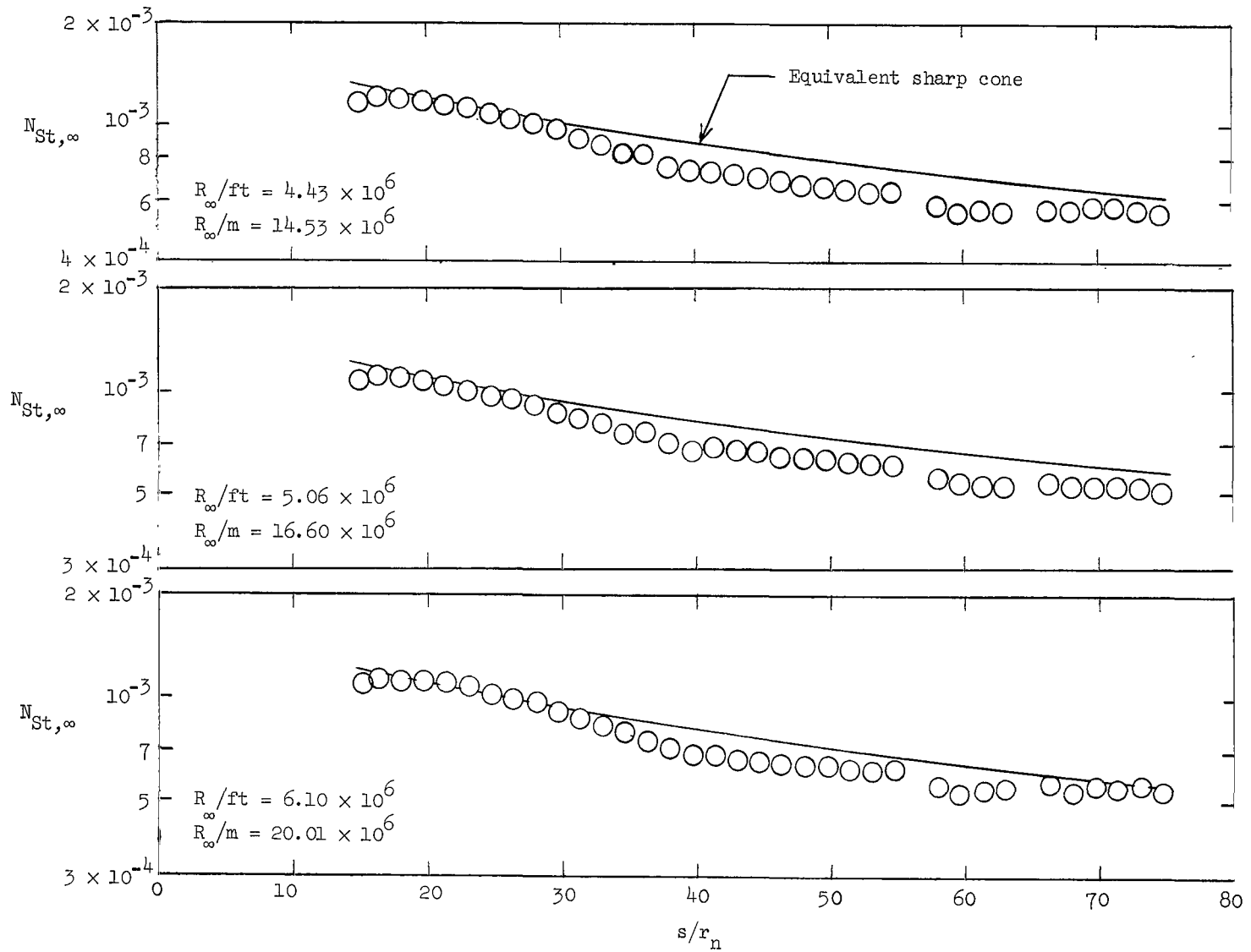
(b) $\alpha = 2^\circ$ to 8° (windward ray).

Figure 12.- Concluded.



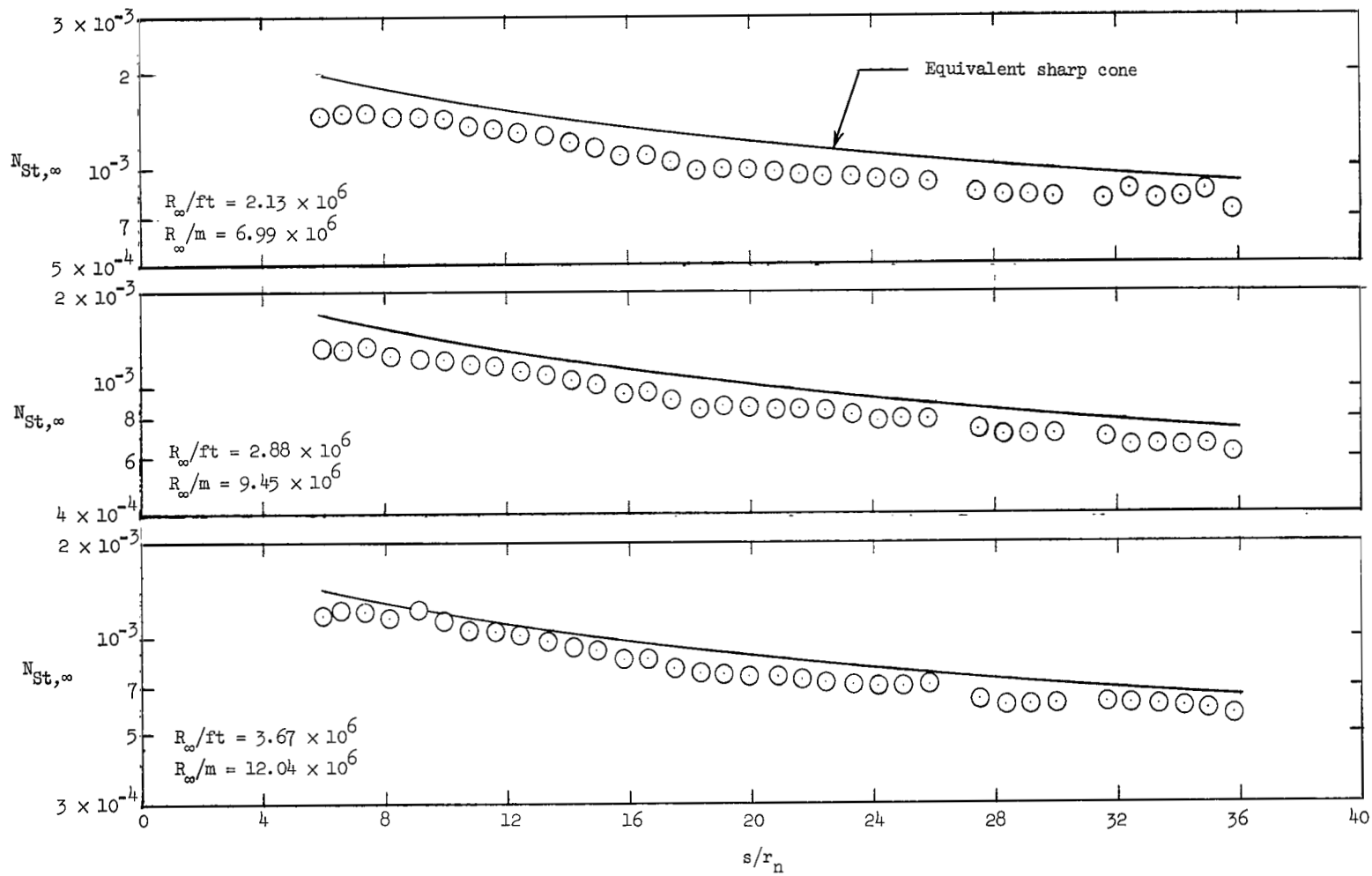
(a) Nose B; $R_\infty/ft = 2.01 \times 10^6$ to 3.80×10^6 ($R_\infty/m = 6.59 \times 10^6$ to 12.46×10^6).

Figure 13.- Stanton number distributions for blunt-tipped metal cone. $\alpha = 0^\circ$.



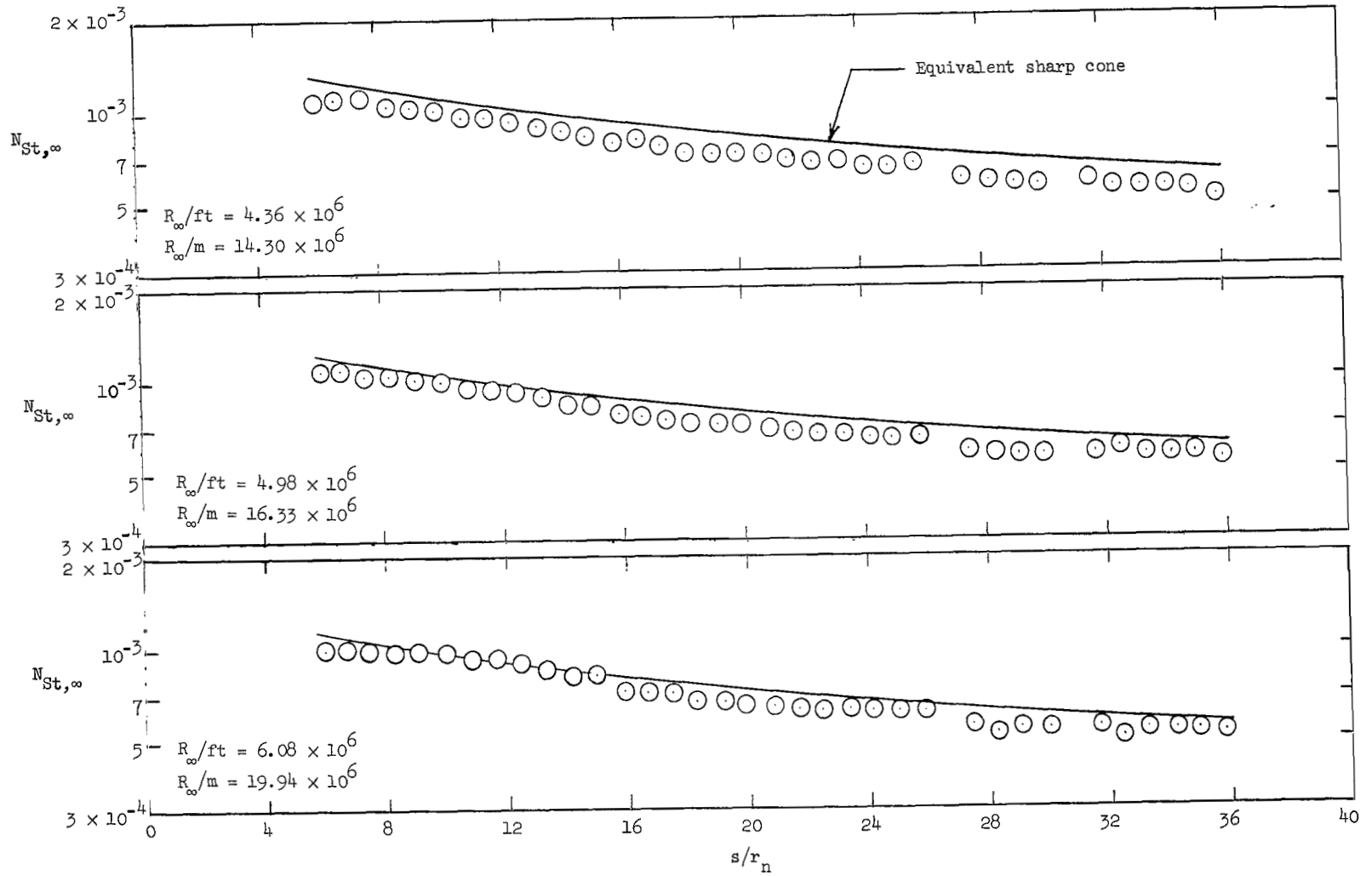
(b) Nose B; $R_\infty/ft = 4.43 \times 10^6$ to 6.10×10^6 ($R_\infty/m = 14.53 \times 10^6$ to 20.01×10^6).

Figure 13.- Continued.



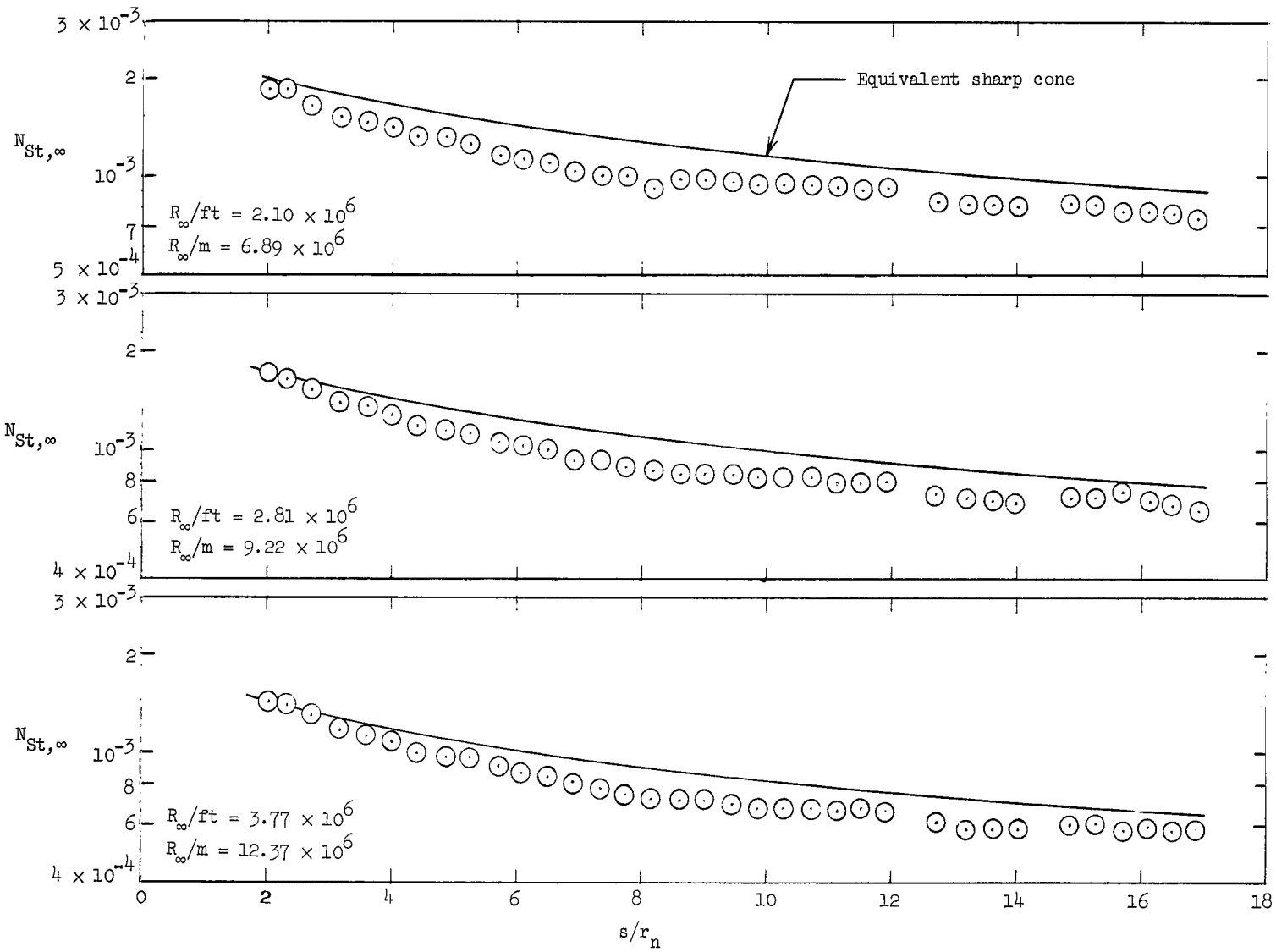
(c) Nose C; $R_\infty/ft = 2.13 \times 10^6$ to 3.67×10^6 ($R_\infty/m = 6.99 \times 10^6$ to 12.04×10^6).

Figure 13.- Continued.



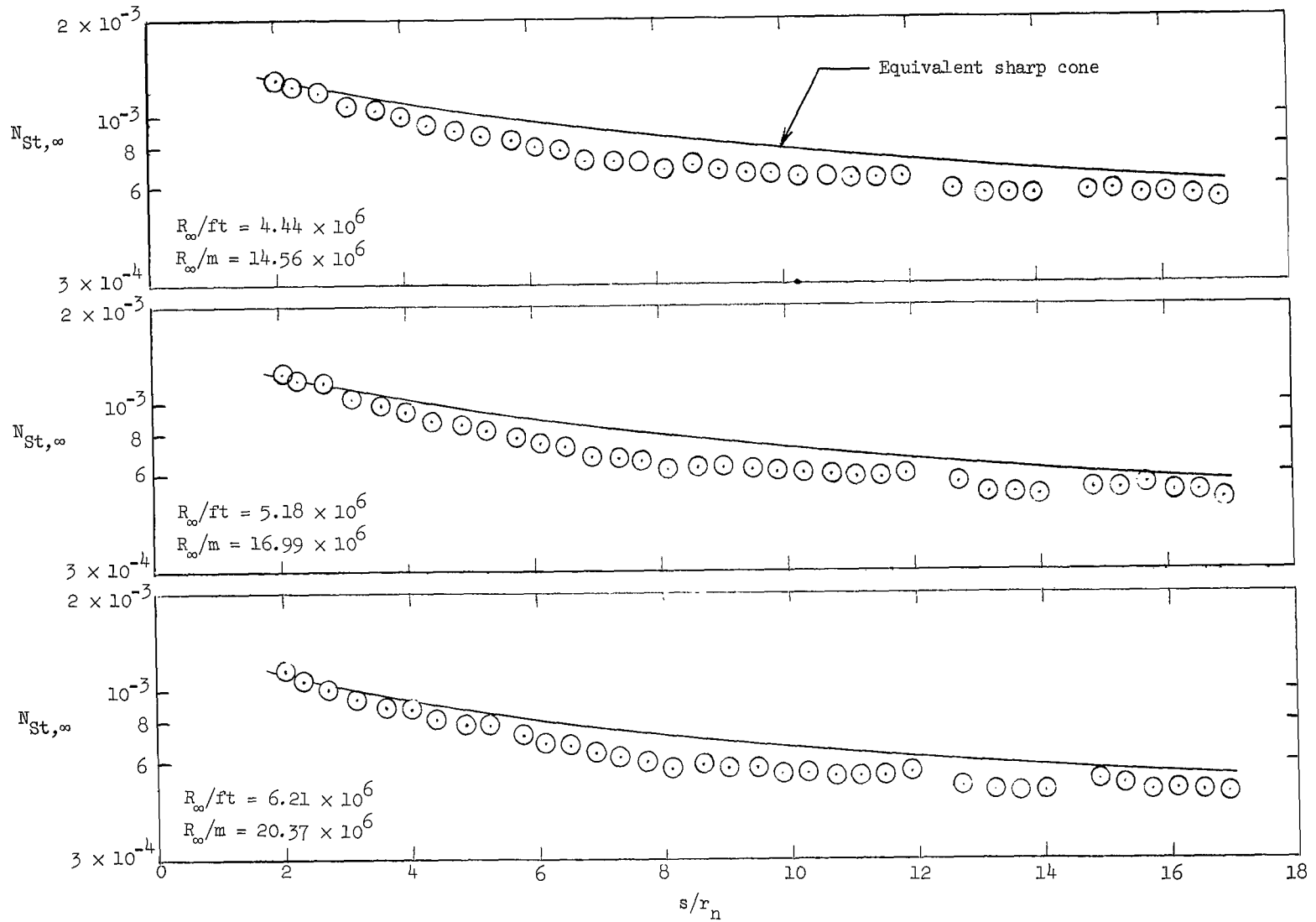
(d) Nose C; $R_{\infty}/ft = 4.36 \times 10^6$ to 6.08×10^6 ($R_{\infty}/m = 14.30 \times 10^6$ to 19.94×10^6).

Figure 13.- Continued.



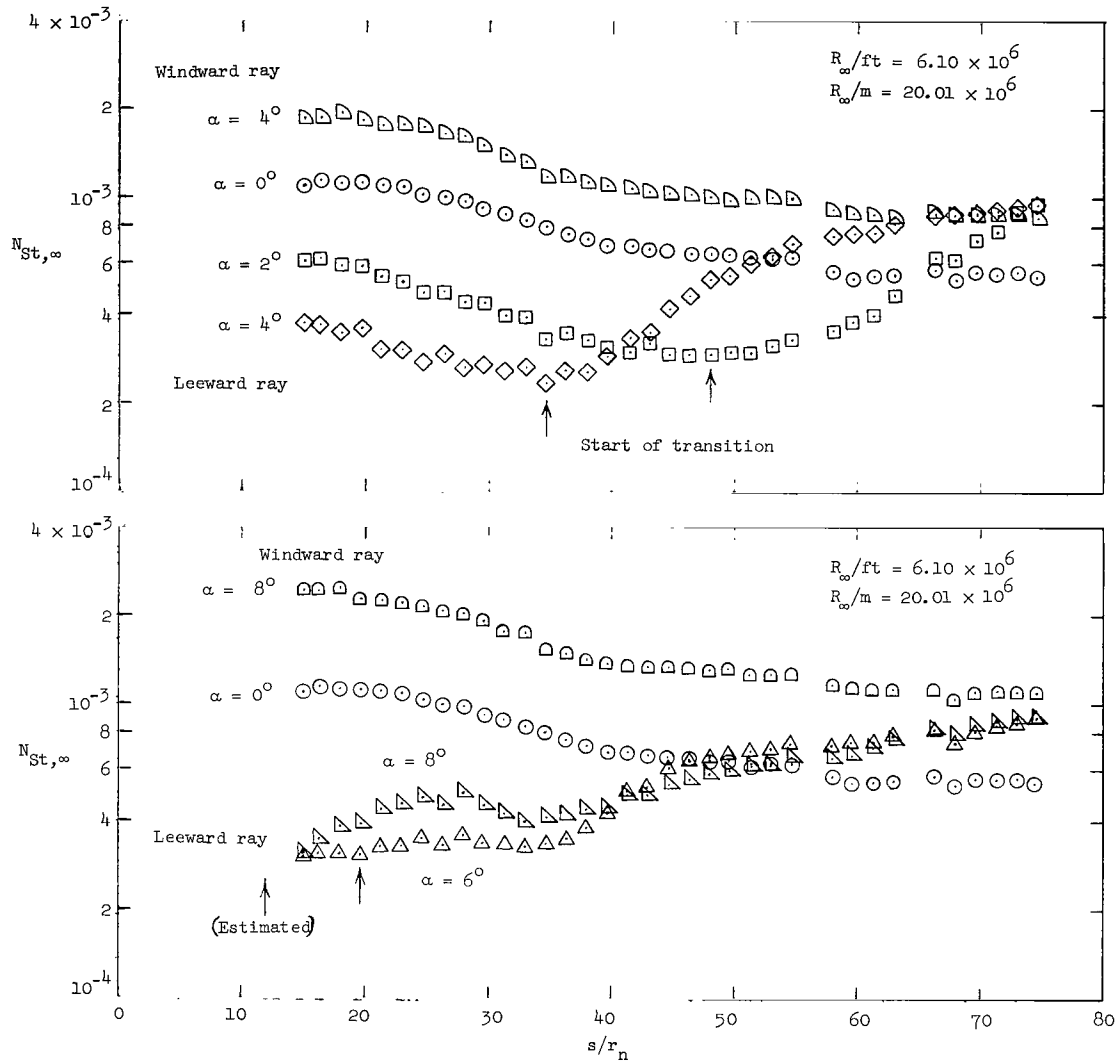
(e) Nose D; $R_{\infty}/ft = 2.10 \times 10^6$ to 3.77×10^6 ($R_{\infty}/m = 6.89 \times 10^6$ to 12.37×10^6).

Figure 13.- Continued.



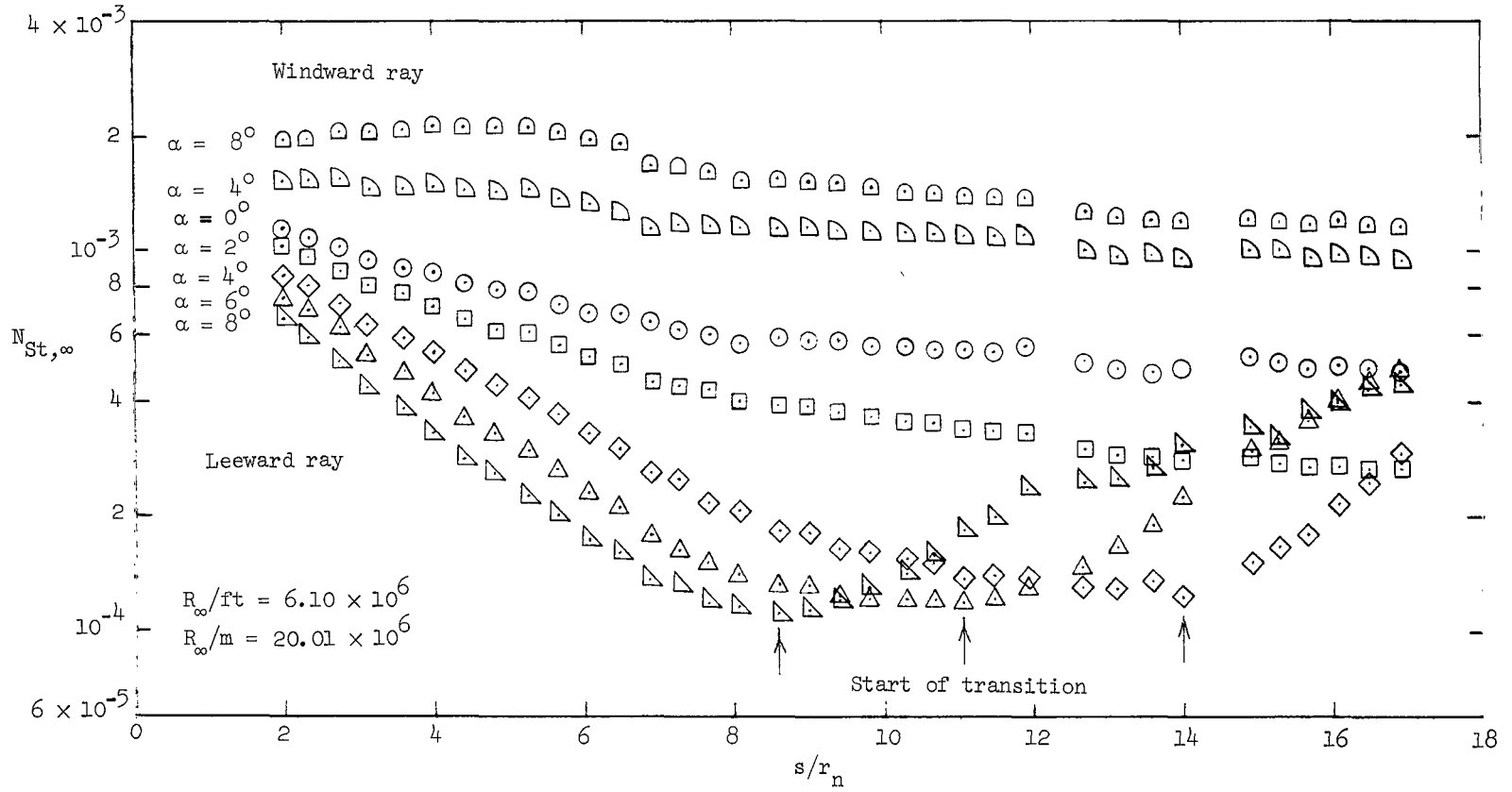
(f) Nose D; $R_\infty/ft = 4.44 \times 10^6$ to 6.21×10^6 ($R_\infty/m = 14.56 \times 10^6$ to 20.37×10^6).

Figure 13.- Concluded.



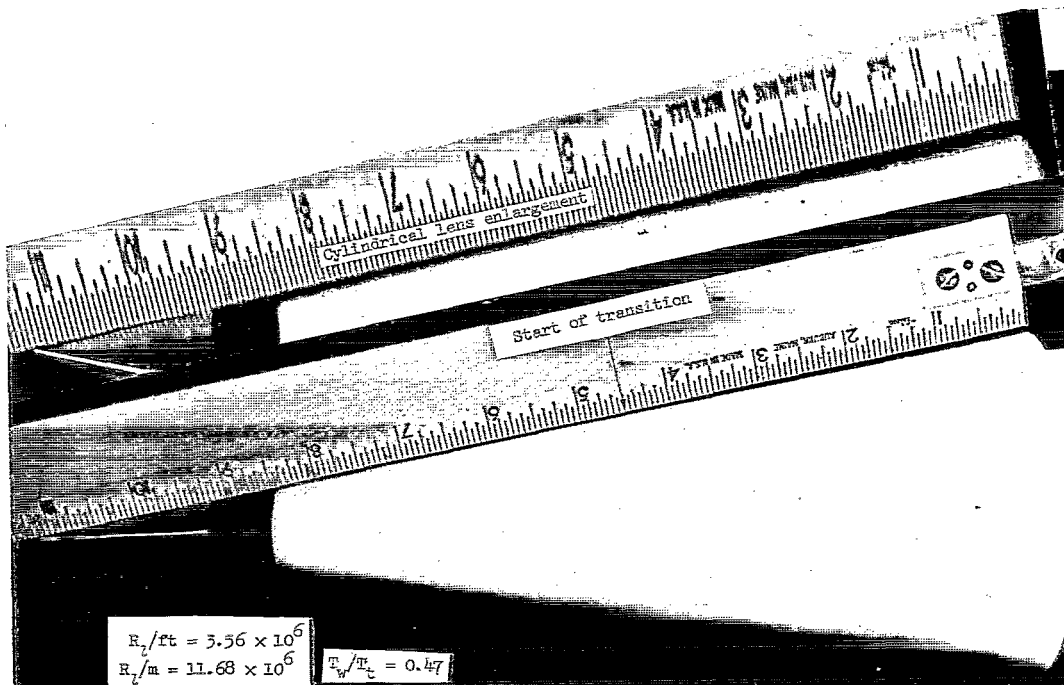
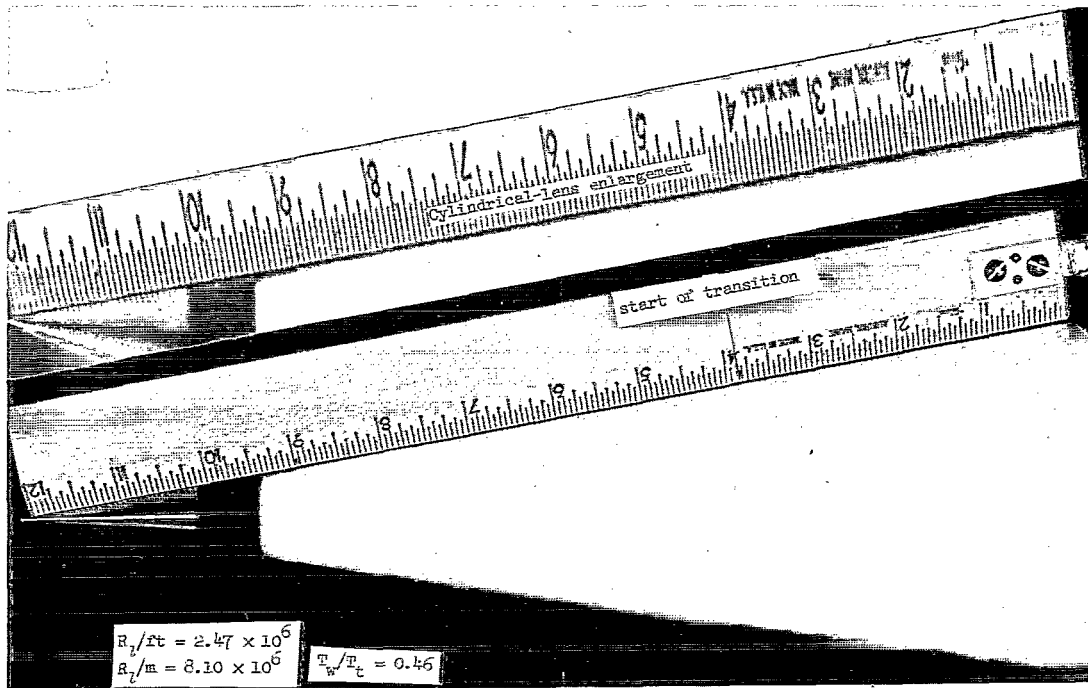
(a) Nose B; $\alpha = 0^\circ$ to 8° .

Figure 14.- Stanton number distributions for blunt-tipped metal cone at angle of attack.



(b) Nose D; $\alpha = 0^\circ$ to 8° .

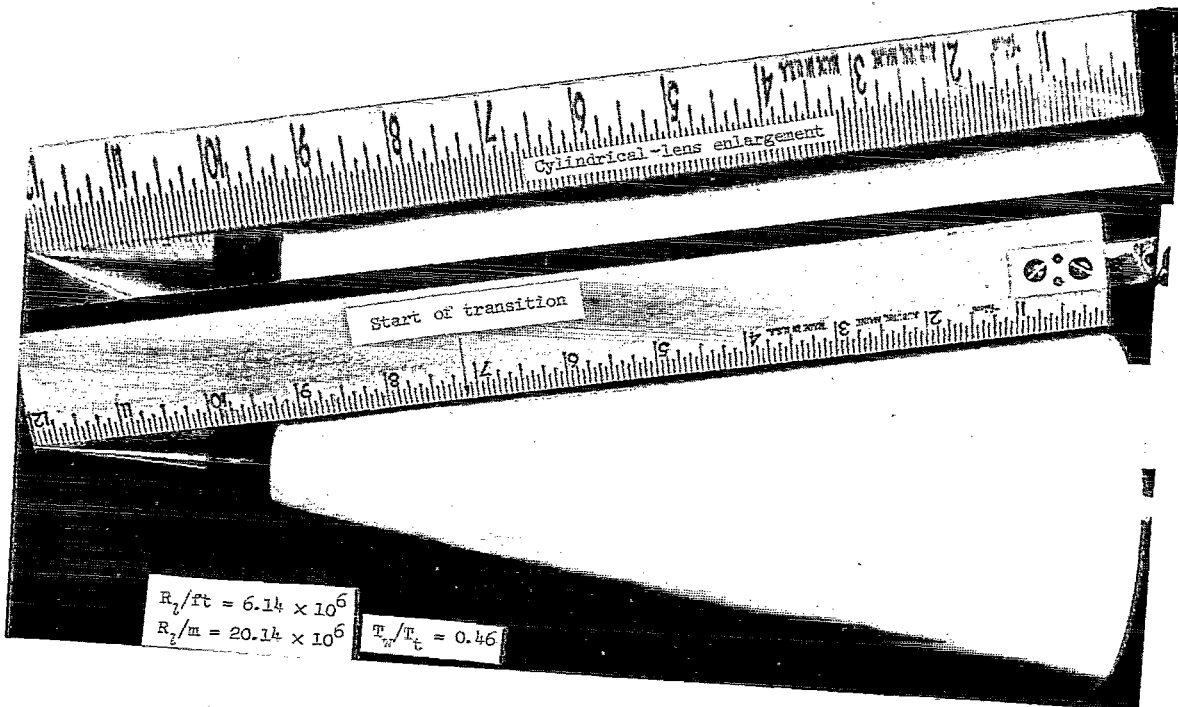
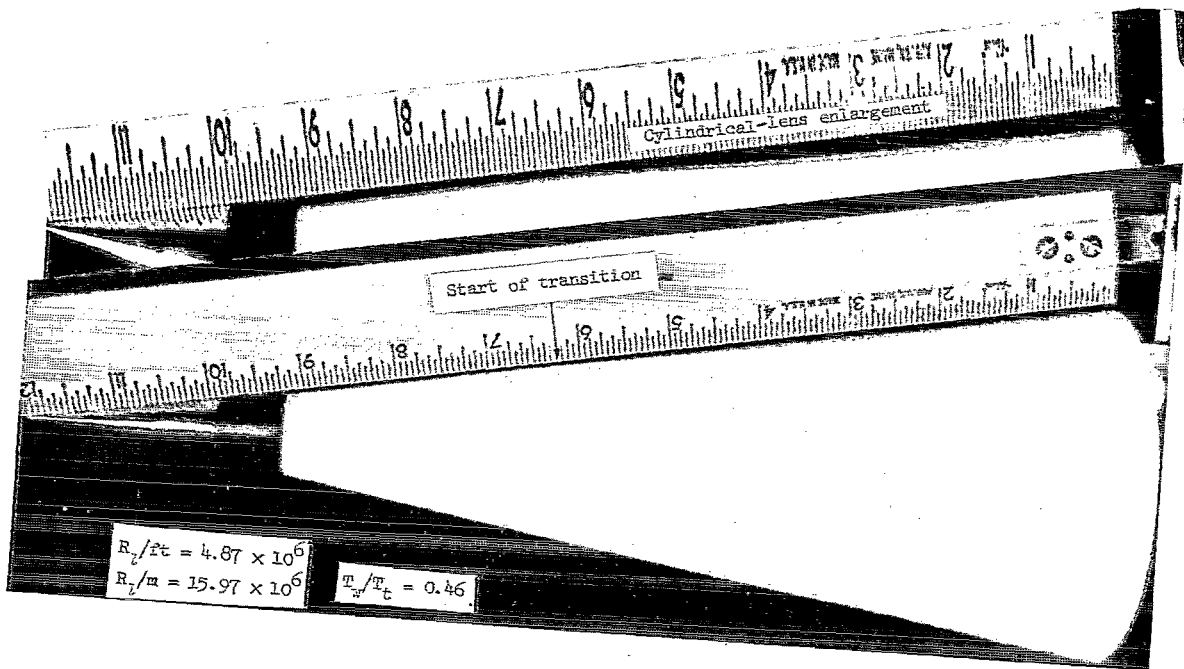
Figure 14.- Concluded.



(a) $R_c/ft = 2.47 \times 10^6$ to 3.56×10^6 ($R_c/m = 8.10 \times 10^5$ to 11.68×10^6).

Figure 15.- Photographs of surface recession on ablated models.

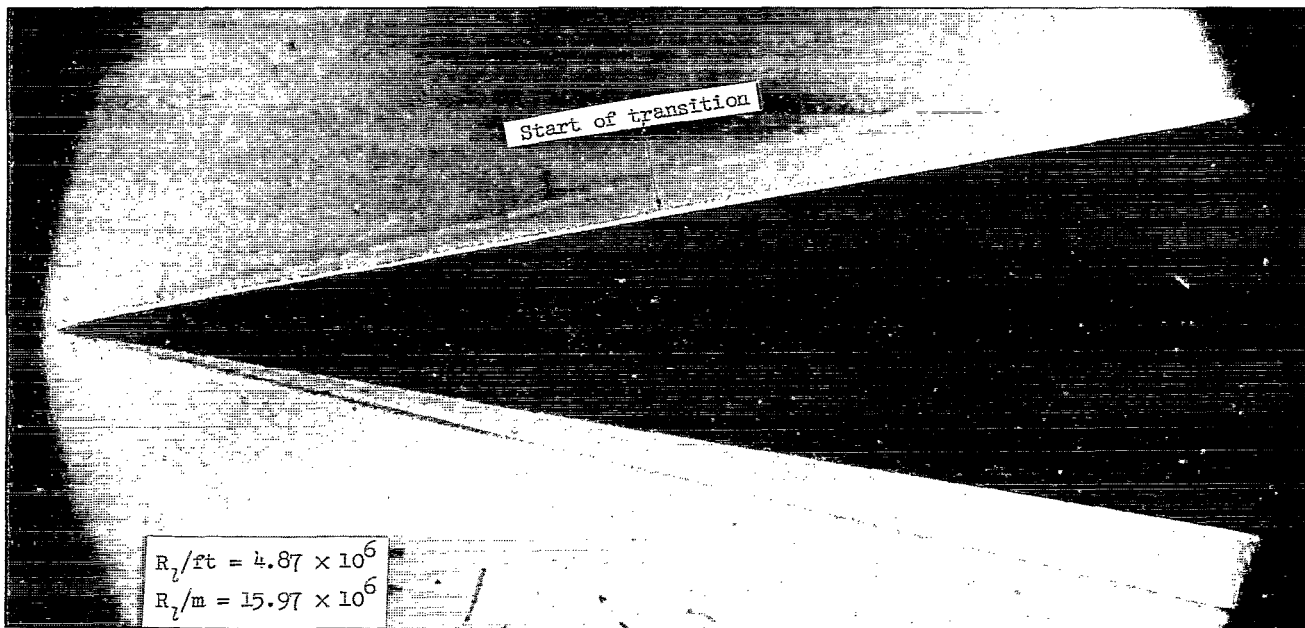
L-70-1543



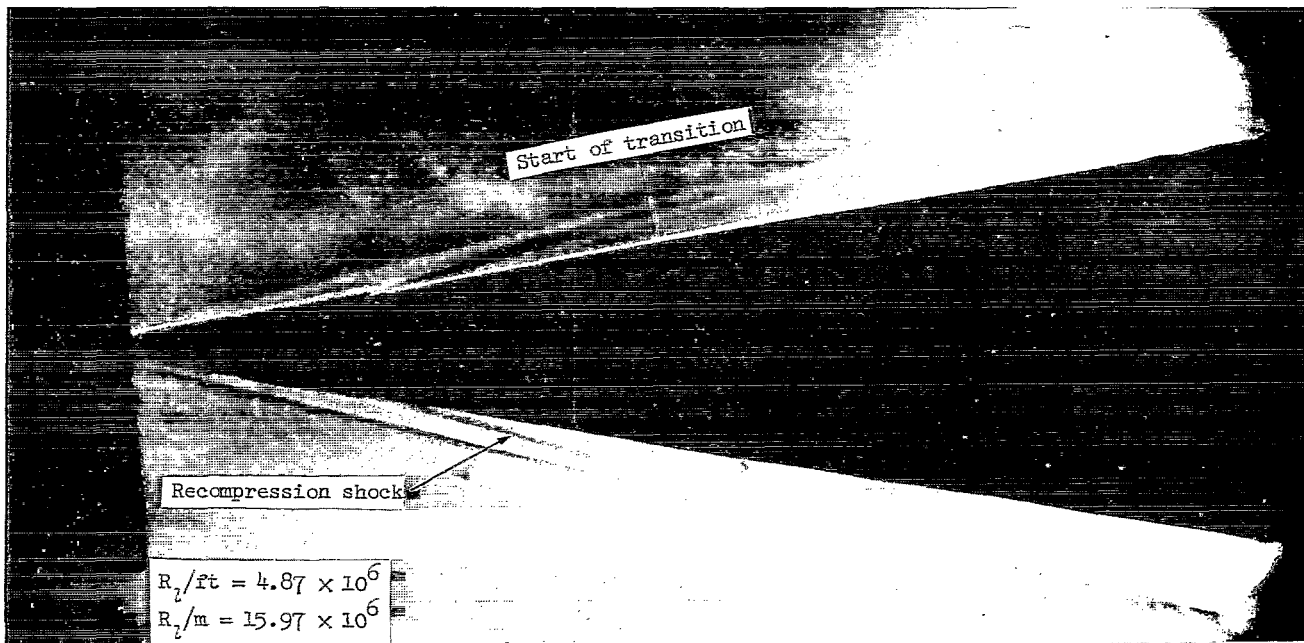
(b) $R_l/ft = 4.87 \times 10^6$ to 6.14×10^6 ($R_l/m = 15.97 \times 10^6$ to 20.14×10^6).

Figure 15.- Concluded.

L-70-1544



$t = 3 \text{ sec}$



$t = 30 \text{ sec}$

Figure 16.- Typical schlieren photographs of an ablating cone.

L-70-1545

FIRST CLASS MAIL



POSTAGE AND FEES PAID
NATIONAL AERONAUTICS AND
SPACE ADMINISTRATION

OIU 001 37 51 3DS 70103 00903
AIR FORCE WEAPONS LABORATORY /WLOL/
KIRTLAND AFB, NEW MEXICO 87117

ATTN: LOU BOWMAN, CHIEF, TECH. LIBRARY

POSTMASTER: If Undeliverable (Section 158
Postal Manual) Do Not Return

"The aeronautical and space activities of the United States shall be conducted so as to contribute . . . to the expansion of human knowledge of phenomena in the atmosphere and space. The Administration shall provide for the widest practicable and appropriate dissemination of information concerning its activities and the results thereof."

— NATIONAL AERONAUTICS AND SPACE ACT OF 1958

NASA SCIENTIFIC AND TECHNICAL PUBLICATIONS

TECHNICAL REPORTS: Scientific and technical information considered important, complete, and a lasting contribution to existing knowledge.

TECHNICAL NOTES: Information less broad in scope but nevertheless of importance as a contribution to existing knowledge.

TECHNICAL MEMORANDUMS: Information receiving limited distribution because of preliminary data, security classification, or other reasons.

CONTRACTOR REPORTS: Scientific and technical information generated under a NASA contract or grant and considered an important contribution to existing knowledge.

TECHNICAL TRANSLATIONS: Information published in a foreign language considered to merit NASA distribution in English.

SPECIAL PUBLICATIONS: Information derived from or of value to NASA activities. Publications include conference proceedings, monographs, data compilations, handbooks, sourcebooks, and special bibliographies.

TECHNOLOGY UTILIZATION PUBLICATIONS: Information on technology used by NASA that may be of particular interest in commercial and other non-aerospace applications. Publications include Tech Briefs, Technology Utilization Reports and Notes, and Technology Surveys.

Details on the availability of these publications may be obtained from:

SCIENTIFIC AND TECHNICAL INFORMATION DIVISION
NATIONAL AERONAUTICS AND SPACE ADMINISTRATION
Washington, D.C. 20546